Title
Droplet-based microfluidics in biomedical applications

Journal
Biofabrication, 14(2)

ISSN
1758-5082

Authors
Amirifar, Leyla
Besanjideh, Mohsen
Nasiri, Rohollah
et al.

Publication Date
2022-04-01

DOI
10.1088/1758-5090/ac39a9

Peer reviewed

TOPICAL REVIEW

Droplet-based microfluidics in biomedical applications

To cite this article: Leyla Amirifar *et al* 2022 *Biofabrication* **14** 022001

Biofabrication

TOPICAL REVIEW

Droplet-based microfluidics in biomedical applications

RECEIVED
19 August 2021

REVISED
9 November 2021

ACCEPTED FOR PUBLICATION
15 November 2021

PUBLISHED
24 January 2022

Leyla Amirifar[1,11], Mohsen Besanjideh[1,11], Rohollah Nasiri[1,2,3,4,11], Amir Shamloo[1,10,*], Fatemeh Nasrollahi[2,3,4], Natan Roberto de Barros[2,3,4], Elham Davoodi[2,3,5], Ahmet Erdem[2,3,6], Mahboobeh Mahmoodi[2,3,7], Vahid Hosseini[2,3,4], Hossein Montazerian[2,3], Jamileh Jahangiry[2,3], Mohammad Ali Darabi[2,3,4], Reihaneh Haghniaz[2,3,4], Mehmet R Dokmeci[2,3,4], Nasim Annabi[8], Samad Ahadian[2,3,4,*] and Ali Khademhosseini[2,3,4,8,9,*]

[1] Nano-Bioengineering Lab, Department of Mechanical Engineering, Sharif University of Technology, Tehran, 11365-11155, Iran
[2] Center for Minimally Invasive Therapeutics (C-MIT), University of California—Los Angeles, Los Angeles, CA 90095, United States of America
[3] Department of Bioengineering, University of California—Los Angeles, Los Angeles, CA 90095, United States of America
[4] Terasaki Institute for Biomedical Innovation (TIBI), Los Angeles, CA 90024, United States of America
[5] Multi-Scale Additive Manufacturing Lab, Mechanical and Mechatronics Engineering Department, University of Waterloo, Waterloo, ON N2L 3G1, Canada
[6] Department of Biomedical Engineering, Kocaeli University, Kocaeli, 41001, Turkey
[7] Department of Biomedical Engineering, Yazd Branch, Islamic Azad University, Yazd, 8915813135, Iran
[8] Department of Chemical and Biomolecular Engineering, University of California—Los Angeles, Los Angeles, CA 90024, United States of America
[9] Department of Radiological Sciences, University of California—Los Angeles, Los Angeles, CA 90024, United States of America
[10] Stem Cell and Regenerative Medicine Center, Sharif University of Technology, Tehran 11365-11155, Iran
[11] Equal contributions.
[*] Authors to whom any correspondence should be addressed.

E-mail: shamloo@sharif.edu, sahadian@terasaki.org and khademh@terasaki.org

Keywords: microfluidics, droplet, drug delivery, detection, particle synthesis, diagnostics, cell

Abstract

Droplet-based microfluidic systems have been employed to manipulate discrete fluid volumes with immiscible phases. Creating the fluid droplets at microscale has led to a paradigm shift in mixing, sorting, encapsulation, sensing, and designing high throughput devices for biomedical applications. Droplet microfluidics has opened many opportunities in microparticle synthesis, molecular detection, diagnostics, drug delivery, and cell biology. In the present review, we first introduce standard methods for droplet generation (i.e. passive and active methods) and discuss the latest examples of emulsification and particle synthesis approaches enabled by microfluidic platforms. Then, the applications of droplet-based microfluidics in different biomedical applications are detailed. Finally, a general overview of the latest trends along with the perspectives and future potentials in the field are provided.

1. Introduction

Droplet-based microfluidics aims at the generation and manipulation of discrete volumes of fluids in the immiscible phases, such as the generation of oil-in-water (O/W) or water-in-oil (W/O) droplets. This technology offers several advantages, including high control over small volumes of fluids and droplet characteristics, the possibility of performing high throughput experiments with an enhanced mixing mechanism, and a high surface-area-to-volume ratio, and enhanced reaction rate [1]. Various applications, including drug delivery, emulsification, nano/micro-particles synthesis, and cell encapsulation, are offered using droplet microfluidics [2]. In many lab-on-chip applications, there is a need to make uniform droplets as microreactors in biochemical or chemical reactions to enable predictable and controlled outcomes [3]. Furthermore, generating well-controlled sequences of droplets with different volumes is desired for some applications, a typical example is the multi-volume droplet digital polymerase-chain-reaction (PCR) for quantitative and accurate detection of genetic information [4, 5]. Additionally, this technology enables the possibility of performing large-scale phenotypic or genotypic screens at the single-cell level. Furthermore, droplet-based microfluidics has diverse

applications in drug discovery, antibody screening, and multiplexed genomic applications such as single-cell studies, targeted genetic workflows, single-cell RNA sequencing (RNA-seq), and chromatin immunoprecipitation (ChIP)-sequencing (ChIP-seq) [6, 7].

Droplet-based microfluidic systems have emerged as a promising technology for droplet generation for different applications. This contrasts with mechanical mixing, which relies on Rayleigh instabilities to generate droplets because of shearing of two immiscible phases [8, 9]. Studies conducted on droplet microfluidics exhibit the creation of a convective flow profile inside the droplets, which speeds up the mixing process. Hence, understanding the physics of fluid flow inside the droplets is critical for designing an efficient microfluidic device. The dynamics of droplet generation in microfluidics are governed by the Stokes equation; however, a nonlinear behavior is observed in droplet microfluidics due to the deformable interfaces between droplet and the carrier fluid. Injection of two immiscible fluids into a microfluidic channel leads to the formation of continuous and dispersed phases and generation of stable droplets in the dispersed phase. The controlled generation of droplets is required for expanding their applications in various biomedical areas, including drug and gene delivery and lab-on-a-chip systems [10–12]. Flow rate and viscosity ratios of two immiscible phases and the interfacial tension are the most influential parameters on the generation of droplets. Droplets are generated when the viscous drag force applied by the continuous phase on the dispersed phase overcomes the interfacial surface tension force of the fluid pair. Droplet generation can also occur when the dispersed fluid can fill and plug the continuous channel. This process causes a pressure change, which then creates the plug to shear off and generate a droplet [13].

In this review, first different approaches for droplet generation, including passive and active methods are presented. Then, the application of droplet-based microfluidics in emulsification and particle synthesis is discussed. Later, different applications of this technology in biomedical engineering including biomolecular analysis (DNA and genomics, RNA and transcription, protein analysis, and directed evolution of enzymes), cell biology (intracellular and extracellular interactions, and artificial cell generation), and diagnosis (microbial infections, oncology assays, genetic mutations, drug delivery systems (DDS), drug screening platforms), and tissue engineering are reviewed. Finally, the opportunities for further developments and potential applications enabled by droplet-based microfluidic devices are presented.

Previous review papers published in this field are mostly focused on a specific area of droplet-based microfluidics. The presented review paper is more comprehensive compared to the previous published papers in this area and it covers the droplet generation methods and most of its applications in biomedical engineering. Another specific feature of this review is its special attention to the engineering aspects of the droplet-based microfluidic systems. It also reveals the importance of the engineered droplet-based microfluidic systems in advancing biomedical applications. Additionally, because the field of droplet-based microfluidics is progressing rapidly, a new review paper in this field that covers the recent advances in this field is crucial.

2. Droplet generation methods

The process of droplet formation occurs due to interfacial instability between the immiscible phases. In this process, the interface of the continuous and dispersed phases is deformed, leading to pinching off the dispersed phase and droplet generation [14, 15]. Compared to the conventional droplet generation methods, droplet-based microfluidics is more capable of high-throughput generation of monodisperse droplets. Droplet monodispersity is determined by calculating the coefficient of variation (CV), which is calculated by dividing the standard deviation of the size distribution of a set of droplets by its arithmetic average. The CV values are typically less than 5%, even for the complex droplet architectures generated in microfluidic devices [16, 17]. These low CV values reveal the ability of the microfluidic methods for producing monodisperse droplets. From a physical point of view, droplet formation is controlled by inertial, viscous, interfacial, and gravitational forces, as well as other applied external force fields [18]. The significance of these forces can be revealed by introducing the relevant dimensionless parameters. The most common dimensionless parameters in droplet microfluidics are Reynolds number (Re), Capillary number (Ca), Weber number (We), Bond number (Bo), as well as flow rate ratio (φ) and viscosity ratio (λ), which are defined and listed in table 1. These parameters are calculated by determining the interfacial tension (σ), fluid velocity (V), fluid density (ρ), and dynamic viscosity (μ). In addition, the characteristic length, l, is usually considered as the channel width. The subscripts c and d also denote the continuous and dispersed phase, respectively. Assuming that inertial and gravitational forces to be of less significance, droplet formation modes can be characterized by the capillary number, as well as the flow rate and viscosity ratios. The capillary number is commonly calculated based on the viscous force induced by the continuous phase ($\mathrm{Ca}_c = \mu_c V_c/\sigma$). At low capillary numbers, $\mathrm{Ca}_c < \mathrm{O}(0.01)$, the viscous force is not dominant during droplet formation, and the plug-like droplets are detached from the dispersed phase in the squeezing regime [19]. In this mode, the dispersed phase protrusion completely blocks the path of the continuous phase fluid, which leads to an increase in upstream pressure and drop detachment by squeezing pressure. The size of droplets generated in the squeezing regime

Table 1. Dimensionless parameters in droplet-based microfluidics.

Parameter	Formula	Physical description
Reynolds number	$\mathrm{Re} = \frac{\rho V l}{\mu}$	$\frac{\text{Inertial force}}{\text{Viscous force}}$
Capillary number	$\mathrm{Ca} = \frac{\mu V}{\sigma}$	$\frac{\text{Viscous force}}{\text{Interfacial force}}$
Weber number	$\mathrm{We} = \frac{\rho V^2 l}{\sigma}$	$\frac{\text{Inertial force}}{\text{Interfacial force}}$
Bond number	$\mathrm{Bo} = \frac{\Delta\rho g l^2}{\sigma}$	$\frac{\text{Gravitational force}}{\text{Interfacial force}}$
Flow rate ratio	$\varphi = \frac{Q_d}{Q_c}$	$\frac{\text{Dispersed phase flow rate}}{\text{Continuous phase flow rate}}$
Viscosity ratio	$\lambda = \frac{\mu_d}{\mu_c}$	$\frac{\text{Dispersed phase viscosity}}{\text{Continuous phase viscosity}}$

is independent of the capillary number and depends solely on the flow rate ratio [19, 20]. As the capillary number increases, the role of viscous force becomes more apparent, and transition from the squeezing regime to the dripping regime occurs. In the dripping regime, highly monodisperse droplets are formed with a length smaller than the channel width. The CV values of less than 3% are achievable in the dripping regime [21, 22]. Moreover, droplet size, as well as droplet generation frequency, strongly depends on the capillary number [20, 21, 23]. Owing to high monodispersity and ease of manipulation, dripping is the most preferable mode of droplet formation in biomedical applications [24]. Jetting is another droplet formation regime that occurs due to Rayleigh plateau instability along a stretched dispersed thread. Compared to the dripping regime, jetting takes place at relatively higher capillary numbers and flow rate ratios [25]. In this mode, in addition to the viscous force, the dispersed phase inertia can also be involved in overcoming the surface tension [26]. In other words, the jetting mode can be characterized by $\mathrm{Ca_c}$ and $\mathrm{We_d}$, where $\mathrm{We_d}$ is defined based on dispersed phase inertial force ($\mathrm{We}_d = \rho_d V_d^2 l/\sigma$). The size of droplets generated in the jetting regime depends on capillary and Weber numbers, flow rate ratio, and capillary perturbations [26, 27]. Droplet monodispersity in the jetting regime is remarkably less than those of dripping and squeezing regimes [25]. Hence, except for specific applications [28], the jetting mode is not preferred for the encapsulation of bioactive compounds. More details about the microfluidic droplet generation regimes can be found in a review paper by Zhu *et al* [25].

To establish the desired state of droplet formation, in terms of droplet size and generation rate, there are two main approaches in microfluidics: passive and active methods. The passive methods operate based on the channel geometry and the physical properties of the immiscible phases. On the other hand, active methods take advantage of the external force fields to control droplet breakup dynamics. Figure 1 schematically represents different passive and active methods, which are reviewed in this paper. Moreover, a summary of the pros and cons of these methods is given in table 2.

2.1. Passive methods for droplet generation

The passive mechanisms rely on channel geometry, flow rate, and intrinsic properties of the immiscible phases without adding any external force fields to the fluid flows [25, 29, 30]. These mechanisms are commonly classified based on channel geometry. As depicted in figures 1(a)–(c), cross-flow, flow-focusing, and co-flow configurations are the most usual passive droplet generation designs applied in biomedical applications [16, 18, 25]. Moreover, these standard geometries may be modified to induce higher shearing force and achieve the desired modes of droplet formation [31, 32]. Droplet manipulation in passive methods is normally carried out by varying the flow rates or driving pressures of the dispersed and continuous phases injected into the microfluidic device [33, 34]. Using surfactants can be another alternative to adjust the droplet size and droplet generation frequency. Surfactants are amphiphilic molecules that are frequently added to the continuous or dispersed phases to prevent droplet coalescence. However, these molecules can alter the interfacial tension, which, in turn, leads to a change in the capillary number. Different concentrations of Tween 20 surfactant were used by Peng *et al* [35] to generate W/O droplets in a flow-focusing device. It was observed that interfacial tension significantly decreases by adding a specific amount of surfactant to the dispersed phase, which results in a reduction in droplet size and enhancement of droplet generation frequency. Adjusting the rheological properties of

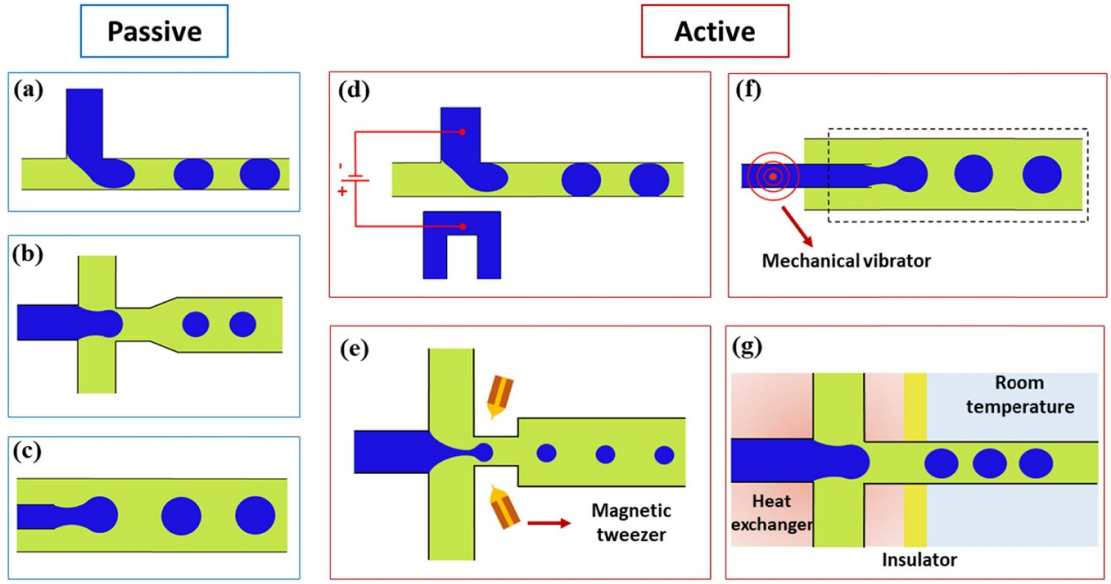

Figure 1. Schematic of different passive and active microfluidic droplet generation methods. (a)–(c) Different channel geometries in passive approach; (a) cross-flow, (b) flow-focusing, and (c) co-flow geometries. (d)–(g) Implementing different active methods in microfluidic droplet generators; (d) electrical control of droplet generation with direct current in a cross-flow configuration [48], (e) employing magnetic field by a magnetic tweezers instrument to control ferrofluid droplet generation in a flow-focusing device [56], (f) applying mechanical vibration on the microtubing of the dispersed phase fluid to stimulate droplet generation in a co-flow geometry [64], and (g) thermal control of droplet generation in a flow-focusing device [46].

the immiscible phases is another passive strategy to achieve desired droplets in terms of size, shape, and generation frequency. Biological samples are commonly highly viscous such as polymeric solutions, cell suspensions, and samples containing proteins and enzymes. Using these samples as the dispersed phase may lead to pinching resistance due to high viscosity ratios. In this situation, the normal process of droplet generation is disrupted by emerging satellite droplets [36], laminar flow [37], or unstable modes of droplet formation [24]. Therefore, the concentration of the polymeric precursors and biological components should be optimized such that they have minimum adverse effects on the process of droplet generation. Nanofluids can also be employed in droplet-based microfluidic to regulate the viscosity ratio. Nanofluids provide different rheological properties base on nanoparticle concentration [38]. They can protect droplets against coalescence [39], enhance shear stress during droplet formation [20], and have an intermediate role to change the fluid flow patterns under the presence of magnetic fields or thermal sources [40]. Nevertheless, the channel geometry still plays the most important role in the passive droplet generators and is discussed in more detail in this review.

2.1.1. Cross-flow design

In a cross-flow design, the continuous and dispersed phases meet in a junction with an arbitrary angle. From a geometrical point of view, the cross-flow designs are classified into T-junction and Y-junction geometries. In the former group, the two inlet channels are perpendicular (figure 1(a)), while in the latter group, they are connected in other angles between 0° to 180° [14, 25]. Figure 2(a) displays different modes of droplet formation in a T-junction microfluidic device [37]. Although plug-like droplets are usually formed in cross-flow microfluidic devices, spherical droplets can also be generated at relatively higher capillary numbers and lower flow rate ratios. Meanwhile, high monodispersity can be achieved using cross-flow geometries [25]; however, droplets may be damaged by the shear stress or adhere to the channel walls sine breakup occurs at the vicinity of the wall. Compared with the other configurations, cross-flow designs need a small space on microfluidic platforms and can be easily combined by the other microfluidic units [41].

2.1.2. Flow-focusing design

The flow-focusing devices are usually employed to generate spherical monodisperse droplets rather than plug-like ones [18]. The continuous phase is flowed into two side channels and surrounds the flow of dispersed phase in a constriction channel (figure 1(b)). In such a situation, the dispersed phase is squeezed on both sides by the two streams of the continuous phase, and spherical droplets are generated in the dripping or jetting regimes [16]. The width and length of the constriction channel can remarkably affect the breakup process by adjusting the shear stress imposed on the dispersed phase. Compared with cross-flow configurations, flow-focusing devices are used to generate smaller droplets at higher generation rates [25]. Furthermore, droplets are less threatened by the wall

Table 2. Comparison of different droplet generation methods.

Generation method	Advantages	Disadvantages	Implementation
Passive methods:	In general: ✓ ease of implementation	In general: ✘ long response time, ✘ high breakup resistance	In general: using different geometrical design, adjusting flow rate ratio, interfacial tension, and rheological properties
Cross-flow	Ease of integration with other units	Low sphericity in products	
Flow-focusing	High-throughput generation of small droplets	Requiring large space	
Co-flow	Ease of fabrication	Susceptible to constitute jet	
Active methods:	In general: ✓ small response time ✓ low breakup resistance	In general: ✘ complexity ✘ susceptible to produce satellite and secondary droplets	—
Electrical	General advantages	Electrode fouling and damaging bioactive components	DC and AC voltages
Magnetic	Contactless actuation	Damaging bioactive components	Permanent magnets and electromagnets
Mechanical	Variety in the execution mechanisms	General disadvantages	Hydraulic and pneumatic valves, piezoelectric actuators, and mechanical vibrators
Thermal	Usable for gene amplification	Small response time is only attainable using focused laser beam	Heat exchangers, resistive heaters, and laser beams

shear stress since breakup occurs in the middle region of the channel. Typically, flow-focusing devices are employed to encapsulate sensitive biological components such as cells [42]; but they need relatively large space on microfluidic platforms due to three inlet branches and cannot be easily integrated by the other units in a confined space.

2.1.3. Co-flow design

In the co-flow design, the continuous and dispersed phases are flown in parallel while the dispersed phase is enclosed by the continuous phase (figure 1(c)). The breakup dynamics is controlled by shear force at the end of the dispersed phase channel, leading to droplet generation by either dripping or jetting modes [16, 27]. Although droplets generated in the dripping regime are highly monodisperse, those generated in the jetting regime are polydisperse. The characteristics of droplets generated by co-flow microfluidic devices are similar to those generated by the flow-focusing channels [42]. However, droplet size can be controlled by the width of the dispersed phase channel. In addition, droplet size is usually larger than this size in the dripping mode [25]. Fabricating co-flow droplet generators can be simply done by inserting a microcapillary tube (dispersed phase channel) into another capillary glass (continuous phase channel). Besides, conventional microfabrication methods such as the standard soft-lithography method can be employed to construct 2D planar co-flow configurations. The co-flow designs can also be modified to the step emulsification configuration where an expansion step is located downstream of the microchannel to trigger droplet formation [42].

2.2. Active methods for droplet generation

Active methods are commonly combined with the passive configurations to facilitate the droplet generation process by exerting different external force fields [25]. The passive methods usually suffer from the long response time origins from large fluidic resistance of the tubing and compressibility of the

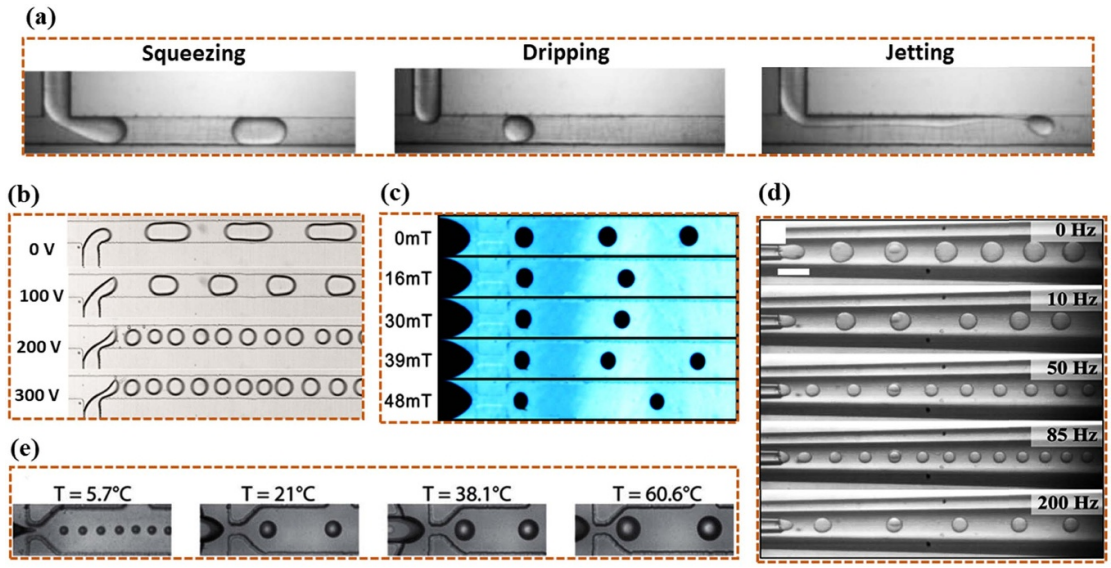

Figure 2. Images of passive and active droplet formation in different microfluidic devices. (a) Different modes of passive droplet generation for a highly viscous dispersed phase (IL-2) using a cross-flow geometry (reprinted from [37], Copyright (2016), with permission from Elsevier). (b)–(e) Active droplet generation methods; (b) electrical control of the aqueous droplet generation at different DC voltages in a T-junction microchannel (reprinted from [48], with the permission of AIP Publishing), (c) ferrofluid droplet formation under various magnetic flux densities in a flow-focusing microfluidic device (reprinted by permission from Springer Nature Customer Service Centre GmbH: Springer Nature, Microfluidics and Nanofluidics [56] Magnetically controllable generation of ferrofluid droplets, Q Yan, S Xuan, X Ruan, J Wu, X Gong, (c) 2015), (d) mechanical control of aqueous droplet formation at different vibration frequencies in a co-flow microfluidic device (reprinted by permission from Springer Nature Customer Service Centre GmbH: Springer Nature, Microfluidics and Nanofluidics [64] Droplet generation in co-flow microfluidic channels with vibration, P Zhu, X Tang, L Wang, (c) 2016), (e) images of water droplets generated at different temperatures of the upstream part of the flow-focusing device (reprinted with permission from [46]. Copyright (2009) American Chemical Society).

channel materials [43]. Moreover, biological fluids may exhibit pinching-resistance behavior due to their complex rheological properties during passive droplet generation processes [24]. In these situations, the fluid dynamics can be controlled by applying external force fields [40, 44]. In droplet microfluidics, an external energy source is locally focused on the droplet generation region, leads to rapidly obtain the desired modes of droplet formation. In addition, active methods may be involved in droplet sorting [45] or assist in conducting some biological processes such as DNA amplification [46]. Herein, a brief description of the most common active methods for droplet formation, including electrical, magnetic, mechanical, and thermal control methods, are presented (figures 1(d)–(g)).

2.2.1. Electrical method

In this method, electrical direct current (DC) or alternative current (AC) is applied to manipulate the droplet formation process within the microfluidic channels [25]. The electrodes can be in direct or indirect contact with the fluids in the microfluidic device; however, electrode fouling and sample contamination can be avoided with indirect electrode contacts [43, 47]. In the DC control approach, droplet size and generation frequency depend on applied DC voltage and the electrical conductivity of the aqueous phase. As DC voltage increases, droplet size is decreased due to the accumulation of the free charges in the water-oil interface [43, 48]. Figure 1(d) schematically shows an example of DC control of droplet generation in a T-junction microchannel, where the electrodes are connected to the aqueous phase channel and a U-shape side-channel close to the junction. As shown in figure 2(b), the droplet size decreases by enhancing DC voltage up to a voltage around 200 V, where a saturation state is established, i.e. the droplet size does not decrease further by applying higher voltages [48]. In AC control methods, the applied voltage fluctuates with a frequency either more or less than that of droplet generation. In such a situation, droplet size depends on the root mean square (RMS) amplitude of the AC voltage and the voltage frequency [43]. The AC voltage is also preferred for applying the electrowetting on dielectric (EWOD) approach for droplet generation [49]. The function of the EWOD mechanism is to decrease the contact angle during droplet formation. By employing the electrical control methods, the response time is significantly reduced during droplet formation without using moving instruments; however, the microfluidic device becomes more complex due to the electrical connections, fouling may occur due to the contact of electrodes with the aqueous phases, and bioactive components may be damaged due to the effect of strong electric fields.

2.2.2. Magnetic method

The external magnetic field generated by the permanent magnets or electromagnets can be used as an active contactless mechanism to manipulate droplet formation [50, 51]. To apply the magnetic force, one of the dispersed or continuous phases should have magnetization capability. Ferrofluids, fluids with suspended magnetic particles, are commonly used to exert magnetic force to the fluid flows [52]. The stabilized ferrofluids can be prepared with both water- and oil-based fluids [53, 54]; hence, there is no limitation to exert magnetic field to either continuous or dispersed phases. Magnetic particles can substantially change the viscosity of the ferrofluids [55]. Therefore, droplet generation can be affected by the rheological properties of the ferrofluids even in the absence of a magnetic field [56]. Using ferrofluids in biomedical applications may be harmful to bioactive components such as cells. Therefore, the direct contact of such components with ferrofluids should be avoided in microfluidic systems. To this end, it is recommended that ferrofluid is used as the continuous phase while the delicate components are encapsulated in the non-magnetic dispersed phase [57]. Also, embedding washing mechanisms in microfluidic systems can help minimize the contact of ferrofluids with those components that are not compatible with them [58, 59]. The droplet formation process under the magnetic field depends on several parameters, including ferrofluid magnetization, magnetic flux density, magnetic field gradient, and the direction of the magnetic field toward the fluid stream [43, 50, 60]. Tan *et al* [50] demonstrated that by locating a permanent magnet downstream of a T-junction device, the size of ferrofluid droplets increases with enhancing magnetic flux density; however, as the magnet is placed upstream, droplet generation is delayed, and the larger droplets are detached from the aqueous ferrofluid. Figure 1(e) displays the schematic of droplet manipulation with a magnetic tweezers instrument in a flow-focusing device. The ferrofluid droplets generated under various high-level areas of a square wave signal are shown in figure 2(c). It is observed that by increasing magnetic flux density, magnetic drag force enhances such that the breakup process is more accelerated. However, droplet monodispersity may be reduced at high magnetic flux density by emerging secondary droplets [56]. The magnetic method of droplet manipulation can provide quick response times. Besides, droplet sorting can be well done using this method [45, 57, 61].

2.2.3. Mechanical method

Mechanical methods of droplet manipulation are based on inducing a disruption in the liquid interface using mechanical actuators. Various mechanical elements, such as hydraulic and pneumatic valves and choppers [62], piezoelectric actuators [63], and mechanical vibrators [64] can be integrated with the passive droplet generation devices. Using mechanical approaches, the amplitude and frequency of the perturbing factor and the natural droplet generation frequency, i.e. droplet generation frequency in the absence of perturbing factors, are the main parameters to determine droplet size and droplet generation frequency [43, 64]. Figure 1(f) shows the schematic of using an off-chip mechanical vibrator to induce fluctuations in the flow of dispersed phase during droplet formation in a co-flow microfluidic device. Also, figure 2(d) displays the effect of vibration frequency on the generation of aqueous droplets in such a device [64]. It is observed that monodisperse droplets are generated with a natural frequency of 25 Hz without using mechanical vibration. At vibration frequencies lower than 25 Hz (10 Hz), droplet formation may be disrupted by the mechanical force, resulting in polydisperse droplets. However, at vibration frequencies above the natural frequency and lower than a critical frequency around 86 Hz (50 and 85 Hz), the generation frequency is synchronized with the vibration frequency, and monodisperse droplet formation is accelerated. Beyond the value of the critical frequency (200 Hz), varying vibration frequency has no considerable effect on the droplet formation process, but droplets are generated at a higher frequency compared with the natural frequency. Vibration amplitude can also affect droplet generation such that the large amplitudes may lead to a reduction of monodispersity and formation of satellite droplets [64]. Mechanical control methods significantly reduce the response time, especially using piezoelectric actuators [43]. On the other hand, integrating microfluidic devices with mechanical components leads to more complexity in microfluidic platforms.

2.2.4. Thermal method

A change in fluid temperature can result in changes in interfacial tension and fluid viscosity. For most fluids, the interfacial tension decreases by enhancing temperature, while the surfactant stabilized fluids behave oppositely [42]. The viscosity of liquids is also decreased as temperature rises. Therefore, the capillary number and viscosity ratio are affected by varying temperatures, and consequently, droplet size and generation rate are modified. Different mechanisms, such as heat exchangers, resistive heaters, and laser beams, can be used to locally heat the liquid interface during droplet formation [43]. Figure 1(g) demonstrates the schematic of integration of a flow-focusing device on a heat exchanger to propound the effect of thermocapillary and temperature-dependent viscosity in droplet generation. Figure 2(e) shows that the size of water droplets generated in mineral oil increases by almost two orders of magnitude as the upstream part of the flow-focusing device is heated from 5.7 °C to 60.6 °C [46]. The thermal control of the droplet generation process is remarkably based on the temperature dependency of the fluid properties

and the physical properties of additives such as surfactants and nanoparticles [65]. Moreover, thermal methods can incorporate in controlling droplet velocity and performing thermal cycles for on-chip gene amplification [46].

3. Emulsification and particle synthesis

Droplet microfluidics offers a facile and promising route for emulsification and particle fabrication processes. In this way, a precise amount of substance can be encapsulated within the particles in a controllable and desirable fashion. Compared to the conventional emulsification and encapsulation methods, droplet-based microfluidic devices consume fewer costly materials and can accurately control the size, structure, and combination of droplets with a high degree of monodispersity. Droplet templates constructed by the microfluidic devices can undergo an off- or on-chip solidification process to synthesize microparticles with different shapes. Moreover, inorganic nanoparticles can be synthesized using microfluidic droplet platforms. These precious features can be employed in a broad range of biomedical applications, especially for fabricating pharmaceutical products and conducting biological assays.

3.1. Emulsification

Emulsions are the mixture of two or more immiscible liquid phases in a way that an external (continuous) phase surrounds all the internal (dispersed) phases as minute droplets. The microfluidic emulsification devices are usually employed in dripping or jetting regimes [22, 66, 67]. Single emulsions can be formed by overcoming viscous shear forces over the surface tension between two liquid phases. W/O emulsions can be formed inside the hydrophobic channels, while the formation of O/W emulsions requires the hydrophilic channels [68]. Surfactants are conventionally used to prevent the coalescence of droplets. Moreover, emulsions can be stabilized by adding a specific amount of nanoparticles [39, 69]. These kinds of emulsions are known as Pickering emulsions. In the Pickering emulsions, nanoparticles act as a mechanical barrier at the liquid-liquid interface to prevent the coalescence of droplets [70, 71].

Double emulsions are nested droplets in droplets suspended in a continuous phase. These emulsions can be architected in the form of water-in-oil-in-water (W/O/W) [72] or oil-in-water-in-oil (O/W/O) [73] within a microfluidic device. Figure 3(a) displays the creation of monodisperse double emulsion droplets inside a microfluidic device [74]. The core–shell structure of double emulsions makes it possible to compartmentalize both polar and nonpolar substances and generate microcapsules by consolidating the shell layers. This hierarchy can be continued to construct triple, quadruple, or multiple emulsions. For example, figure 3(b) schematically depicts the formation of monodisperse quadruple emulsion droplets by a four-stage microfluidic device [17], while the generated droplets are displayed in figure 3(c). By compartmentalizing distinct smaller droplets inside a larger one, multi-component double emulsions can be constructed. Figure 3(d) shows how multi-component double emulsions are architected by a single-step emulsification device [67]. The number and size of inner droplets can be precisely regulated by adjusting the generation frequencies of inner and outer droplets as well as utilizing different droplet formation modes. In the dripping mode, the number of inner droplets is equal to the ratio of the generation frequencies of the inner droplets to that of the outer droplets (figure 3(e)). By employing the jetting regime for one of the inner phases, the larger inner droplets are generated compared to those fabricated by the dripping regime (figure 3(f)). Multicomponent multiple emulsions can also be developed by adding more emulsification processes. Figure 3(g) shows an example of a multicomponent triple emulsion, which is precisely engineered through a microfluidic capillary device [28].

Emulsions established by droplet-based microfluidics can be employed in several biological applications. In addition to the controlled compartmentalizing of desired substances, two other reasons lead to such a wide range of applications. First, functional shells can be precisely created via microfluidic capillary devices. Second, the trapped substances can be released through different programmed mechanisms. As an example, the quadruple emulsion droplets depicted in figure 3(c) provide a template to generate capsule-in-capsule structures. By loading chitosan in the aqueous phases and adding terephthalaldehyde (TA) in the oil phases, chitosan is crosslinked in the aqueous phases, and the capsule-in-capsule structures are formed. The optimum combination of each phase is designated by adjusting the viscosity and density of the phases. In this way, the stable capsule-in-capsule structure with an average size of 419 μm and CV $<$ 4% is attained for both the inner and outer capsules. TA-crosslinked chitosan can be degraded in a low pH environment. Therefore, by adding a buffer solution with pH 2.5, the sequential release of outer and inner oil cores is carried out. In addition to acidic-triggered release profiles, thermal release methods can also be exerted on the shells. Wax is a preferable material that can be used to thermally release ingredients. In figure 3(e), wax is used as the middle phase. In this situation, the inner droplets are prevented from cross-contamination and coalescence without using any surfactant. Furthermore, the coalescence of inner droplets was carried out by increasing the temperature to the wax melting point. The combination of temperature- and acid-triggered release methods is also feasible. In figure 3(h), poly(N-isopropylacrylamide) (PNIPAM) and TA-crosslinked chitosan are used respectively in

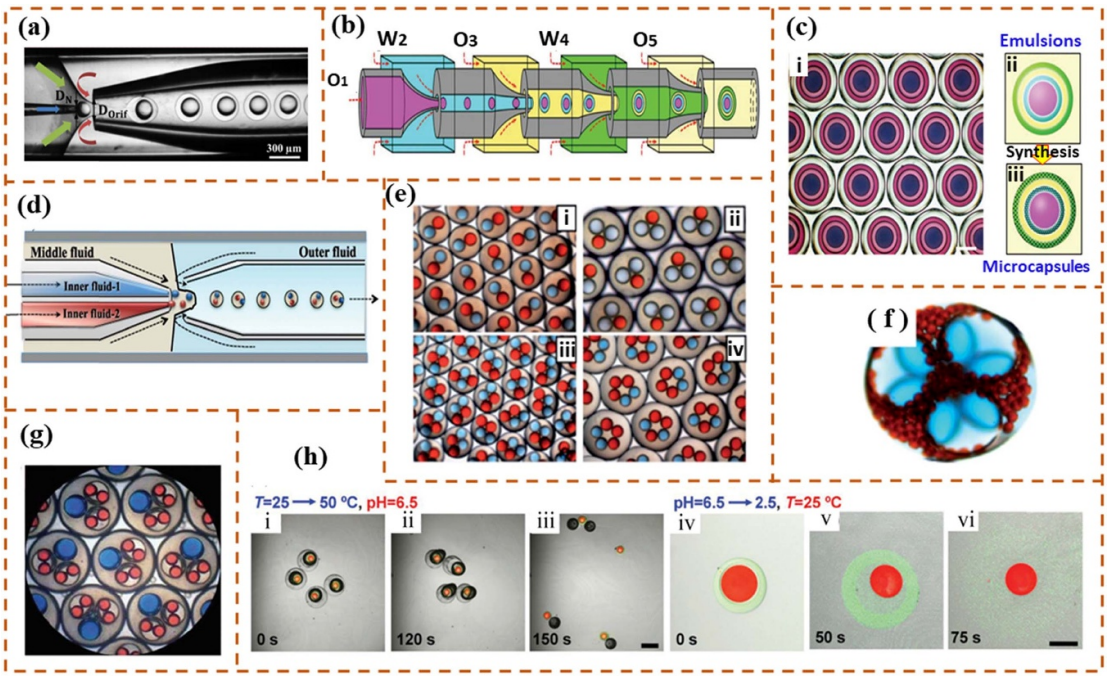

Figure 3. Formation of monodisperse (a) double and (b) quadruple double emulsions. (c) (i) Quadruple emulsion droplets generated by the microfluidic device in (b). (ii), (iii) Synthesizing capsule-in-capsule structures by crosslinking chitosan in the aqueous phases. (d) Schematic of generating multi-component double emulsion droplets via a microfluidic capillary device. (e) Different structures of multi-component emulsions created by tuning the generation frequencies of the inner phases in the dripping regimes. (f) A multi-component double emulsion droplet with two different sizes of inner droplets. The large blue and small red droplets are respectively generated in jetting and dripping regimes. (g) A multicomponent triple emulsion droplet. (h) (i)–(iii) The sequence of thermal-triggered release and (iv)–(vi) acid-triggered release of capsule-in-capsule structures. Scale bares are 400 μm in (iii), and 100 μm in (vi). (a) Reprinted from [74], Copyright (2015), with permission from Elsevier. (b), (c), (h) [17] John Wiley & Sons. (d)–(f) Reproduced from [67] with permission of The Royal Society of Chemistry. (g) Reproduced from [28] with permission of The Royal Society of Chemistry.

outer and inner shells. As the temperature increased beyond the volume phase transition temperature of PNIPAM, the PNIPAM shell shrinks and raptures due to high inner pressure. Then, the inner shell is decomposed in an acidic environment. Therefore, the sequential and independent release of substances can be achieved by consecutive temperature-triggered (in the outer shell) and acid-triggered (in the inner shell) release methods.

3.2. Particle synthesis

Emulsion templates can be served to fabricate functional micro- and nanoparticles with various biological applications. From an architectural point-of-view, these particles can be categorized in different shapes. Figure 4 summarizes the most practical particle shapes applicable in biomedicine. The simple particles are spherically built up in micro and nanoscales through droplet microfluidics. Core–shell and Janus particles are made up of two distinct regions that exhibit different properties in terms of polarity, solubility, degradability, etc. The core–shell particles are commonly used to synthesize microcapsules and vesicles, while both core–shell and Janus particles are appealing structures for drug and gene delivery systems [11, 75]. Using the core–shell particles, the components in distinct layers can symmetrically release in a programmed manner. However, the Janus particles result in an asymmetric release of the components. All the mentioned particles can be formed with non-spherical configurations, as depicted in figure 4.

Compared with conventional batch methods, microfluidics offers several advantages for generating monodisperse engineered particles [76, 77]. Using this technique, the reagent consumption and all physical and chemical phenomena are precisely controlled inside individual microreactors. Thereby, functional particles with the desired size and shape can be easily constructed. From the compositional point-of-view, the particles can be grouped into polymeric and non-polymeric (inorganic) particles. The former group has been commonly used in pharmaceutical applications [78, 79], while the latter group has a wide range of applications in bio-sensing [80], bio-imaging [81], and cell labeling [82]. Besides, the particles with a combination of polymeric and non-polymeric components can be formed using droplet microfluidic devices [83, 84].

Polymeric particles are commonly made up of poly(lactic acid) (PLA), polycaprolactone (PCL), poly(lactic-co-glycolic acid) (PLGA), and poly(vinyl alcohol) (PVA), as well as polysaccharides, including chitosan, alginate, and pectin, which are appealing

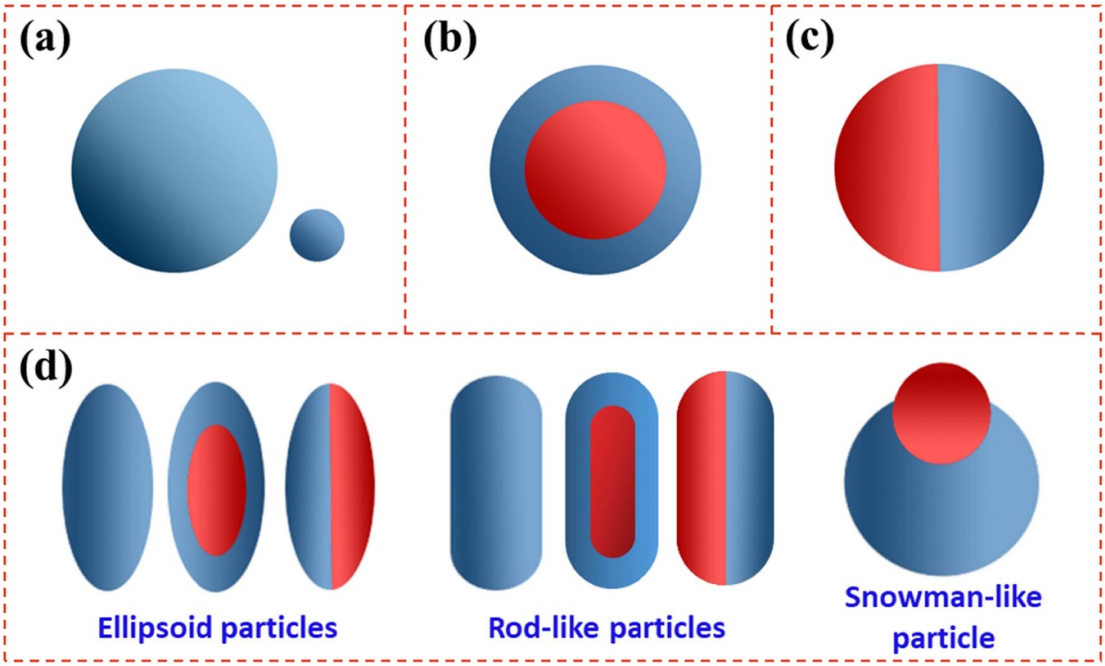

Figure 4. Most applicable particles in biomedicine. (a) Simple micro- and nanoparticles, (b) core–shell particle, (c) Janus particle, and (d) non-spherical particles, including ellipsoid, rod-like, and snowman-like particles.

materials for preparing functional microparticles owing to their biodegradability, biocompatibility, and high solubility [11]. Droplet microfluidics can also be used for consolidating the polymeric structures. Consolidation commonly occurs through polymerization, crosslinking, or evaporation processes. These processes can be controlled in microreactors provided by droplet microfluidics. Hence, in addition to the size and shape, particle solidity can be accurately adjusted. This issue is more significant for particles with complex structures. On the other hand, inorganic particles such as gold (Au), silver, and magnetite nanoparticles can be efficiently synthesized by droplet microfluidic devices. Gold nanoparticles (AuNPs) are broadly used in many biomedical applications from cancer therapy [85] to diagnostic devices such as rapid lateral flow strips [86]. Conventionally, AuNPs are produced by the reduction of gold salt precursor in the presence of a stabilizing reagent. The batch methods usually suffer from inhomogeneous mixing, which leads to polydisperse particle size distribution and large batch-to-batch variations. Lazarus *et al* [87] revealed the capabilities of droplet microfluidics to synthesize monodisperse and controlled-sized AuNPs. They injected gold precursor as well as reducing and stabilizing reagents in parallel inside a flow-focusing device and allowed the interdiffusion of three laminar streams. They observed when the oil focusing flow rate increases, the middle flow turns into droplets, and more monodisperse and smaller AuNPs are formed, compared with the case of low oil flow rates that drops are not formed. Particle synthesis inside droplets enhances the mixing and consequently accelerates the chemical reactions. Since the reagents are protected inside the droplet microreactors, the device fouling issues is less significant in the droplet microfluidic devices compared with the other devices. Furthermore, silanization and pH adjustment techniques can be employed to minimize the adsorption of nanoparticles by the channel walls [87, 88]. Bandulasena *et al* [88] employed a droplet-based microfluidic device to synthesize different-sized AuNPs. As shown in figure 5(a), 1 mM tetrachloroauric acid ($HAuCl_4$) stream comprising 1% (w/v) polyvinylpyrrolidone (PVP), as the gold precursor, and 20 mM L-ascorbic acid solution, as reducing reagent, are injected through the co-flow capillary tubes. The counter flow of oil Miglyol 840 turns the central flow into monodisperse droplets that facilitates the mixing of gold precursor and the reducing reagent. The effect of different flow rate ratios and geometrical parameters on the size and polydispersity of synthesized NPs were investigated. Characterization of particles was performed through dynamic light scattering, transmission electron microscopy (TEM), and ultraviolet–visible (UV–Vis) spectroscopy. To study the effect of continuous phase flow rate on characteristics of NPs, gold precursor and reductant flow rates were set to 2 ml h^{-1} and 12 ml h^{-1}, respectively, and the oil flow rate was varied from 30 to 60 ml h^{-1}. As depicted in figure 5(a), the size of droplets and NPs are decreased by increasing the carrier oil flow rate. Nevertheless, the polydispersity index of NPs enhances by increasing the continuous phase flow rate. It was inferred that generating smaller droplets enhances reagent mixing,

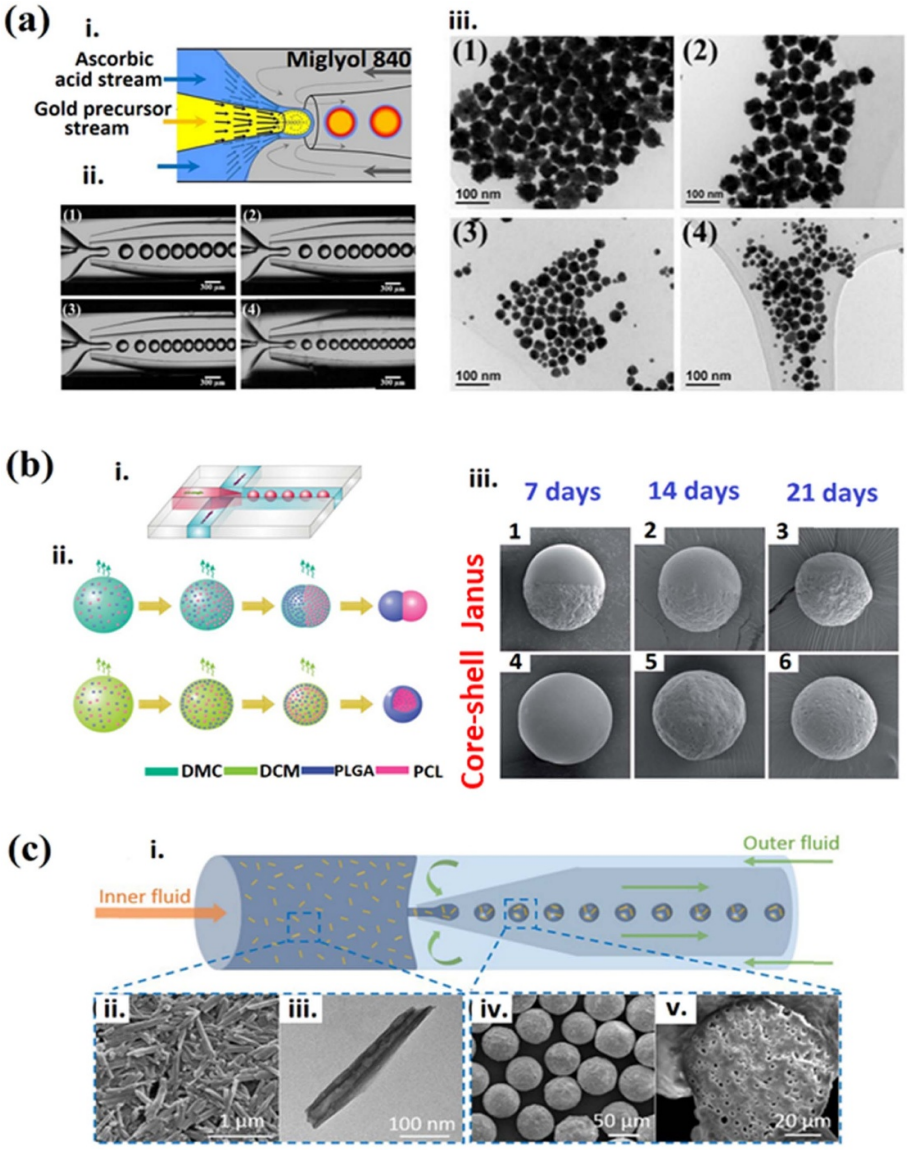

Figure 5. (a) Microfluidic synthesis of gold nanoparticles. (i) Schematic of the droplet-based microfluidic device. (ii) Different-sized droplets generated at 30 ml h^{-1} (1), 40 ml h^{-1} (2), 50 ml h^{-1} (3), and 60 ml h^{-1} (4) flow rates of the continuous phase. (iii) Representative TEM images of synthesized AuNPs with the sizes of 276 nm (1), 365 nm (2), 257 nm (3), and 240 nm (4) corresponding to the mentioned flow rates. (b) Fabrication of core–shell and Janus particles. (i) Flow-focusing microfluidic device. (ii) Schematic illustration of PLGA/PCL particle synthesis in the form of Janus and core–shell particles using different solvents in the dispersed phase. DMC: dimethyl carbonate; DCM: dichloromethane. (iii) Comparing *in vitro* degradation of Janus (1–3) and core–shell (4–6) PLGA/PCL particles within 21 d. The smooth and rough parts display PLGA and PCL parts, respectively. (c) Fabrication of HPMCAS microparticles containing HTNs. (i) Microfluidic device, (ii) a representative SEM image of surface morphology of HNTs, (iii) a representative TEM image of the nanotubular structure of HNTs, (iv) monodisperse HNT-loaded HPMCAS particles, and (v) a representative SEM of the cross-section of an HNT at HPMCAS particle. (a) Reprinted from [88], Copyright (2019), with permission from Elsevier. (b) Reproduced from [90] with permission of The Royal Society of Chemistry. (c) Reprinted from [91], Copyright (2017), with permission from Elsevier.

so that particle nucleation dominates over particle growth. Thus, smaller and more polydisperse NPs are synthesized within the smaller droplets.

Core–shell and Janus particles are synthesized through a roughly similar procedure using droplet-based microfluidic devices. Double emulsion templates are commonly employed to synthesize core–shell particles. On the other hand, Janus droplets are formed using single emulsions so that two immiscible fluids are injected in parallel inside an individual channel and then sheared by a continuous fluid flow [89]. Nevertheless, both core–shell and Janus particles can be synthesized using single emulsion templates through the phase separation mechanism. Li *et al* [90] implemented a controlled phase separation mechanism on O/W single emulsions and fabricated both core–shell and Janus PLGA/PCL particles, as shown in figure 5(b). PLGA and PCL are respectively hydrophilic and hydrophobic polymers. Thus, such particles can be a favorable template for loading both hydrophilic and hydrophobic substances in a single particle. To synthesize Janus

particles, an aqueous solution having 2 wt% PVA is employed as the continuous phase, and the dispersed phase is prepared by dissolving PCL and PLGA (7:3 or 1:1 w/w) in dimethyl carbonate with a total concentration of 40 mg ml^{-1}. The flow rates of dispersed and continuous phases are designated as 0.16 and 0.4 ml h^{-1}, respectively. Finally, the Janus particles are collected in a bath containing a 2 wt% aqueous solution of PVA at room temperature, and solidification occurred by solvent evaporation. The core–shell particles with PCL core and PLGA shell are fabricated following a similar protocol. The exceptions are that dichloromethane is used as the solvent (instead of dimethyl carbonate), and the dispersed and continuous phase flow rates are adjusted as 0.45 and 0.25 ml h^{-1}, respectively. For the identical weight ratio of PLGA/PCL, the average sizes of Janus and core–shell particles are 28.42 and 47.00 μm, respectively. Besides, the CV values of 4.25% for the Janus and 2.74% for the core–shell particles represent excellent degrees of monodispersity. To figure out the particle characteristics, attenuated total reflection Fourier transform infrared spectroscopy (ATR-FTIR) and acetone treatment were performed. The sequential degradation of PLGA/PCL Janus and core–shell particles inside phosphate-buffered saline (PBS) is also shown in figure 5(b). As demonstrated in figure 5(b), after 14 d of incubation inside the PBS bath, the PLGA part (smooth part) of the Janus particle is more degraded compared with the PCL part. Besides, the PLGA shell in core–shell particle is degraded, such that ATR-FTIR detected both PLGA and PCL on the surface of the particles. After 21 d, the Janus particle mostly loses its PLGA part, and the core–shell particle turns into a PCL microsphere. This different degradation behavior can be advantageous for programmed DDS.

Recently, the fabrication of microparticles loaded with nanoparticles has been enabled via droplet-based microfluidic devices. This class of particles is appealing for developing oral DDS. Some nanoparticles, such as halloysite nanotubes (HNTs) [91] and porous silicon (Psi) [92], have high drug loading capacity. By encapsulating the drug-loaded nanoparticles into the polymeric microparticles, it is possible to subsequently release different physiochemical drugs in a single formulation. Li *et al* [91] presented a flow-focusing O/W microfluidic platform to encapsulate HNTs in hydroxypropyl methylcellulose acetate succinate (HPMCAS) polymer (figure 5(c)). The inner dispersed phase is the 20 mg ml^{-1} solution of HPMCAS in ethyl acetate (EA) containing HNTs at a concentration of 4 mg ml^{-1}, and the outer continuous phase is 2% w/v Poloxamer 407 aqueous solution. Figure 5(c) depicts HNTs embedded in monodisperse HPMCAS microparticles with an average size of 70 μm. Drugs with different physiological properties can be loaded respectively in HPMCAS and HNTs, and the programmed release can be performed by pH stimulation.

Particles with non-spherical architectures are also fabricated by droplet-based microfluidic devices. The special shape of particles is usually the result of the external stresses exerted on emulsions during the droplet generation process or the difference in interfacial tensions or chemical properties of the adjacent phases. Ellipsoid [93], rod-like [93, 94], and snowman [95] shaped particles are some prevalent non-spherical particles that are fabricated by droplet-based microfluidic devices.

4. Applications of droplets in biomedicine

4.1. Biomolecular analysis

Biomolecules are chemical compounds produced by living organisms. They are vital for many endogenous and exogenous processes in cells. Therefore, understanding their structure and function has been the subject of numerous studies over the years [96, 97]. In the following sections, deoxyribonucleic acid (DNA), ribonucleic acid (RNA), enzymes, and proteins are described as four important biomolecules, and the droplet-based microfluidic platforms used for analyzing these biomolecules are presented.

4.1.1. DNA and genomics

Droplet-based microfluidic systems has attracted increasing attention in studying single-cell genomics, which plays a significant role in the understanding of individual cell function in both normal development and disease [98]. DNA is one of the two main classes of nucleic acids that carry the genetic instructions for building a life form. Hence, the characterization of DNA is of interest in many fields, such as clinical diagnostics and pharmaceutical research. PCR was first performed in a droplet-based microfluidic platform by Beer *et al* [99]. Since then, droplet-based microfluidic devices have been employed for DNA extraction [100] and sequencing [101]. Zubaite *et al* used a droplet-based microfluidic system for isolation, amplification, and condensation of single-DNA molecules in 3 pL volume droplets and converted into ∼1300 nm-sized DNA-magnesium-inorganic pyrophosphate particles [102]. The droplets were generated by a simple T-junction device, and the condensed DNA particles were purified using centrifugation with a recovery rate of ∼60%–90%. An *in vitro* transcription-translation reaction was then performed with re-encapsulated purified particles as the template and expression of the β-galactosidase enzyme was successfully obtained. Large quantity of functional gene copies ($\sim 10^5$ copies per particle) can be provided and a variety of enzymes or proteins can be synthesized using droplet microfluidics, making it adaptable to many *in vitro* assays. In droplet PCR platforms, adding a piezoelectric diaphragm micropump to the T-junction channel, for

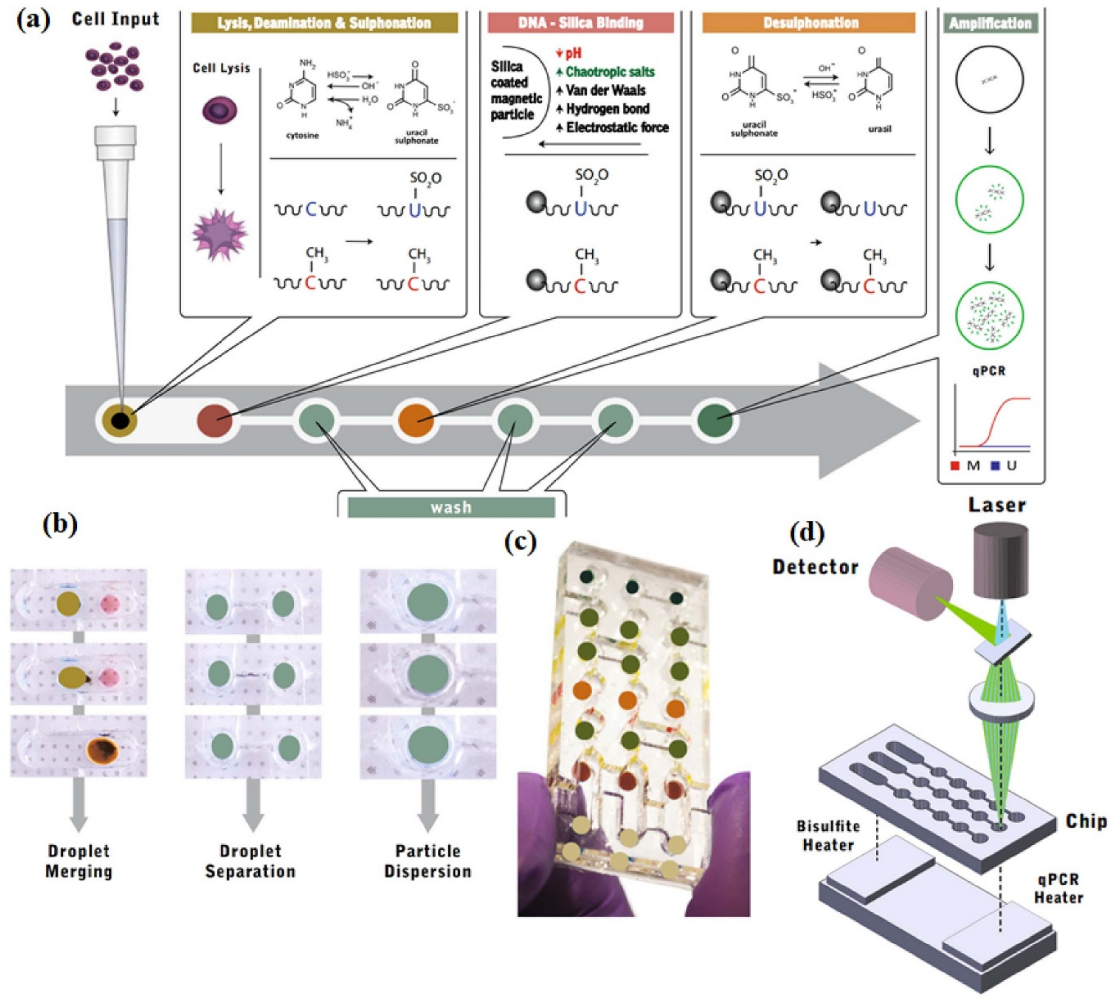

Figure 6. Droplet magnetofluidic chips for quantitative MSP was developed by Stark *et al.* (a) Human cell suspension was loaded to the 1st chamber from the left along with droplets containing magnetic particles and bisulfite conversion reagent. Bisulfite conversion and cell lysis were achieved through droplet merging. In the 2nd chamber, the resulting droplets were merged with secondary droplets containing reagents for binding DNA to magnetic particles. In the next well, DNA-containing beads were washed by a buffer and transferred to the 5th chamber for desulphonation. After two more washing steps, the beads entered the 7th chamber for MSP. (b) Three operations were distinguished within the platform: droplet merging in which the entire droplet was moved and merged due to DNA bounding onto magnetic particles, droplet separation in which DNA was transported across different droplets, and particle dispersion in which the particles plug was released upon removal of the magnetic field. (c) Three identical and parallel lanes of the fabricated microfluidic device. Droplets were mixed with food dye for better visualization. (d) A thermal control unit with two heating blocks was placed below the chip lysis and bisulfite conversion in the 1st chamber and PCR thermal cycling in the last chamber. A fluorometer with laser and detector on top of the chip provided real-time signal detection during PCR. Reprinted by permission from Springer Nature Customer Service Centre GmbH: Springer Nature, Biomedical microdevices [104] A sample-to-answer droplet magnetofluidic assay platform for quantitative methylation-specific PCR, A Stark, D J Shin, T-H Wang, (c) 2018.

the evacuation of air from the outlet reservoir, can enhance the production of W/O emulsion droplets to the rate of ~1000 droplets per second [103]. Although this approach leads to low material cost due to the small sample dead volume, the throughput of the microfluidic chip would need improvement. A fully integrated droplet magnetofluidic assay platform was introduced by Stark *et al* [104] for DNA extraction, quantitative PCR of biological samples, and bisulfite conversion. Instead of following a 13 steps methylation-on-beads (MOB) protocol for benchtop methylation-specific PCR (MSP) assay, a seven-step streamlined MOB protocol was developed which reduced the total handling time from 4.5 to 7 h. Details of the magnetofluidic system are depicted in figure 6. Considering the importance of single-stranded DNA (ssDNA) as a molecular recognition element, a droplet-based microfluidic chip can be implemented in conjugation with microsphere-PCR to amplify ssDNA and reduce contaminations of double-stranded DNA [105]. Using this platform, the droplets can be formed with the aid of a flow-focusing geometry using an orifice-diffuser structure with a rate of 30 microspheres per second, then moved to a serpentine mixing channel followed by a polymerization channel for microsphere solidification, and finally subjected to PCR. Pathogens such as *Escherichia coli* (*E. coli*) O157 and *Listeria monocytogenes* [106] can also be detected by taking advantage of droplet PCR platforms. To characterize the genetic

variety within cancer cell populations, Pellegrino *et al* designed a microfluidic device for high-throughput single-cell DNA sequencing of acute myeloid leukemia tumors [107]. Their workflow was comprised of two steps: first, the cell suspension and lysis buffer, including protease were injected into the device, formed droplets, and incubated to encourage proteolysis. Then, the droplets containing genomes of individual cells were combined with droplets containing molecular barcode-carrying hydrogel beads and PCR reagents. The above method could produce sequence-ready libraries in less than 2 d cost-effectively due to the use of picoliter volume droplets and was able to detect cells harboring pathogenic mutations as few as 3 out of about 4000 genotyped cells.

4.1.2. RNA and transcription

RNA is the other main class of nucleic acids that carries out the genetic instructions encoded in DNA and converts them into proteins. A particular segment of DNA is copied into a messenger RNA (mRNA) via transcription and then decoded to produce a specific amino acid chain via translation. Therefore, performing the process in a reverse manner provides a significant genetic database. Besides, RNA released from a cellular material can be extracted and reverse transcribed into complementary DNA (cDNA), followed by a PCR process to amplify regions of interest. This procedure is called reverse transcription PCR (RT-PCR) and has the advantage of reverting single-stranded unstable RNA to cDNA, which is easy to work with [108]. As it is mentioned in previous sections, the first droplet-based RT-PCR was introduced by Beer *et al* [109]. Thereafter, significant progress has been made in the field of pathogens detection whose genomes are composed of RNA such as influenza viruses [110, 111], retroviruses (e.g. human immunodeficiency virus (HIV)) [112, 113], and flaviviruses (e.g. hepatitis C virus (HCV)) [114]. Single-copy RT-PCR in a droplet-based microfluidic device was first presented by Zhang *et al* [115], where a single RNA molecule or cell was encapsulated within agarose droplets. Their chip had four inlets: one for an aqueous solution of cell lysis and RT-PCR chemicals in 2% agarose solution, one for aqueous solution of cells or RNA in 2% agarose solution, and the remaining two for oil injection. In the case of 0.1/1.8 ml h^{-1} (agarose/oil) flow rate, the sizes of the produced droplets were 48 $\pm$ 5 μm. Using agarose in droplet formation was beneficial for long-term downstream processing; agarose droplets were cooled to form agarose beads after performing RT-PCR to avoid diffusion of RT-PCR products in neighboring droplets. However, the agarose is incompatible with using TaqMan probes. In droplet-based microfluidic devices, conducting single-cell RT-PCR assays are challenging; cells must be lysed to release RNA, while lysis reagents and lysate can prevent identification of the target sequences in RT-PCR reaction. As a result, cell lysis and RT-PCR reagent addition are often carried out in separate microfluidic devices with labor-intensive process of collecting droplets from one device and injecting them to another. To address the aforementioned issues, Eastburn *et al* [116] proposed a droplet-based microfluidic device that integrated cell lysis and reagent addition in a single chip and could perform ~5000 single-cell TaqMan RT-PCR reactions in a single experiment. 40 μm-droplets were produced by regulating the flow rates of cell suspension, lysis buffer, and focusing oil. This ultrahigh-throughput platform could always identify a unique cell type among a heterogeneous cell sample due to the droplet compartmentalization, which offered the possibility of simultaneous use of TaqMan probes and cell-viability dyes. In another study, to make the integrated single-cell droplet RT-PCR chip in a more efficient manner, Kim *et al* [117] used alkaline lysis, in which isolated single cells were exposed to a buffer with high pH that could be rapidly neutralized by RT-PCR buffer. The above chemical strategy enhanced the throughput from 168 droplets per second in two-step workflows to 411 droplets per second in the integrated one, decreased the consumption of RT-PCR reagent at a 10% cell loading ratio for 100 000 cells from 660 μl to 270 μl and reduced the preparation time of 47 078 single-cell RT-PCR droplets from 120 min to 19 min. The detailed schematic of this microfluidic platform can be seen in figure 7.

In addition to RT-PCR, reverse transcription loop-mediated isothermal amplification (RT-LAMP) has been applied, in which the target sequence is amplified at a constant temperature in contrast to temperature cycling in RT-PCR [118]. In one study, Azizi *et al* [119] combined droplet-based microfluidics and LAMP to design a sensitive biosensor for *Salmonella typhimurium* detection. To examine the detection limit of the *Salmonella typhimurium* in the latter device, droplets with diameters of 20 μm and 40 μm were generated via a T-junction device, and eight LAMP reaction cocktails were prepared using the extracted RNA, including a negative control and seven positive samples with different dilution factors. By implementing a mathematical model, it was shown that in a pure culture condition, the detection limits were at an approximate dilution factor of $10^5\times$ and $10^7\times$ for 20 μm and 40 μm droplets, respectively. The detection limit was two orders of magnitude lower in the contaminated milk sample. However, it was noted that in the case of larger droplets, a longer incubation time, or a more precise method was required to distinguish positive and negative droplets. Another way of cDNA amplification in reverse transcription is RNA sequencing (RNA-seq).

While RT-PCR can only identify known transcripts, RNA-seq can detect both known and sequences with a low amount of RNA and high productivity. However, this broader range of information often needs bioinformatics for analysis, increasing

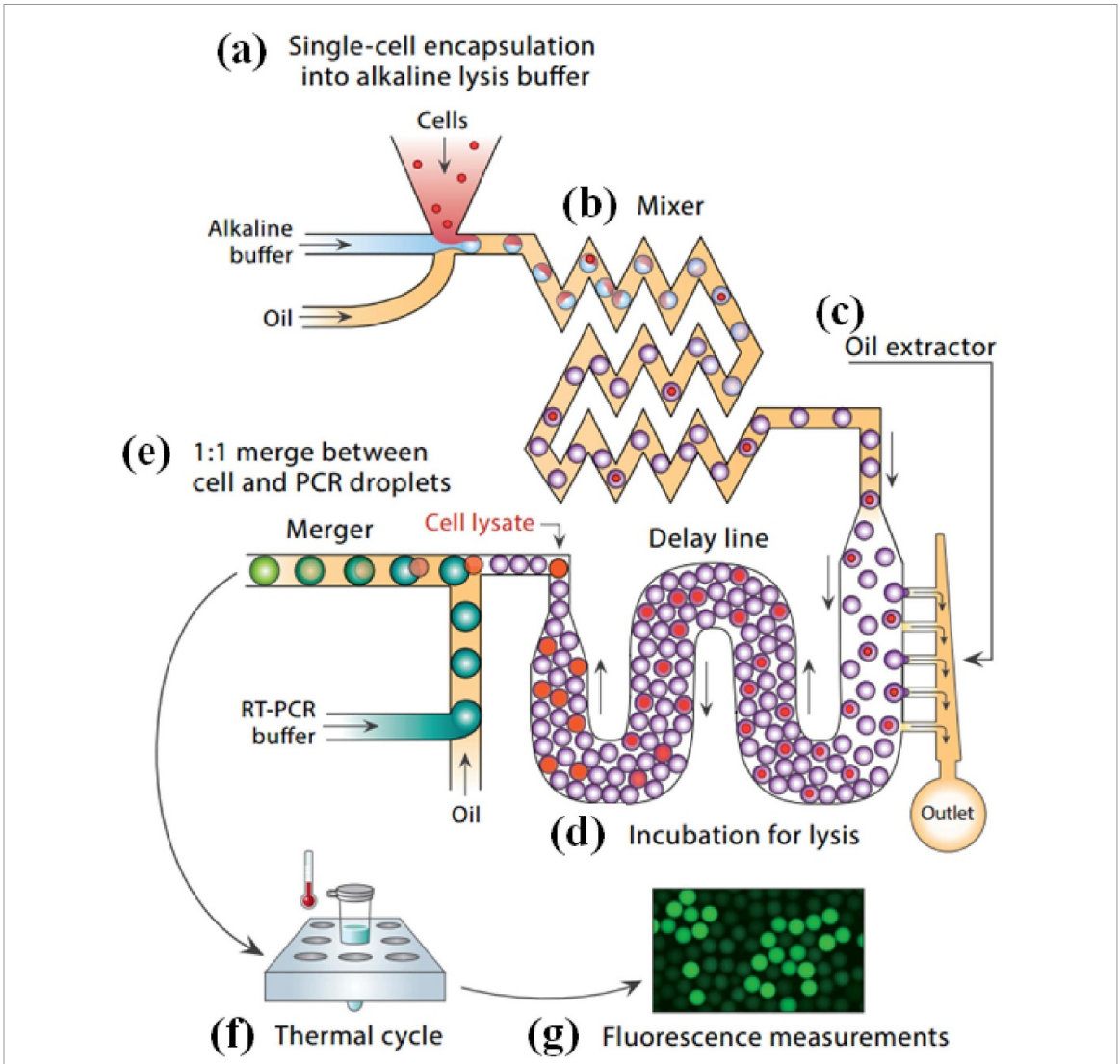

Figure 7. Schematic representation of the integrated droplet-based microfluidic device presented by Kim *et al* for performing single-cell RT-PCR using chemical lysis. Single cells were encapsulated with the alkaline buffer in a modified T-junction (a) and moved towards a serpentine microchannel for homogenous mixing of the droplet contents (b). Then the excess oil was removed to pack the droplets together (c) as they entered the delay line for incubation (d). By the end of the delay line, cell lysis was completed, and lysis droplets were merged with RT-PCR droplets generated by a parallel T-junction (e). The pairing occurred via electrocoalescence, and the lysis buffer was instantly neutralized by RT-PCR buffer. The resulting droplets were collected and amplified by RT-PCR procedure (f) and TaqMan-positive droplets were achieved (g). Reprinted with permission from [117]. Copyright (2018) American Chemical Society.

the cost of the process [120]. RNA-seq has also been conjugated with droplet-based microfluidics due to their efficient droplet generation for low input RNA samples. Mouse embryonic stem cells before and after removal of leukemia inhibitory factor and their differentiating cells were profiled in a droplet-based RNA-seq microfluidic device called inDrop [121]. In this study, to ensure that the primers required for encoding every barcode were present in each droplet, a library of barcoded hydrogel microspheres (BHMs) was produced and then co-encapsulated with cells. In a similar approach named Drop-seq, individual mouse retinal cells and barcoded primer beads were encapsulated within nanoliter-sized droplets along with lysis buffer [122]. Droplets were formed by a droplet-based microfluidic chip capable of producing more than 100 000 droplets per minute. Single-cell transcriptomes attached to microparticles were then subjected to RNA-seq. The Drop-seq method was able to identify 39 distinct populations from 44 808 cell profiles. Perturb-seq is the name of another platform that combined droplet-based single-cell RNA-seq with barcoding clustered regularly interspaced short palindromic repeats-mediated perturbations in companion with an analytical pipeline to decompose massive generated datasets [123]. High amplification of RNA was achieved via applying a new method called easier-seq (emulsion-based amplification of sequence-independent uniformly transcribed RNA sequencing), followed by droplet generation in a microfluidic device [124]. Sequencing could be performed on RNAs with or without polyadenylate tails using random N_6 hexamers as the reverse transcription primers. The cDNA product

was then encapsulated within 1.5 × 10^5 65 pL droplets in microfluidic channels and exposed to isothermal amplification. Coupling multiplexed droplet single-cell RNA sequencing (dscRNA-seq) with a computational algorithm, demuxlet assisted in the investigation of gene expression in eight pools of peripheral blood mononuclear cells (PBMCs) from lupus patients [125]. With the aid of demuxlet, droplets containing a single cell and two cells, singlets, and doublets respectively, were distinguished. Thus, the cost of per-cell and per-sample library preparation was reduced. The strategy of multiplexed profiling and demultiplexing of transcriptomes by demuxlet was proven to be robust and unbiased.

4.1.3. Protein analysis

Proteins are bridges between genetic information and cellular biological functions. Copying genetic sequences of DNA into RNA is followed by translation, in which chains of amino acids are generated. Amino acids are building blocks of proteins; 20 different chains of amino acids must be combined in a specific sequence to produce a unique type of protein. Characterization of proteins and their function at the single-cell level were exploited by droplet-based microfluidic platform due to their improved reliability and scalability in comparison to conventional techniques [126]. Protein crystallization has been in the spotlight of research as understanding protein structures can shed light on their regulatory patterns. When Protein Data Bank was founded in 1971, it contained only seven protein structures [127] which increased to more than 151 000 structures in 2020 due to the growing attention. Protein crystallization includes two steps: nucleation in which a stable nucleus is formed by aggregation of protein molecules in a solution and growth where more molecules attach to the nucleus, and the crystal becomes bigger [128]. Protein crystallization requires a complimentary analysis such as x-ray diffraction to obtain protein structure. Hence, to achieve high-resolution data, the process must be controlled to prevent the aggregation of protein crystals [129]. To address this problem, droplet-based microfluidic devices have come to aid to produce engineered droplets for encapsulating a specific number of proteins [130, 131]. Screening of protein crystallization in nanoliter volume droplets was first implemented by Zheng *et al* [132], where thousands of protein crystallization conditions were achieved by controlling the flow rates of the solution. Small-angle x-ray scattering (SAXS) is another screening technique that has been coupled with droplet-based microfluidic devices for protein crystallization [133]. In the study, proteins were encapsulated in aqueous droplets with buffer and crystallization agents. The resulting droplets were then passed through the x-ray beam to record SAXS data. The structural stability of proteins in droplets was tested in rasburicase, which demonstrated no radiation damage. Likewise, the effect of protein saturation on weak interaction variations was investigated on lysozyme. Both experiments showed good agreement with previously reported data, making the latter platform a powerful tool in the field of protein crystallization. Lysozyme was also used as a model protein for a parametric study of the crystallization mechanism within droplets conducted by Ferreira *et al* [134]. They performed a hydrodynamic study on the formation of droplets and the effect of their volume on the phase behavior of lysozyme with numerical and experimental approaches. Using the designed microfluidic device, they could generate the droplets with volumes of 0.9–18 μl at the frequency of up to 250 droplets per assay. Lysozyme crystals formed in these droplets are demonstrated in figure 8. Protein and protein-ligand crystallization were explored in a versatile microfluidic platform with droplet factory, droplet characterization, and droplet incubation and observation compartments [135, 136]. In the droplet factory, droplets as small as 2–10 nl were generated. The size, frequency, and composition of the droplets were determined by spectrophotometry in the droplet characterization unit, and a thermostat and an *XYZ*-motorized camera were placed within the incubation and observation part. Instead of microfabrication techniques, they applied commercial microfluidic tubing and junctions to create the desired geometry and chose lysozyme and human quinone reductase 2 (QR2) for protein and protein-ligand experiments, respectively. These three independent units along with the easily constructed geometry of droplet generator provided precise control over the crystallization process. As an alternative to conventional polydimethylsiloxane (PDMS)-based microfluidic devices, Selzer *et al* [137] developed a polycarbonate-based microfluidic chip designed for generation of droplets used in crystallization. Using polycarbonate not only made the fabrication process simpler and more flexible to chip geometry, but also provided a platform for droplet generation requiring hydrophobic or hydrophilic surface properties.

In addition to protein crystallization, droplet-based microfluidic platforms have been employed to detect cell membrane proteins [138, 139], investigate protein–protein interactions [140–142], and perform single-cell proteomic analysis [143, 144].

4.1.4. Directed evolution of enzymes

Enzymes are biological catalysts that accelerate chemical reactions within cells. Malfunction or deficiency of a single enzyme can lead to disease [145]. Most enzymes are proteins except ribozymes, which are catalytic RNA molecules. In the present review, enzymes are surveyed in a separate section due to their significant roles in many biological processes. The directed evolution of enzymes is a topic of interest that has been coupled with droplet-based microfluidic devices [146]. The principle of

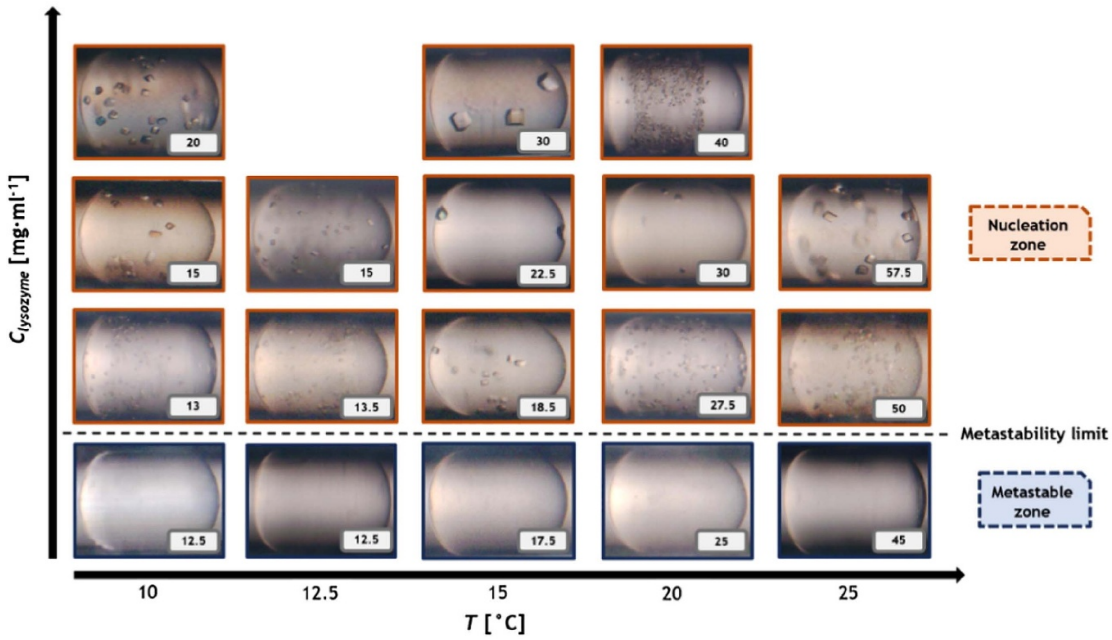

Figure 8. Formation of lysozyme crystals at sodium chloride 3% (w/v) and pH 4.7 within droplets generated by the microfluidic device introduced by Ferreira *et al*. Below the metastability limit, clear droplets were obtained with no nucleation and growth of crystals because the critical supersaturation state was not achieved. Above the metastability limit, lysozyme crystals were formed, and their number and size depended on initial lysozyme temperature and concentration. The numbers indicated in each picture are lysozyme concentrations in mg ml^{-1}. Reprinted from [134], Copyright (2018), with permission from Elsevier.

directed evolution is to choose an enzyme with similar properties to the desired ones and introduce random mutations into its encoding gene. The library of mutations is then cloned into bacteria to produce randomly mutated enzymes. The resulting enzymes were tested, and the best ones were selected and subjected to further rounds of evolution. After a few generations, new variants of enzymes are achieved [147]. In this method, it is important to recover the DNA sequences of the selected enzymes. A droplet-based study enables the simultaneous screening of enzymatic activity and its genetic source. Fluorescence-activated droplet sorting (FADS) is the most commonly used screening technique in the droplet-based directed evolution of enzymes such as arylsulfatase [148], CotA laccase [149], novel lipolytic enzyme EstT1 [150], and retro-aldolase RA95 [151] all via *E. coli* cells. Since just one type of substrate was used in the aforementioned platforms, the capability of FADS was limited to screen only simple enzymatic properties. Ma *et al* [152] employed a dual-channel microfluidic droplet screening device (DMDS) to improve the monitoring efficiency to more than 10^8 droplets with up to $\sim 10^7$ enzyme variants per day. The basis of their screening approach was FADS, but enzymatic activities could be simultaneously evaluated on two substrates. Hence, more complex enzymatic properties such as enantiospecificity, regiospecificity, and chemospecificity were screened via this device. The details of this droplet-based microfluidic platform are depicted in figure 9. Screening methods are not limited to FADS. Gielen *et al* [153] developed an efficient microfluidic absorbance-activated droplet sorter (AADS) for directed enzyme evolution with sorting rates of around 300 droplets per second. This AADS module was based on two optical fibers placed face to face across the droplet microchannel that could sense the concentration of dye within each passing droplet and record the decrease in transmittance. Another challenge in directed enzyme evolution is that by using *E. coli* as host, lysis must be carried out within the droplets to reach enzymatic activity. Using yeast cells simplifies the process by deleting the lysis step [154]. In this regard, Beneyton *et al* [155] took advantage of the yeast *Yarrowia Lipolytica* in their droplet-based chip. Five fungal genes encoding hydrolytic enzymes were successfully secreted and overexpressed in an active form.

4.2. Cell biology

Encapsulation and compartmentalization of cells in droplets simplify manipulation and screening in cell-based assays. Each droplet plays the role of microenvironment for the cells; hence intracellular and extracellular responses to a controlled stimulus can easily be detected [156]. As microfluidic devices have shown their capability in generating droplets with tunable properties, they have been used to expand current knowledge in the field of cell biology [157]. Cell biology research in droplet-based microfluidic chips covers single-cell analysis [158, 159] and organ-in-a-droplet [160]. Artificial cell generation is another

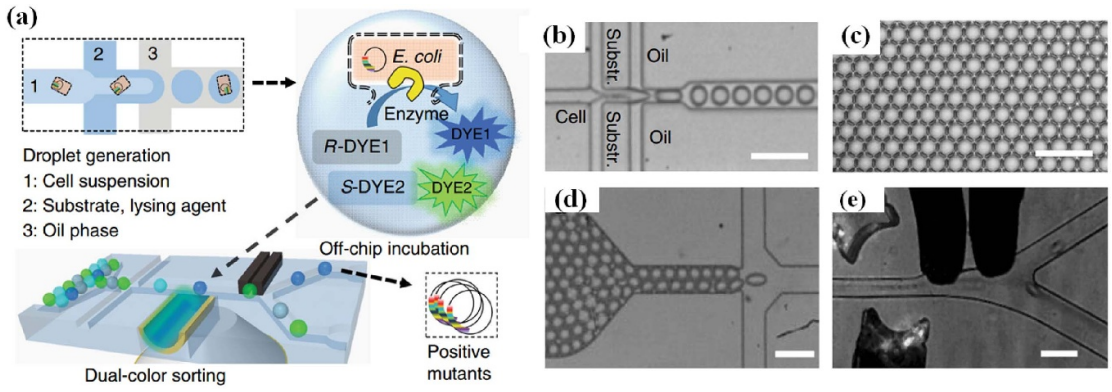

Figure 9. DMDS platform was designed by Ma *et al* for improved screening of directed evolution of enzymes in droplet-based microfluidics. (a) Schematic illustration of DMDS operation which included flow-focusing droplet generation and a dual-channel FADS. Monodisperse droplets with diameters of 24–42 μm were formed to encapsulate mutant enzyme-expressing single cells along with two fluorogenic substrates and lysis buffer. After off-chip incubation and reinjection of the droplets, two spatially separated lasers producing two temporally separated emissions were used to identify the mutant-enriched droplets. Optical images of droplet generation (b) off-chip incubation, (c) reinjection, (d) and sorting within the platform, (e) FADS. Scale bars are 100 μm. Reprinted by permission from Springer Nature Customer Service Centre GmbH: Springer Nature, Nature Communications [152] Efficient molecular evolution to generate enantioselective enzymes using a dual-channel microfluidic droplet screening platform, F Ma, M T Chung, Y Yao, R Nidetz, L M Lee, A P Liu, Y Feng, K Kurabayashi, G-Y Yang, (c) 2018.

attractive approach in cell biology research that mimics only specific characteristics of a living cell [161].

4.2.1. Intracellular and extracellular interactions

In living cells, intracellular processes are as essential as the communication of cells with each other and their extracellular matrix (ECM). Regulation of cellular function is highly dependent on the signals received from inside and outside of the cell membrane. Thus, isolating an individual cell or a group of cells within a droplet enables the characterization of the underlying mechanism of cellular responses. Encapsulation of mitochondria within aqueous droplets was the first application of droplets in cell-based assays [162]. Droplet size is a deterministic factor in cell division and viability. In an instructive example, three different sizes of droplets were generated via a microfluidic droplet generator system to evaluate the effect of the aforementioned parameter on the Chinese Hamster Ovary (CHO) cell culture [163]. Cells were encapsulated in three different volumes including 33 180, and 320 pL droplets and cultivated for three days. It was demonstrated that by the end of the 1st day, cell division stopped in 33 pL droplets followed by decreasing cell viability. This is due to the high density of cells in a small volume as one cell in 33 pL volume corresponded to 3×10^7 cells ml^{-1}. Although high viability above 90% and continuous cell division were observed in both 180 pL and 320 pL droplets after 72 h, droplets with volume of 180 pL were considered as the most efficient for screening since they contained more concentrated cell products.

In a droplet, cell growth as an important indicator of cell response to the desired manipulation is different from bulk culture; the adherence of cells to droplet boundaries is less than cell attachment to a culture plate, the amount of nutrients provided for cells encapsulated within a droplet is smaller, and the permeability of gases to the droplets is different [164]. Correspondingly, careful adjustments must be made in microfluidic devices to generate droplets specified for a certain type of cell and test condition. Oxygen supply to the cells has been improved using a dynamic droplet incubation method, in which flow-induced convection was created to enhance average inter-droplet distances among accumulated droplets and increase oxygen transfer into them [165]. Cell-laden hydrogel microcapsules are also capable of mimicking *in vivo* microenvironment for 3D cell culture in droplet-based microfluidic devices [166]. Siltanen *et al* [167] proposed a droplet microfluidic chip to encapsulate hepatocytes in droplets with liquid core and polyethylene glycol (PEG) shell. Cell–cell contacts were facilitated by liquid core, while the hydrogel shell acted as a damper so that fluidic shear stress within the system could not damage the cells. Using the above approach, the hepatic function was maintained for over 10 days. Headen *et al* [168] introduced a droplet microfluidic device with six parallel flow-focusing nozzles to enhance microgel fabrication throughput. In this platform, mesenchymal stem cells (MSCs) encapsulation was achieved in very high cell densities of 2×10^7 cell ml^{-1} within small microgels with diameters less than 100 μm, and secretion of vascular endothelial growth factor (VEGF) was monitored in microgels. Detection of cytokines such as IL-2,TNF-α, and IFN-γ secreted by encapsulated Jurkat T cells in agarose microgels is another application of droplet-based microfluidic systems [169].

The co-culture of different cell types in a single droplet plays a crucial role in allowing one to study cell–cell interactions. The hydrogel-based droplet microfluidic chips can be employed for the co-culturing of cells within a droplet [166]. Two

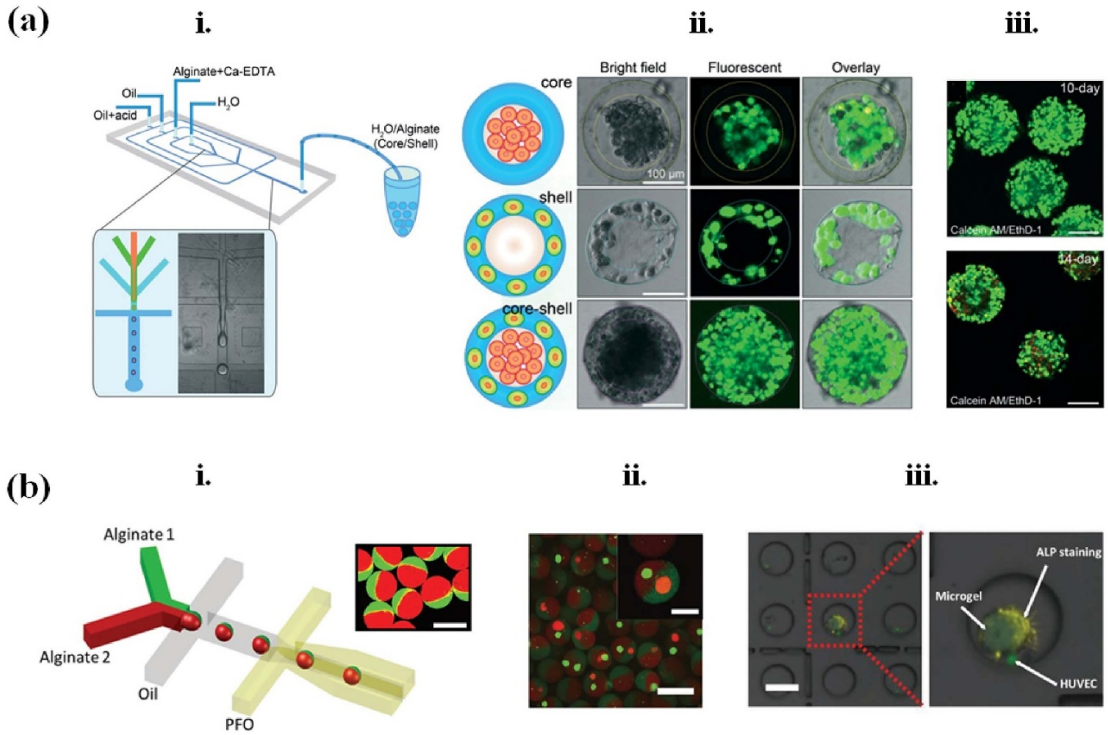

Figure 10. Cell co-cultures in droplets. (a) Replication of stromal-parenchymal interactions in droplets. (i) A microfluidic device to generate core–shell droplets so that hepatocytes and fibroblasts are embedded in the core and shell, respectively. The alginate shell is crosslinked on-chip through additional oil flow containing acetic acid. (ii) Different assemblies of cells in the core and shell of droplets. (iii) High cell viability was recorded after 10 and 14 d through calcein and Ethidium Homodimer-1 (EthD-1) staining. Reproduced from [160] with permission of The Royal Society of Chemistry. (b) Pairing different cells within the Janus microgels. (i) A microfluidic device to construct the alginate Janus microgels. The fluorocarbon oil and perfluoro-n-octane (PFO) solution are introduced as the continuous and washing solution into the device. The inset shows the confocal image of Janus particles. (ii) NIH3T3 cells were labeled with red and green cell trackers encapsulated into the distinct compartments of the Janus particles. Microgels are labeled with fluorescein (green) and rhodamine (red) to distinguish each compartment. (iii) Microgels containing MSCs and/or HUVECs after 8 d of coculture in a PDMS microwell. Positive ALP activity is observed inside the microgels with the presence of HUVECs. Scale bars are 100 μm. [173] John Wiley & Sons.

blood progenitor cell lines MBA2 and M07e were co-encapsulated in agarose microgels using a microfluidic chip for droplet generation, and as a result of 1:1 co-culture, IL-3 secreted by MBA2 cells enhanced the viability of M07e cells to 65.9% $\pm$ 8.4% in comparison to 20% in the case of individually encapsulated M07e cells [170]. When heterogeneous umbilical cord blood cells were cultured with MBA2 cells within agarose microgels using the same chip, subpopulations of hematopoietic cell types were recognized based on their level of viability in response to the secreted IL-3. Co-encapsulation of invasive MDA-MB-231 and non-malignant MCF-10A human breast epithelial cell lines in alginate/Matrigel microgels led to a core–shell structure where MCF-10A cells aggregated in the center, surrounded by MDA-MB-231 cells [171]. A different level of E-cadherin expression by the two cell types was claimed to be the reason for the segregation within particles. The co-culture of hepatocytes and stromal cells within alginate/matrigel capsules resulted in the aggregation of hepatocytes and improved their survival as indicated by increased levels of albumin secretion [171]. Endothelial progenitor cells have also been used as a supporting cell type for hepatocytes in alginate/collagen microgel co-cultures [172]. Paracrine co-culture of hepatocytes encapsulated in PEG microgels atop a feeder layer of 3T3 fibroblasts also resulted in their prolonged survival [167].

To construct a more realistic model of stromal-parenchymal interactions, Chen *et al* [160] established the core–shell structures which could replicate the crosstalk between hepatocytes (HepG2) and fibroblasts (NIH-3T3). As depicted in figure 10(a), hepatocytes were confined in the central aqueous phase, and fibroblasts were embedded in the alginate shells. The on-chip crosslinking of shells was carried out via an additional oil channel containing 0.15% acetic acid. Hepatocytes formed the aggregates after several days, and the hydrogel shell was permeable enough to pass nutrients and metabolites. The proposed droplet-based microfluidic device was able to separately encapsulate different cells in the core and shell with high viability. Therefore, stromal-parenchymal interactions can be well replicated in such structures. Albumin secretion and urea synthesis were monitored over time. It was observed that the concentration of albumin and urea in the core–shell structure (fibroblasts in the shell and hepatocytes in core) increased compared

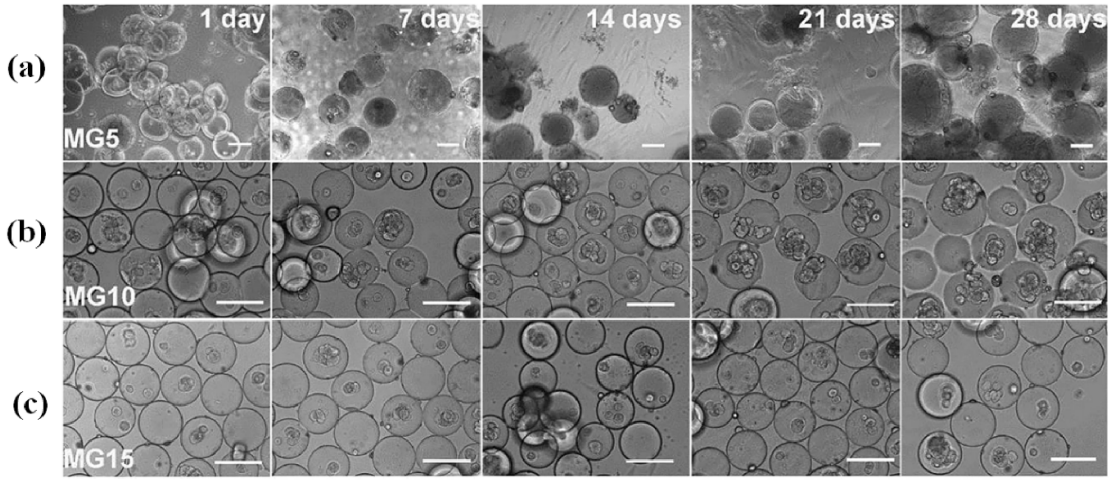

Figure 11. Optical images of BMSC culture within PVA-based microgels generated by a microfluidic platform introduced by Hou *et al*. In 7 d, degradation occurred in (a) MG5 microgels, followed by the migration of encapsulated cells towards the culture plate. By day 28, only a few intact MG5 microgels were present. The degradation process was slower for (b) MG10 and (c) MG15 microgels; proliferation and migration were decelerated accordingly. Scale bars are 150 μm. Reprinted from [176], Copyright (2018), with permission from Elsevier.

to the monotypic culture of hepatocytes. In another approach, Zhang *et al* [173] generated monodisperse multicompartment microgels with up to four distinct compartments. As shown in figure 10(b), the Janus microgels constructed with this technique were employed to pair single cells in a highly biocompatible manner. NIH3T3 cells, with different fluorescent labels, were dispersed within the RGD-alginate solution and then employed as dispersed phases to form Janus microgels. Moreover, to evaluate the feasibility of constructing stem cell niche microenvironment, human umbilical vein endothelial cells (HUVECs) and, MSCs were encapsulated inside the Janus microgels and then seeded inside PDMS microwells. After 8 days, the positive activity of alkaline phosphatase (ALP) was observed, which indicates the osteogenic commitment of MSCs.

Hydrogel encapsulation of stem cells in droplet-based microfluidic devices has been widely used to promote directed differentiation. Endodermal differentiation of mouse embryonic stem cells was successfully achieved by microfluidic encapsulation within microgels composed of PEG and heparin [174]. For osteogenesis, droplets containing bone marrow-derived MSCs (BMSCs), bone morphogenic protein-2 (BMP-2) osteogenic growth factor, and photo-crosslinkable gelatin-methacryloyl (GelMA) were formed via a microfluidic platform and then transformed into microgels [175]. Microspheres obtained by this strategy yielded high cell viability and proliferation, cell migration from the interior of the microsphere to its surface, and differentiation of BMSCs into osteoblasts. Hence, they could be implemented as injectable cell vehicles for bone regeneration purposes. As another example of droplet microfluidics application in osteogenic differentiation of BMSCs, Hou *et al* [176] fabricated degradable PVA-based microgels encapsulated with BMSCs and BMP-2. Three PVA concentrations (MG5, MG10, and MG15) were used to form cell-laden microgels for studying cellular behavior and microsphere degradation in four weeks. The highest proliferation and degradation were observed when the lowest concentration of PVA (MG5) was used, where after only 1 week, cells began to migrate out of the microgels. MG10 and MG15 microgels demonstrated slower degradation rates. Hence, their cell proliferation and migration were more restricted compared to the MG5 samples. Optical images of microgels and cells during 4 weeks of incubation are shown in figure 11.

4.2.2. Artificial cell generation

To simplify the complexity of living cells and provide a bottom-up reconstruction approach, artificial cells were introduced [161]. Artificial cells are engineered cell-like structures that allow the isolated study of specific aspects of cell biology in a tunable microenvironment such as droplets. Droplet-based microfluidic systems can be employed for generating artificial cells [177]. Culture conditions like delivery of oxygen and nutrients are not a concern in artificial cells since they are not living systems. Diverse cellular processes such as gene expression, cytoskeleton biophysics, membrane operations, and cell division have been investigated using artificial cells [161].

The cell membrane, a selectively permeable barrier that controls the transport of biological substances in and out of a cell, can be constructed using droplet-based microfluidic devices to mimic the morphology and function of the natural cell membrane. Several techniques are developed for fabricating the lipid bilayer of the cell membrane [178]. In an example of how emulsion works in artificial membrane generation, Elani *et al* [179] designed a

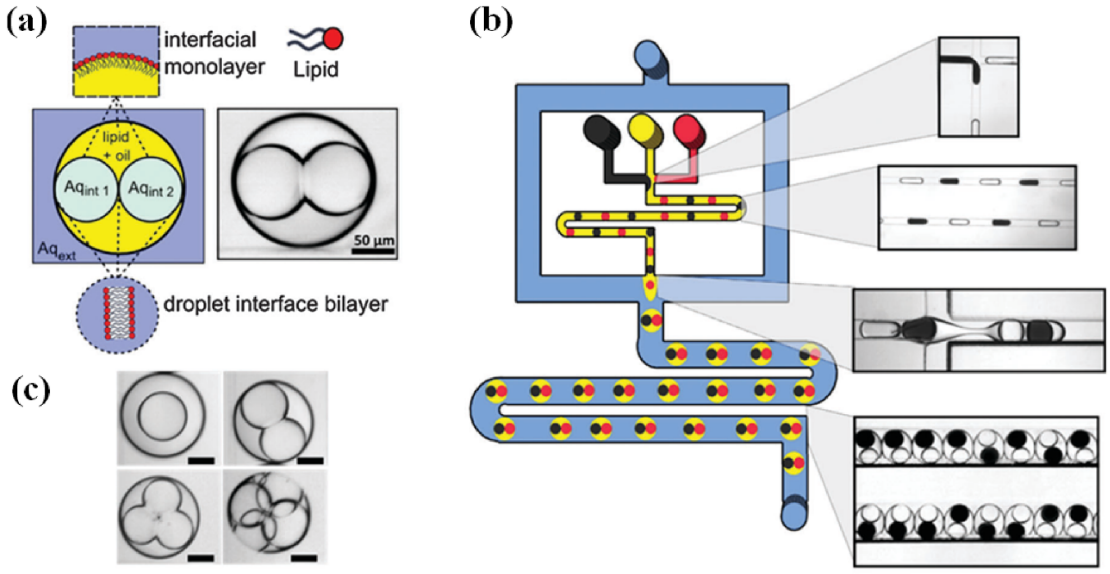

Figure 12. (a) Schematic and optical image of a multisome with two compartments generated in the work of Elani *et al*. DIB was formed at the point of contact of the inner droplets, and a monolayer was distinguished at the interface of the outer droplet and external aqueous phase. (b) Representative illustration of the droplet-based microfluidic platform for generation of multisomes, comprised of two opposing T-junctions to form inner aqueous droplets and a flow-focusing channel to encapsulate them in an oil droplet. (c) Encapsulation of 1–4 aqueous droplets was achieved by changing the frequency of inner droplet formation. Reproduced from [179] with permission of The Royal Society of Chemistry.

droplet-based microfluidic chip to produce up to four compartment multisomes with aqueous and oil phases. In this platform, first water-in-oil droplets were produced by a primary T-junction structure, and then several the aqueous droplets were encapsulated within larger oil droplets in a flow-focusing microchannel (figure 12). Droplet interface bilayers (DIB) were recognized at the interfaces of inner droplets and between the inner droplets and the external aqueous phase, while interfacial monolayers were formed between the outer droplet and the outside aqueous phase. Multisomes with two inner droplets were then proven to be practical microreactors for biological reactions, where one of the inner droplets was considered as a chemical reservoir to a membrane-permeable substance and the other as a chamber to carry out the reaction. It has been shown that by adding an extra step to this double-emulsion method and creating a hydrogel shell as the outer layer of the droplets, the stability and mechanical properties of such multisomes were improved [180]. The hydrogel shell sustains structural rigidity and allows the permeation of biological compounds from the surrounding to the droplets. Czekalska *et al* [181] developed a passive method using a droplet-based microfluidic device to create a parallel array of up to 12 DIBs in less than 5 min. Each artificial bilayer was generated at the interface of two aqueous nanoliter droplets. By precisely controlling the contents of each droplet, the permeability coefficient of fluorescein was determined, and by detecting calcium ions passing through the nanopores of the artificial membrane, the activity of α-hemolysin membrane protein was measured. The transport activity of DIBs could be further controlled and specified by incorporating secondary transporters such as lactose permease in their structure [182]. Moreover, the electrical properties of the membrane could be explored by conjugating sensitive electrodes to an automated microfluidic system in which chains of four connected droplets were generated to obtain three lipid bilayers at their interfaces [183]. By adding α-hemolysin to the droplets, nanopores capable of ion transport were created within the DIBs, so that the electrodes could record the corresponding picoampere currents.

To mimic the cytoskeleton in artificial cells, dynamic morphological changes of the membrane due to continuous remodeling of the actomyosin network are explored by encapsulating actin and myosin II within water-in-oil droplets. Besides, an equation of DIB motion based on the non-periodic oscillatory deformations of the interface, derived from the randomly exerted normal stress made by actomyosin filaments, is presented [184]. Contractile ring assembly in cell division is also explored using the cell-sized W/O droplets generated via a microfluidic platform [185]. Actin filaments spontaneously form a single ring-shaped bundle at the equator due to elastic energy minimization, although the analogous process *in vivo* occurs in the presence of spatial regulatory signals. This finding indicates that because of the point symmetry of the cell boundary, the assembly of the cytokinetic ring in spherical-shaped mitotic cells is more stable than the non-spherical-shaped ones.

4.3. Diagnosis

4.3.1. Microbial infections

Exploring microbial physiology, detecting microbial infections, and testing microbial susceptibility have been enabled by droplet-based microfluidic systems [186]. Plasmodium parasite, which causes malaria infection, can be detected from blood and saliva samples using a rolling-circle-enhanced-enzyme-activity-detection-on-a-chip system that includes a microfluidic droplet generator [187]. In this platform, double amplification is enabled by generating a multitude of DNA circles by each target enzyme to enhance the signal by a rolling-circle-amplification technique. Double amplification combined with rapid reaction kinetics and efficient mixing, enabled by droplet-based microfluidic systems, leads to a highly sensitive and quantitative platform. Besides, to identify *E. coli* in spiked blood, a platform called 'Integrated Comprehensive Droplet Digital Detection' (IC3D) was developed by integrating real-time sensors, microfluidic droplet generators, and 3D particle counting systems [188]. IC3D enabled amplification-free quantification and detection of *E. coli* in concentrations of 1–10 000 bacteria ml^{-1} within ∼1.5–4 h, which was less than ∼15 h of PCR test.

In addition to detection, treatment of microbial infections has been advanced with the aid of droplet-based microfluidic devices. In bacterial studies, different concentrations of antibiotics such as ampicillin, chloramphenicol, and tetracycline were encapsulated with *E. coli* via a microfluidic droplet generator to screen bacteria–antibiotic interactions and determine the minimum inhibitory concentration (MIC) values of the drugs [189]. In another droplet-based microfluidic chip, morphological changes and proliferation of *E. coli* spiked to urine samples at the concentration of 5×10^4 CFU ml^{-1} were monitored in response to antibiotics ceftazidime and levofloxacin [190]. In this antimicrobial susceptibility testing (AST) system, three concentration values were chosen for each antibiotic: below, above, and at the exact amount of MIC reported by the Clinical Laboratory and Standards Institute. Then, cell division and filament formation as signs of antibiotic-induced stress on bacterial cells encapsulated in the droplets were compared. Besides, simultaneous screening of four antibiotics/pathogens in a parallel droplet-based microfluidic device was reported, in which doubling times of *S. aureus* 29 213, *E. faecalis* 29 212, *E. coli* 25 922, and *K. pneumoniae* 700 603 bacteria and the corresponding MIC values of oxacillin and tetracycline were evaluated [191]. This system accelerated the AST process to 30 min compared to traditional AST assays, which take 16–24 h. The impact of the initial concentration of bacteria on the efficiency of antibiotic treatment has also been investigated by taking advantage of microfluidic technology to generate droplets encapsulated with different numbers of cells along with antibiotics [192] (figure 13).

Droplet-based microfluidic devices have opened new possibilities in viral diagnostics as well [193]. Murine noroviruses (MNVs) and murine macrophage RAW cells encapsulated in picoliter droplets were detected using droplet-based microfluidics and plaque-based assay through an RT-PCR process [194]. In this system, the droplet generation rate was 2000 droplets s^{-1}, and it was followed by genome replication and amplification. The neutralizing rate of viruses in droplets was also measured in the presence of antibody MAb A6.2 and showed good agreement with the traditional plaque reduction neutralization assay. The neutralization effect of the aforementioned antibody on MNVs was also explored in another droplet-based microfluidic device, focusing on amino acid mutations as escaping the strategy of viruses against neutralization [195]. In the latter study, the evolution of a single virus encapsulated with a single cell was compared to bulk assays, showing that due to lack of competition from other virions, the number of infecting viruses was equal to the number of viral genomes in droplets. Fusion kinetics of influenza A virus was also investigated in a droplet-based microfluidic chip with high temporal resolution [196].

4.3.2. Oncology assays

The utilization of droplet-based microfluidics in cancer research improves our understanding of the complex nature of tumors at the single-cell level [197]. In a study by Yu *et al*, the enzymatic activities of matrix metalloproteinases (MMPs), which indicate degradation of ECM leading to metastasis of cancer cells, was detected by a droplet-based microfluidic approach through generating single-cell droplets at a high throughput of 2.4×10^3 droplets min^{-1} [198]. MMP9 activity was quantified in the encapsulated lymphoma cells (U937), invasive breast ductal carcinoma cells (MCF-7) cells, and mouse embryonic fibroblast cells (NIH3T3) as the negative control, to differentiate cancer and normal cells as well as different cancer cell lines by monitoring their enzymatic fingerprints. To study cancer cell heterogeneity, the patient-derived glioblastoma samples were introduced to a droplet-based microfluidic system, where encapsulation of the cells within droplets was followed by screening and computational analysis of single-cell protease profiles [199]. A library of cell types including HUVECs, astrocytes (NHAs), fibroblasts (NHDFs), white blood cells (WBCs), and cell lines associated with brain tumors were generated based on their distinct MMP/ADAM activity profiles within 2 h with the throughput of ∼100 cells s^{-1}. Droplet-based microfluidics is proven to be effective in the single-cell level study of cancer metabolism. As an example, evaluating glucose consumption and lactate release, as indicators of the metabolic process,

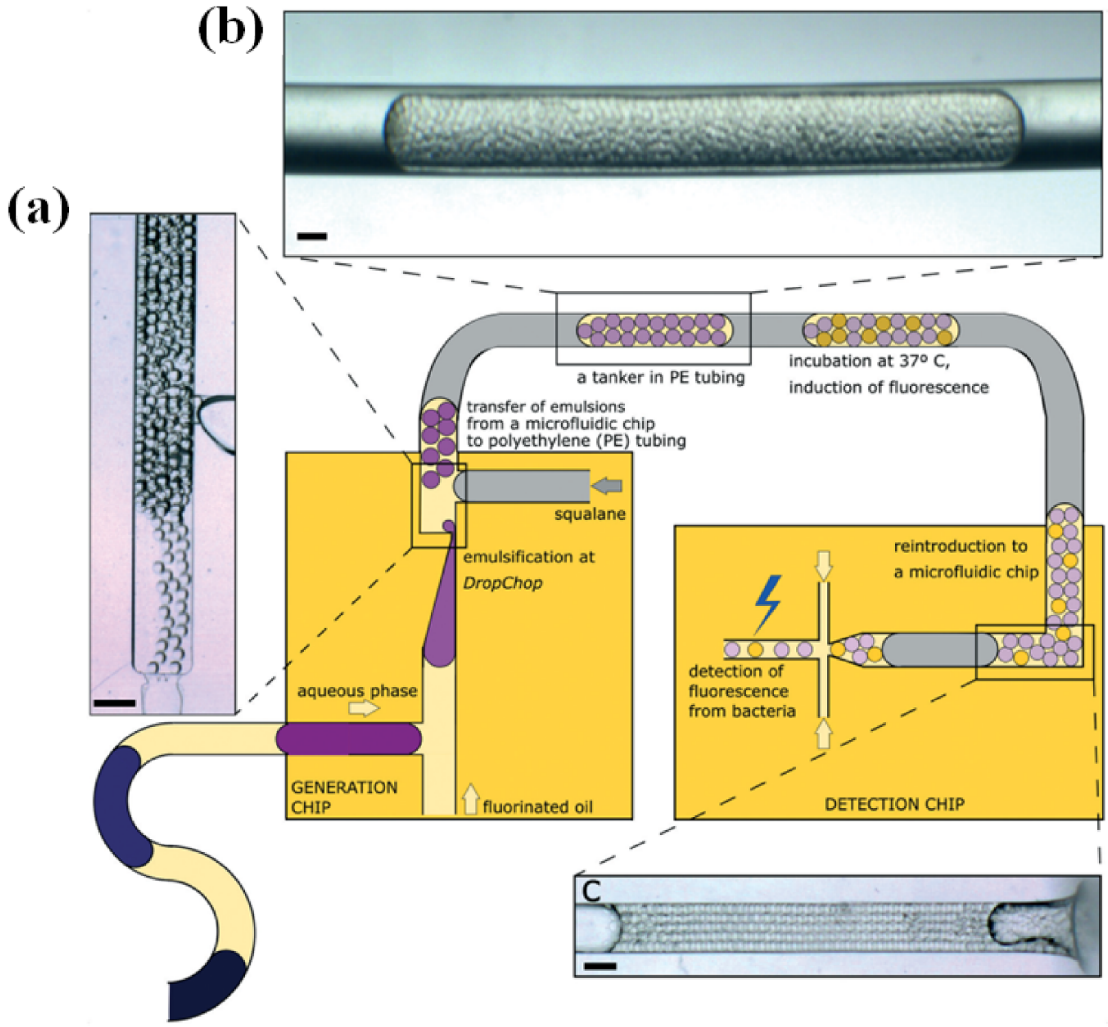

Figure 13. The workflow of the microfluidic droplet generator developed by Postek *et al* for detecting the effect of antibiotic cefotaxime on *E. coli*. Thousands of sub-nanoliter daughter droplets were encapsulated in a larger mother droplet, called a tanker (a). Each tanker had a specific number of bacterial cells and antibiotic concentrations. Tankers were then incubated in polyethylene (PE) tubing for the growth of bacteria and fluorescence activation (b) and finally guided towards the detection chip (c). Scale bars are 400 μm. Reproduced from [192] with permission of The Royal Society of Chemistry.

for MDA-MB-231 human breast cancer cells encapsulated within microfluidic droplets revealed a lack of correlation between these two parameters and confirmed the existence of heterogeneous metabolic pathways even in the homogeneous cell lines [200]. Measuring lactate concentration combined with pH screening was another approach pursued in a microfluidic droplet generator for compartmentalization of A549 lung cancer lines and WBCs samples [201]. Higher levels of the secreted lactate and lower values of pH represent the droplets containing cancer cells. Hence, this platform is a suitable diagnostic tool for the detection of circulating tumor cells. It has been reported that cancer cells express significantly higher amounts of sialic acid than normal cells [202]. To detect the cancer biomarkers, a metal nanoparticle-based probe was conjugated to a droplet-based microfluidic platform, and surface-enhanced Raman spectroscopy, plasmonic imaging of MCF-7, SGC, HepG2, and BNL.CL2 cell lines were obtained. Although the single-cell encapsulation rate at the cell density of 3×10^6 cells ml^{-1} was almost 21%, this system enabled distinguishing different cancer cell lines at a single living cell level.

Besides the wide oncology assays at the single-cell level, droplet-based chips can establish an *in vitro* tumor microenvironment (TME). Tumor cells trapped inside a droplet can constitute multicellular tumor spheroid (MCTS), which enhances cell–cell interactions and molecular pathways. Hence, the real tumor behavior is well recapitulated. On the other hand, droplet microfluidic platforms can offer some advantages over other cell aggregation techniques. Using microfluidics platforms, high-throughput production of uniform-sized spheroids can be achieved. Besides, the cells trapped inside the droplets are well protected from environmental stresses. Furthermore, the tumor cells co-encapsulated with stromal cells in a droplet precisely mimic TME. The later feature is very valuable for a better understanding of tumor

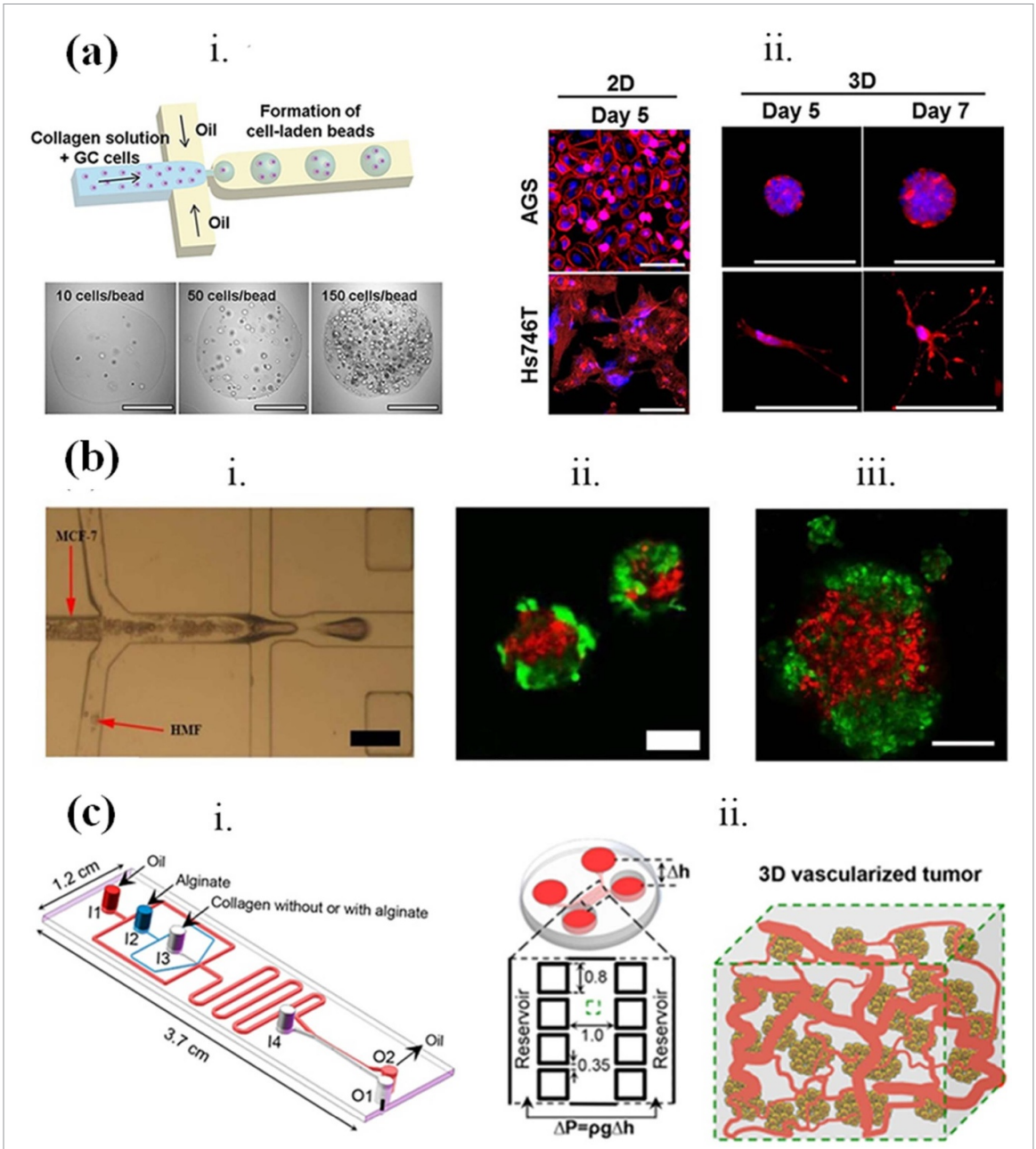

Figure 14. TME formation via droplet-based microfluidic devices. (a) Microtumor model of gastric cancer cells. (i) Schematic of a microfluidic device (top) and multicellular spheroids (MSCs) of gastric cancer cells with different cell concentrations (bottom). Scale bars are 300 μm. (ii) Confocal images of 2D monolayer cultures and 3D microtumors of AGS and Hs746T cells at different times. F-actin and nucleus were stained with TRITC-phalloidin (red) and DAPI (blue), respectively. Scale bars are 100 μm. (b) Fabrication of co-culture tumor spheroids. (i) Microfluidic device employed for fabricating core–shell microparticles. MCF-7 and HMF cells were capsulated in aqueous cores and alginate shells, respectively. The scale bar is 200 μm. (ii) Spheroids fabricated by microfluidic device and (iii) conventional overlay method. MCF-7s and HMFs were stained with DiI-7 (red) and Calcein-AM (green), respectively. Scale bars are 100 μm and 200 μm in (ii) and (iii), respectively. (c) A bottom-up approach for constructing macroscale vascularized tumor. (i) Schematic illustration of a droplet-based microfluidic device for the fabrication of core–shell tumor spheroids. (ii) Microfluidic perfusion device for culturing the building blocks of TME, including TMEs, HUVECs, and hADSCs in collagen hydrogel. A schematic view of a 3D vascularized tumor is depicted as well (all dimensions in (c)-(ii) are in mm). (a) Reprinted by permission from Springer Nature Customer Service Centre GmbH: Springer Nature, Scientific Reports [203] Droplet-based microtumor model to assess cellECM interactions and drug resistance of gastric cancer cells, M Jang, I Koh, S J Lee, J-H Cheong, P Kim, (c) 2017. (b) Reprinted with permission from [204]. Copyright (2018) American Chemical Society. (c) Reprinted with permission from [206]. Copyright (2017) American Chemical Society.

progression, metastasis, and drug resistance. Jang *et al* [203] encapsulated two different types of gastric cancer cells (i.e. AGS and Hs746T cells) inside collagen beads using a cross-junction microfluidic device. Cell morphology, gene expression, and drug resistance were investigated for these 3D culture models, and the results were compared with 2D monolayer models. As depicted in figure 14(a), AGS cells formed well-organized MCTSs, while the Hs746T cells aggregated with a spindle-shape morphology. The gene expressions associated with epithelial-mesenchymal transition were studied through immunofluorescence

staining, RT-qPCR, and western blotting. The results indicated that more mesenchymal markers are expressed in 3D cultured cells compared with the 2D monolayer cultures. This confirmed the pivotal role of the collagen ECM in regulating the physical and biochemical properties of TME. Drug resistance was evaluated by employing different concentrations (0–100 μM) of 5-fluorouracil (5-FU) for both cell lines in 2D and 3D culture models. It was observed that the 3D microtumor models, compared to 2D monolayer cultures, exhibit more resistance to high concentrations of 5-FU. Moreover, comparing drug treatment of AGS and Hs746T cell lines in 3D culture models revealed that Hs746T cells are more resistant to high concentrations of 5-FU due to lower expression of β-catenin. To investigate the tumor-stroma interaction more efficiently, Sun *et al* [204] generated uniform core–shell microparticles so that MCF-7 cells and human mammary fibroblast (HMF) cells were capsulated in aqueous cores and alginate shells, respectively. The cell ratio of 1:1 with a density of 10^7 cells ml^{-1} was selected for tumor and stromal cells. Tumor models with core–shell structures were produced with a rate of 200 spheroids min^{-1} via a cross-junction microfluidic device. Besides, the conventional overlay method was used to generate co-culture tumor spheroids. As depicted in figure 14(b), the microfluidic-based spheroid is more uniform and regular than the one fabricated through the conventional overlay method. Drug efficacy tests were carried out for different culture models consist of the 2D monolayer, 3D tumor spheroids, and 3D co-culture spheroids by using curcumin and paclitaxel drugs at a concentration of 12.8 μM. The microfluidic-based spheroids had higher drug resistance than monolayer cell culture systems but exhibited similar resistance as those made by the conventional overlay method.

The vascular networks within the TME play a crucial role in tumor progression and metastasis. Vascular networks supply nutrients and oxygen to the primary tumor and also facilitate the migration of tumor cells to the secondary site which is known as metastasis. Moreover, multiple signaling pathways among the cells within the TME can lead to angiogenic sprouts. An *in vitro* model of tumor angiogenesis was established in an automated sequential injection droplet array system by 3D encapsulation of tumor cells in Matrigel droplets and 2D culture of HUVECs in another batch of droplets [205]. These two batches of droplets were then paired and fused to co-culture tumor cells and HUVECs in the fused droplet units. After co-culturing, angiogenic sprouts were observed for different tumor cell lines, and it was indicated that the cells with higher metastatic potentials secreted a higher level of human VEGF. An anti-angiogenesis agent, Fingolimod, was added into the TME, and it was revealed that Fingolimod would decrease lumen structures of HUVECs in the context of different tumor cell lines. Agarwal *et al* [206] developed a macroscale vascularized tumor model through a bottom-up method. In their approach, tumor spheroids were fabricated by encapsulating MCF-7 cells within core–shell structures through a microfluidic device. Afterward, the tumor spheroids, together with human adipose-derived stem cells, and HUVECs in 1.5 mg ml^{-1} type-I collagen were introduced into a microfluidic perfusion device. This bottom-up approach is illustrated in figure 14(c). hADSCs were used in this model to stimulate angiogenesis by secreting pro-angiogenic growth factors. VEGF concentration and cell morphology were detected during several days, and the vessel structures were detected on day 4 after culturing the sample. Drug resistance assays showed that this macro model is 4 and 139.5 times more resistant to doxorubicin hydrochloride drug than tumor spheroids and 2D culture models, respectively. Droplet-based microfluidic platforms are efficient for constructing TME and performing drug screening assays. These platforms are separately reviewed in section 4.3.5.

4.3.3. Genetic mutations

As discussed before, PCR and RT-PCR have been widely performed in droplet-based microfluidic devices, which is also extremely practical in the detection of genetic mutations. In this section, we focus on droplet PCR and RT-PCR studies concerning genetic mutation associated with cancer. Extracellular vesicles released from a glioma tumor into cerebrospinal fluid of a patient subjected to BEAMing (beads, emulsion, amplification, magnetics) RT-PCR contains mutant IDH1 transcript [207]. Several mutations in KRAS oncogene, which controls cell proliferation, were detected via microfluidic droplet PCR [208, 209]. In this regard, by implementing a droplet PCR platform, 31 patient-derived primary colorectal tumor samples and corresponding lymph node metastases were tested and high concordance was seen between the presence of KRAS mutations in them [210]. In non-small-cell lung cancer, T790M mutation in the epidermal growth factor receptor was identified in 79.9% of samples obtained from 373 patients by a droplet PCR approach, which indicated higher sensitivity than other methods [211]. Tsao *et al* analyzed the plasma of melanoma patients in a droplet PCR to detect *BRAF* and *NRAS* mutations in circulating tumor DNA (ctDNA) with 0.01% sensitivity [212]. Utilization of the patient's plasma and ctDNA offered a non-invasive and effective way of monitoring cancer post-therapy. An IC3D PCR platform capable of detecting *KRAS G12D* cancer mutation at a high sensitivity of 0.00125%–0.005% as well as analysis of ctDNA from blood samples was recently developed [213]. IC3D technology can complement the existing methods of detection, treatment, and monitoring for early-stage cancer patients.

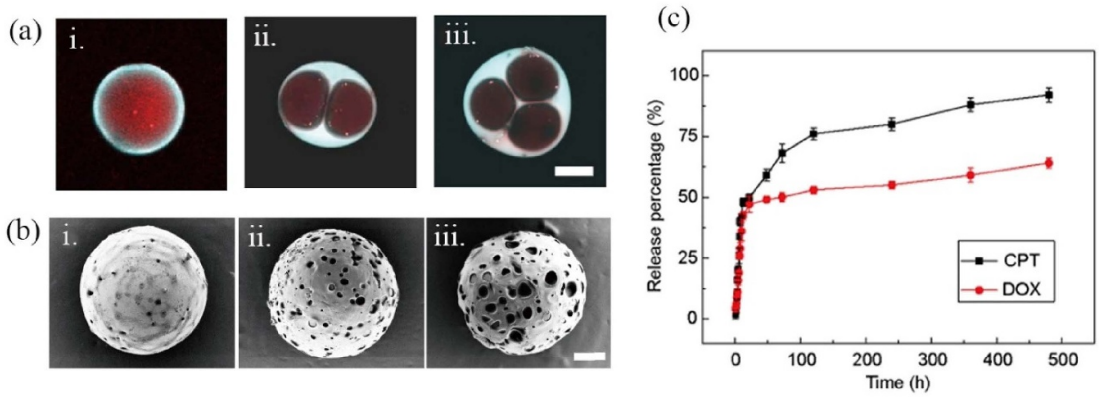

Figure 15. Sustained and synergistic drug delivery via core–shell microparticle. (a) Confocal microscopy images of fluorescent-labeled Dox (red) and CPT (blue) compartmentalized in cores and shells of the microparticles with different numbers of the cores. The scale bar represents 100 μm. (b) SEM images of particle degradation during the release time of 72, 168, and 360 h. The scale bar represents 50 μm. (c) Sustained release of Dox and CPT from core–shell particles. Reprinted by permission from Springer Nature Customer Service Centre GmbH: Springer Nature, Science China Materials [214] Composite core–shell microparticles from microfluidics for synergistic drug delivery, Y Li, D Yan, F Fu, Y Liu, B Zhang, J Wang, L Shang, Z Gu, Y Zhao, (c) 2017.

4.3.4. DDS

Drug encapsulation through droplet-based microfluidics has many advantages compared to other techniques. The precise controlling of the drug combinations, doses, and release rates are the main advantages of the DDSs designed by droplet-based microfluidics over the conventional methods. Indeed, the templates introduced in section 3 can be used for loading the precise amount of the active components in monodisperse microparticles. It should be noted that the risk of burst drug release can be reduced by generating drug carriers with monodisperse sizes [214, 215]. Furthermore, the release rate can be controlled by adjusting the surface to volume ratio of drug carriers, i.e. particle size. Hence, droplet-based methods in microfluidics can be employed to perform successful drug delivery programs by generating monodisperse drug carriers with high encapsulation efficiency and desired sizes. Besides, different drug release programs can be conducted by designing DDSs through microfluidic techniques. Sustained drug release programs are usually developed by loading drugs in the dispersed phase of the single emulsions and converting the droplets to microparticles through different solidification processes [216]. In this manner, the polymeric matrix of the particles degrades slowly in the target site, and drugs sustainably release. On the other hand, the core–shell structures are convenient for conducting the synergistic release of drugs by loading different drugs inside the core and shell structures of the drug carriers. In particular, the core–shell particles are suitable templates to coencapsulate various drugs for the synergistic release of hydrophilic and hydrophobic drugs via a single carrier. The core–shell particles are also attractive for implementing the stimuli-triggered drug release programs so that the core contents are released by changes in the shell structure in response to exogenous stimuli such as pH, temperature, and enzymes. Hence, adjusting the physicochemical properties of the shell layer should be well accomplished to achieve a controlled stimuli-triggered release program. Such adjustment can be well administered via microfluidic devices to construct the shell layer with desired physicochemical properties and thickness. Li *et al* [214] utilized a capillary microfluidic device to generate core–shell microparticles and coencapsulate hydrophilic and hydrophobic drugs in the core and shell portions, respectively. To this end, W/O/W double emulsion templates were produced so that the core was composed of 15% w/v aqueous solution of photo-crosslinkable GelMA with 500 μg ml^{-1} doxorubicin (Dox) hydrochloride as a hydrophilic drug and the shell layer consisted of oil with 10% w/v PLGA and 500 μg ml^{-1} camptothecin (CPT) as a hydrophobic drug dissolved in dichloromethane (DCM). The cores were polymerized by exposing UV-light on droplets at downstream of the microfluidic device, and the shells were solidified through the evaporation of DCM under the reduced pressure at room temperature. Solidification of the cores was carried out to avoid the burst release of the core contents once the shells degrade. Therefore, this approach is suitable for the sustained and synergistic release of drugs with different polarities. Furthermore, the microcapillary device permits assigning multiple cores to the drug template to enable encapsulating different drugs with identical polarity in the separate cores. Figure 15(a) shows the confocal microscopy images of synergistic loading of Dox hydrochloride within the different number of cores and CPT in the shell of the microparticles. It was observed that drugs are loaded uniformly in GelMA cores and PLGA shells with desired encapsulation efficiencies. To evaluate the sustained release of drugs, microparticles were incubated in 1 ml PBS. Then, 200 μl of supernatants

were removed from the centrifuged sample at predetermined time intervals and assayed using a microplate reader. Figure 15(b) shows SEM images of the core–shell microparticles during degradation. The release percentage of CPT and Dox from the core–shell microparticles with 22 μm shell thickness is depicted in figure 15(c). As shown in this figure, the burst drug releases of both core and shell cargoes were prevented. The effect of synergistic drug delivery was also evaluated using *in vitro* tumor models. It was revealed that the synergistic delivery of two anti-cancer drugs is carried out successfully, and the viability of the tumor cells is reduced significantly by employing a synergistic drug delivery program. Trapping drug-loaded nanoparticles in drug-loaded microgels is another strategy that can be applied via capillary microfluidic devices to implement synergistic drug delivery programs. An effective DDS for synergistic and pH-triggered release of drugs was previously introduced in section 3 (figure 5(c)) which takes advantage of drug-loaded nanoparticles [91].

In recent years, liposomes or phospholipid vesicles have attracted immense attention to perform drug delivery programs [215]. Liposomes are lipid bilayer membranes that surround an aqueous content. Hydrophilic-hydrophobic contrast in the liposome structures, along with their biocompatible and biodegradable properties, introduced them as promising templates for compartmentalizing hydrophilic and hydrophobic drugs. These structures can be easily established with a high degree of monodispersity and drug encapsulation efficiency through droplet-based microfluidic devices. Kong *et al* [217] reported constructing Dox-loaded phospholipid vesicles with 94% drug encapsulation efficiency through a capillary microfluidic device. The phospholipid bilayer was formed by removing organic solvents from the shell layer by dewetting. The biocompatibility of this method was validated by AlamarBlue assay, and the results showed that Dox-loaded phospholipid vesicles exhibit a relatively more sustained release profile compared with Dox aqueous solutions. To increase drug retention time in liposomes, drug-loaded liposomes can be embedded in polymeric matrices, and consequently, a more sustained release profile would be obtained. Recently, Yang *et al* [218] designed a DDS based on immobilizing drug-loaded liposomes in GelMA microgels to present an efficient treatment for osteoarthritis via intraarticular injection. In this work, kartogenin (KGN) was considered as the therapeutic agent, which can promote chondrogenic differentiation of BMSCs. KNG-loaded Liposomes (Lipo@KNG) were fabricated with an average size of 250 nm via a thin-film disperse method. Afterward, the liposome-in-GelMA mixture was used as the dispersed phase in a capillary microfluidic device (figure 16(a)) to generate liposome-loaded GelMA (GelMA@Lipo) microgels with an average diameter of 100 μm. In this manner, Lipo@KNG particles were effectively anchored to the GelMA matrix by physical hindrance and non-covalent interactions, which resulted in an extended drug retention time. Figure 16(b) shows the confocal microscopy image of a GelMA@Lipo microgel in which liposomes are labeled with DiI fluorescent dye. The spots with strong red fluorescent determine the location of liposomes inside the microgel. Besides, based on the SEM image of the GelMA@Lipo microgels (figure 16(c)), the monodisperse liposomes are well trapped in the surface cavities of the GelMA microgels. To evaluate the drug release rate, both *in vitro* and *in vivo* assays were conducted. To establish *in vitro* model, drug carriers were incubated in PBS containing 0.1 U ml^{-1} collagenase for 35 d. Figure 16(d) compares the *in vitro* release profile of KGN from GelMA@Lipo microgels with that of the Lipo@KNG particles. As shown in this figure, GelMA@Lipo microgels displayed a sustained release behavior over 5 weeks, while the Lipo@KNG particles were almost completely depleted at the end of the 1st week. Similar behavior was observed for *in vivo* model, where fluorescent-labeled liposomes and GelMA@Lipo microgels were introduced into mouse joint cavities. To realize the therapeutic effects of the employed delivery systems, *in vitro* chondrogenic differentiation of BMSCs under different treatments was investigated by using Alcian blue and Safranin O staining. Besides, the expression level of chondrogenic genes was also determined by qRT-PCR. It was revealed that drug-loaded GelMA@Lipo microgels, compared to drug-loaded liposomes, remarkably promote chondrogenic differentiation of BMSCs. Finally, *in vivo* study confirmed the beneficial effects of the proposed drug carrier on regenerating cartilage and inhibiting the progression of osteoarthritis.

Although droplet-based microfluidics has facilitated sustained and synergistic drug delivery programs, on-demand delivery of biologic drugs, such as proteins and peptides, is still challenging. Small biomolecules can easily escape from the relatively large pores of the microgels. This issue can significantly reduce encapsulation efficiency and drug retention time within hydrogel drug carriers. As an example, alginate is an interesting hydrogel for drug encapsulation due to its proper biocompatibility, biodegradability, and facile gelation process. However, low protein retention efficiency (10%–24%) is reported for alginate microparticles due to the large pores in microparticles (5–200 nm) [219, 220]. On the other hand, electrostatic interaction of the peptides and hydrogel matrix can affect the encapsulation efficiency [221]. Therefore, new strategies have been adopted to increase the efficiency of biomolecule encapsulation as well as release controllability and retention time. Yu *et al* [219] considered different complementary methods to efficiently encapsulate Ovalbumin (OVA), a 42 kDa protein in core–shell alginate microparticles,

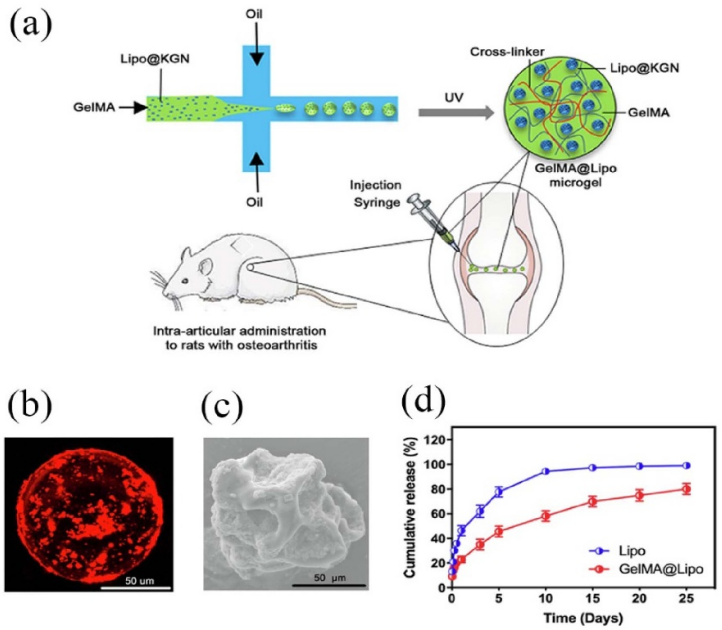

Figure 16. A proposed DDS for extending drug retention time during osteoarthritis treatments. (a) Schematic illustration of the microfluidic device to generate Lipo@KGN-loaded microgel and intraarticular injection of drug-loaded microgels to the animal model. (b) Confocal microscopy image and (c) SEM image of a GelMA@Lipo microgel. Liposomes can be recognized as red fluorescent spots in (b) and particles trapped in microgel cavities in (c). (d) The *in vitro* results of KGN release percentage from liposomes and GelMA@Lipo microgel within 25 d. Reprinted from [218], Copyright (2020), with permission from Elsevier.

via a flow-focusing microfluidic device. First, the authors used FITC-dextran as a model molecule with a molecular weight similar to OVA (40 kDa) to evaluate the retention capacity of the microparticles, and it was observed that the fluorescent intensity of the microparticles quickly weakened due to the burst release of dextran. Hence, the authors decided to coat the surface of the microparticles with other polymers through electrostatic interactions. Due to the inherently negative charge of the alginate microparticles, poly(ethyleneimine) (PEI), a positively charged polymer, was used as the coating layer. Thus, the encapsulated OAV microparticles were collected in a crosslinking bath comprising 0.3 wt% PEI. In this way, the encapsulation efficiency of 88% was achieved, and burst release was avoided due to diffusion barriers on the surface of the microparticles. Figure 17(a) shows the sustained release profile of OAV from PEI-coated alginate microparticles over 120 h (5 d). Chitosan can be utilized as another coating polymer to prevent the burst protein release from alginate microparticles. The encapsulation efficiency of the chitosan-coated alginate microparticles was reported to be 80%. These microparticles can also be used to apply for the stimuli-triggered drug release platforms, especially for oral delivery of the intestinal drugs [220]. Figure 17(b) shows the pH-triggered release profile of OVA from chitosan-coated alginate microparticles. In low pH values (gastric condition), the OVA release is low due to surface protection of chitosan and the shrunken pores of alginate at low pH conditions. In contrast, by increasing pH to 7 (intestine condition), protein release accelerates because alginate pores enlarge in neutral conditions, and chitosan shield cannot resist protein release after experiencing prolonged presence in the acidic environment. The establishment of barriers in the interface of the alginate shell and water core can be another alternative to increase OVA retention time in alginate microparticles. Accordingly, a buffer solution containing OVA and inulin particles with an average size of 2 μm was introduced into the core channel of the microfluidic chip. Then, the generated microparticles were collected in a crosslinking bath containing PEI. In this manner, inulin particles act as a further barrier to increase OVA encapsulation efficiency (91%) and retention time in the aqueous core. As shown in figure 17(c), utilizing inulin particles in the water core of PEI-coated alginate microparticles leads to a more prolonged drug delivery time compared to microparticles without inulin particles.

4.3.5. Drug screening platforms

The advancements in droplet-based microfluidic systems have led to a great evolution in drug screening assays. Previously, 2D monolayer and xenograft models were the acceptable models to conduct the drug assays. However, 2D models cannot offer a realistic model of cell-cell interactions, and they are very sensitive to the cell culture substrates [222]. On the other hand, providing xenograft models imposes high costs and are usually laborious. Therefore, these models are not capable of mimicking human stroma-parenchyma interactions. Although

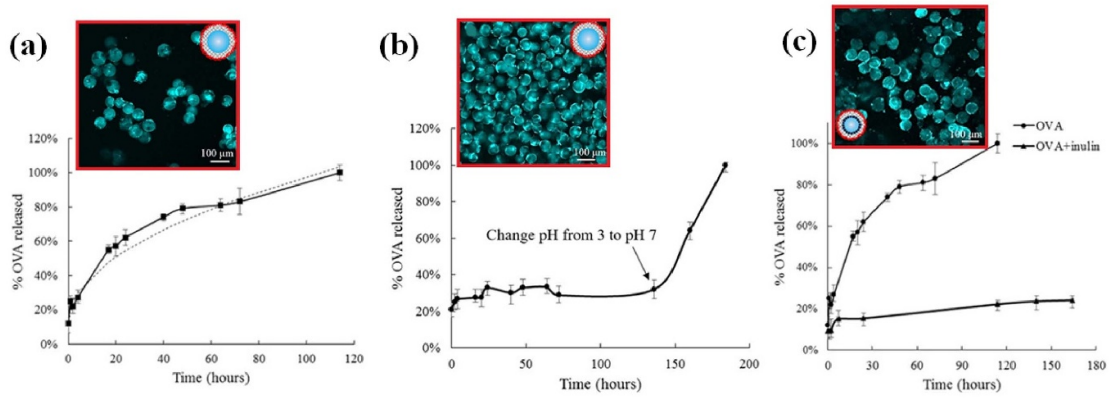

Figure 17. Different strategies to prolong protein release from core–shell alginate microparticles generated by a flow-focusing microfluidic device. (a) OVA release profile for the PEI-coated microparticles; (b) OVA release profile for the chitosan-coated microparticles; (c) comparing OVA release profiles from PEI-coated microparticles containing inulin particles and microparticles without these particles. The insets respectively show the fluorescence images of PEI-coated, chitosan-coated, and PEI-coated + inulin microparticles in (a)–(c). Reprinted from [219], Copyright (2019), with permission from Elsevier.

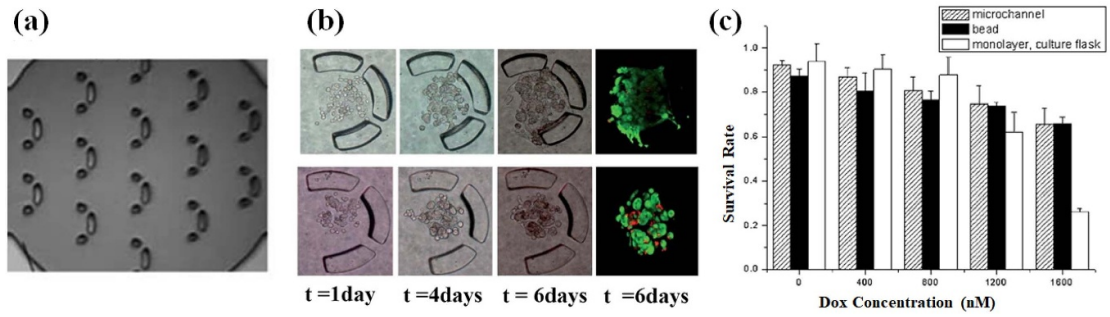

Figure 18. Conducting drug screening assays on the population of tumor spheroids. (a) Cell culture chip with microsieves for locating tumor spheroids. (b) The proliferation of tumor cells during several days; up: without drug injection; bottom: doxorubicin is injected on the 4th day with a concentration of 1200 nM for 2 d. The results of the live/dead assay are presented on the 6th day. (c) Effects of drug concentration and culture method on cell viability; 'microchannel': spheroids cultured in the microfluidic chip; 'bead': spheroids cultured in the standard flask; 'monolayer, culture flask': 2D monolayer culture in the standard flask. Reproduced from [224] with permission of The Royal Society of Chemistry.

several microfluidic models have been presented to compensate for the weakness of the conventional methods of drug screening, among them, droplet-based models are the most efficient and attractive ones for conducting drug screening assays. MCSs can be well established through culturing the intended cell lines in droplets generated by microfluidic devices. These *in vitro* models enhance cell–cell and cell–ECM interactions in a 3D cell culture microenvironment. Furthermore, MCSs with different combinations can be generated and arranged in a precise and high-throughput manner via droplet-based microfluidics. Therefore, droplet-based platforms are appealing for recapitulating *in vivo* like conditions and conducting concurrent drug screening assays.

Thus far, droplet-based microfluidic devices have been widely employed for conducting drug screening assays [61, 203, 204, 223]. In this section, those studies which have taken the advantages of droplet-based microfluidics to provide drug screening platforms are reviewed. Yu *et al* [224] employed a simple microfluidic device to generate alginate droplets with entrapped breast cancer cells with an average diameter of 251 μm. LCC6 cells transfected by *Her2* gene were suspended in DMEM medium with 2 wt.% alginate at a concentration of 10×10^6 cells ml^{-1}. The cell-laden droplets were collected in a Ca^{2+} bath and gelled. Afterward, the generated spheroids were loaded into a perfusion cell culture chip with individual microsieves (figure 18(a)), which settled the spheroids in distinct sites. The microchip allowed the perfusion of culture media and drugs for performing cytotoxicity assays on the population of the settled spheroids. Cell proliferation and viability inside the spheroids were tracked by confocal images. To conduct the cytotoxicity assays, Dox with different concentrations (400, 800, 1200, and 1600 nM) were injected into the cell culture microfluidic chip at a constant flow rate of 0.25 μl min^{-1}. Figure 18(b) shows the cell proliferation and drug effects on cell viability in tumor spheroids. Besides, cell viability rates of different culture techniques were compared. As shown in figure 18(c), cell viability for all cell culture methods

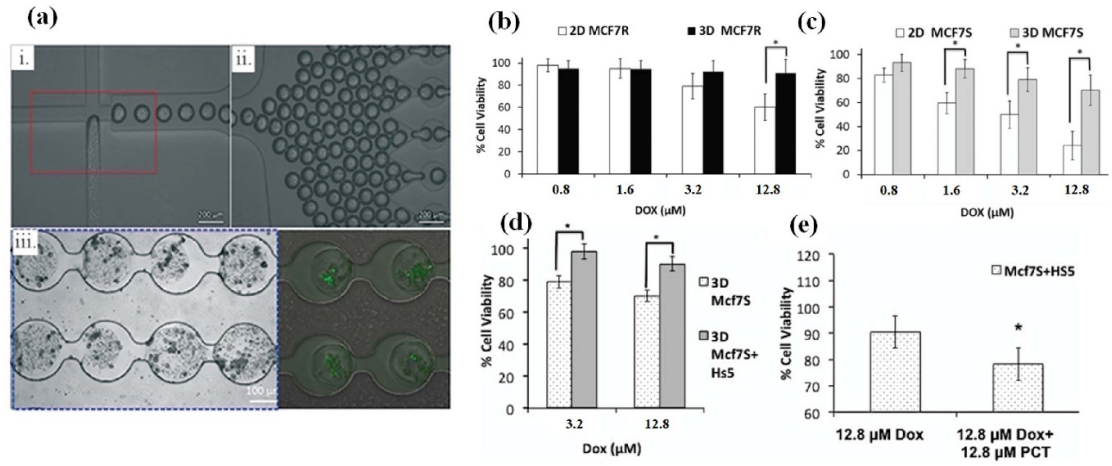

Figure 19. Droplet formation, gelation, and conducting cytotoxicity assays in an integrated droplet-based device. (a) Droplets during formation (i), entering the docking sites (ii), and gelled droplets in the docking sites along with the result of live/dead assay (iii). (b), (c) The results of cell viability for MCF-7R cells (b) and MCF-7S cells (c). (d) Comparing the drug resistance of the composite spheroids with that of tumor spheroids. (e) Effects of different treatments on drug resistance of the composite spheroids. Reproduced from [222] with permission of The Royal Society of Chemistry.

decreases as drug concentration increases. However, the drug resistance of monolayer cultures is significantly less than that of the spheroids at a high concentration of Dox (1200, 1600 nM).

Sabhachandani *et al* [222] provided a microfluidic device to produce cell-laden droplets and immediately settle 1000 droplets in a docking array such that droplet formation, gelation, and cytotoxicity assays were carried out in an integrated microfluidic device (figure 19(a)). In this work, three different cell suspensions in alginate solutions, including MCF-7S (the line sensitive to Dox treatment), MCF-7R (the line resistant to Dox treatment), and coculture of MCF-7S with human bone marrow fibroblasts (HS-5) were employed to generate MCTS. Since fibroblasts are one of the main stromal components of the TME, the composite MCF-7/HS-5 spheroids were employed to study the effects of tumor-stroma interactions on drug resistance. A summary of the results of cytotoxicity assays is represented in figures 19(b)–(e). As shown in figure 19(b), at relatively high concentrations of Dox, the drug resistance of MCF-7R spheroids was higher than that of 2D monolayer counterparts. However, when the MCF-7S cells were employed in tumor spheroids, drug resistance was higher than 2D monolayer cultures for all drug concentrations (figure 19(c)). According to figure 19(d), the coculture of MCF-7S cells and HS-5 cells in tumor spheroids extremely enhances the drug resistance. This observation confirms the effect of cancer cell-fibroblast interactions in the TME on the survival of the cancer cells. This robust droplet-based platform has also been implemented to evaluate the effects of different treatments on the viability of the cancer cells. As depicted in figure 19(e), using a combination of identical doses of Dox and paclitaxel (PCT) can be a more effective treatment for composite spheroids compared to the use of Dox alone.

Recently, Sabhachandani *et al* [225] represented another droplet-based microfluidic device to investigate the effects of immunomodulatory drugs on cell proliferation in TME in the presence of the immunogenic components. To this end, a microfluidic device similar to that of figure 19(a) was employed to settle 250 lymphoma spheroids containing tumor cells (SUDHL-10), fibroblasts (HS-5), and PBMC in the hydrogel combination of alginate and puramatrix. The cell ratio was considered as 3:1 for immune cells: non-immune cells similar to the cell contribution in the lymphoma TME, and the spheroids with an average diameter of 350 μm were located in the docking sites for the cytotoxicity assays. Spheroids were treated by lenalidomide, and the perfused media through the spheroids was collected every day to analyze the secretory factors. The results revealed that lenalidomide treatment, in the presence of activated PBMCs, enhances the overall death of the cancer cells and proliferation of activated PBMCs. This treatment also led to the downregulation of some pro-inflammatory cytokines in lymphoma TME.

4.4. Tissue engineering

The field of tissue engineering is advancing through understanding of biology and function of engineered tissue constructs. Compared to traditional fabrication methods, microfluidics has got a great attention in this field due to its low-cost, reproducible, and accurate characteristics [226]. Among different applications of microfluidics systems, droplet-based microfluidics has provided specific benefits in the field of tissue engineering, such as temporal resolution, cell encapsulation in well-confined

microenvironments, which provide efficient cell–cell and cell–ECM interactions, and screening independent reactions in a high-throughput manner [227]. Additionally, droplet-based microfluidic systems are one of powerful tools to produce shape-controlled hydrogels (i.e. microparticles, microfibers, and hydrogel building blocks) as well as cell-laden hydrogels for making artificial tissues and organs [228, 229]. In this section, we discuss some applications of droplet-based microfluidics in tissue engineering particularly for wound healing, tissue regeneration, and few other applications.

Yu *et al* developed a microfluidic technique to generate hollow bacterial cellulose (BC) microspheres with desirable morphology and structure as the building blocks to construct an injectable porous scaffold for wound healing applications. Tuning porosity in the self-assembled scaffold was done by precisely generating the hollow BC microspheres. Accordingly, the core–shell microparticles with alginate cores and agarose shells were produced via a droplet-based microfluidic device, such that a specific number of a non-pathogenic bacterium, G. xylinus, were encapsulated in the agarose shells as the BC producer. Afterward, G. xylinus secretes BC, which becomes elongated in the confined space of the shell and constructs a hollow cellulose morphology. Finally, a sodium citrate solution and a high-temperature bath were utilized to get rid of the alginate core and agarose shell templates, respectively. Using different-sized alginate particles, monodisperse hollow microspheres were produced with diameters of 20, 40, and 50 μm, which were then assembled as functional elements to create injectable scaffolds. The highly porous scaffold generated in this way demonstrated a proper *in vitro* cell culture with an improved depth distribution and high cell proliferation rate compared with the bulk BC scaffold and that constructed by the solid BC microspheres. This injectable scaffold also enabled tissue regeneration *in vivo*, leading to a fast wound-healing process in a rat skin model [230].

Another core–shell structure was presented by Chen *et al* as niacin metal-organic frameworks encapsulated microcapsules made with alginate shells and copper-/zinc-niacin framework cores through a double-emulsion capillary microfluidic electrospray system [231]. Calcium, copper, and zinc ions were released from the microcapsules in a controlled manner, providing antibacterial, antioxidant, and angiogenesis properties for wound healing. Moreover, niacin improved blood circulation and the uptake of metal ions. *In vivo* experiments were performed on a mouse with *E. coli* infected full-thickness skin defect on its back. It was found that the core–shell structure balanced ion concentration in the wound bed. In the early stages of the wound healing process, calcium ions released from the alginate shells helped skin barrier regeneration by improving angiogenesis. After degradation of the alginate shells, angiogenesis and collagen deposition were induced by the released copper ions, while the regeneration of the ECM was triggered by the release of zinc ions. Hence, the chronic wound healing process was enhanced significantly. Considering that the wound microenvironment has a lower pH value, Shi *et al* designed alginate/$CaCO_3$ composite microparticles with diameters of about 430 μm for sustained and fast release of rifamycin and basic fibroblast growth factor (bFGF) within pH value of 6.4 [232]. Droplets were first generated by a microfluidic device and then solidified and rehydrated to form hydrogel microparticles loaded with antibiotic or growth factor. Mouse fibroblasts (NIH-3T3) *in vitro* and Sprague–Dawley rats *in vivo* were subjected to the resultant microparticles. In both cases, a 1:1 mixture of rifamycin-loaded microparticles with rifamycin concentration of 10 mg ml^{-1} and bFGF-loaded microparticles with bFGF concentration of 10 μg ml^{-1} (named CD-F-R) demonstrated the best performance to inhibit *S. aureus* growth and facilitate wound healing (figure 20(a)). The authors suggested that the biocompatibility and biodegradability of these composite microparticles can be enhanced by modifying sodium alginate in order to establish perfect wound dressing materials. One of the main challenges of tissue engineering in wound healing applications is to develop functional dressings capable of covering the whole healing process. Chitosan microparticles loaded with bFGF generated by a microfluidic electrospray system were introduced to address this issue [233]. The product was claimed to be effective in all four stages of wound healing, including hemostasis, inflammation, proliferation, and remodeling.

Besides wound healing, bone tissue engineering and regeneration is another area for droplet microfluidics applications. Combined with effective therapeutic biomaterials such as calcium phosphate (CaP)-base ceramics, Chacón *et al* produced highly homogeneous CaP microparticles with controlled size and chemical composition [234]. Monodisperse droplets with 75–135 μm in diameters were achieved in this device by keeping the flow rate of the oil phase constant at 8 μl min^{-1} and tuning the flow rate of the water phase. Varying Ca/P ratios resulted in different CaP phases in microparticles. Human mesenchymal stromal cells were then cultured on glass slides covered with the obtained microparticles for up to 14 d. Attachment, metabolic activity, and the expression of osteogenic differentiation markers were observed among cells in contact with 60 μm diameter CaP microparticles. However, the proliferation of cells was limited. The emphasis of the aforementioned study was on the production of CaP microparticles with the aid of droplet-based microfluidics. Although, deeper investigation is required for screening biological response and cell–material interaction to develop bone graft substitutes. In an attempt to achieve a more biocompatible bone

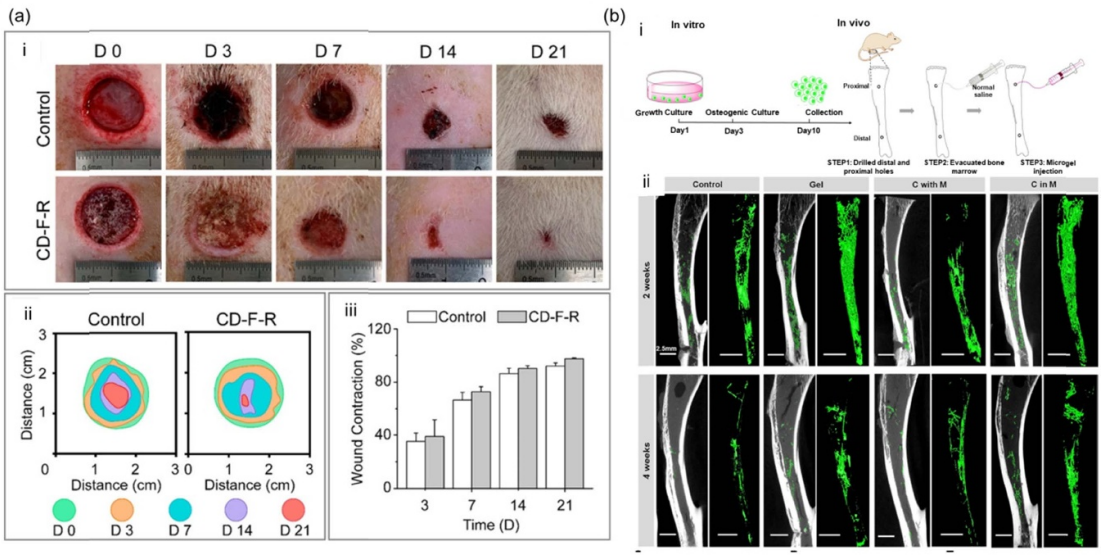

Figure 20. (a)-(i) Digital images of the wound healing process for the same Sprague–Dawley rat over time. The decrease of wound area was faster when CD-F-R microparticles were applied onto the wound surface. After 21 d, the wound was almost completely healed in CD-F-R-treated group, while it was nearly 90% healed in control group. (a)-(ii) Wound-bed closure and (a)-(iii) wound contraction during 21 d. (b)-(i) Schematic illustration of the *in vivo* experiment procedure for bone regeneration with MSC-laden Ca-alginate microgels. The microgels were prepared *in vitro* and then injected into a rat with tibial bone marrow ablation. (b)-(ii) Micro-CT images in 2D and 3D after 2 and 4 weeks of implantation. The regenerated bone tissue is colored with green. C in M groups represent treatment with MSC-laden microgels and C with M groups refer to treatment with empty alginate microgels plus naked MSCs. C in M groups showed the highest new bone formation after both 2 and 4 weeks. Although, decrease in the amount of new bone over time is noticeable in all groups. Scale bars are 2.5 mm. (a) Reprinted with permission from [232]. Copyright (2019) American Chemical Society. (b) Reprinted from [236], Copyright (2020), with permission from Elsevier.

graft, Sun *et al* used silk fibroin (SF) and nano-hydroxyapatite (nHAp) to fabricate a scaffold embedded with SF microspheres and loaded with bone morphogenic protein-2 (BMP-2) as an osteoconductive growth factor and GlyPhe-Hyp-Gly-Glu-Arg (GFOGER) as a peptide sequence, all to support adhesion, proliferation, and osteogenic differentiation of BMSCs [235]. SF microspheres with average diameters of 4.20 $\pm$ 1.76 μm were generated using a coaxial microfluidic device. Alkaline phosphatase activity and calcium content measurements confirmed the enhancement of osteogenic differentiation of BMSCs on the scaffolds loaded with both GFOGER and BMP-2 (G + B). Cell proliferation was higher on GFOGER scaffolds than G + B ones, though. The potential of accelerated bone formation by implementing GFOGER to composite scaffolds was also noticed in their *in vivo* experiments as the defected area was regenerated by a new bone 12 weeks after the implantation. Moreover, *in vitro* and *in vivo* results indicated that G + B scaffolds showed the same level of bone regeneration with roughly one-third dose of BMP-2 as the ones containing only BMP-2. Yet, the effect of size and size distribution of SF microspheres on bone formation were not investigated in this research. A promising approach for bone tissue regeneration is the direct injection of BMSCs encapsulated within microscale hydrogels [176, 236]. With the aid of a microfluidic chip, Hou *et al* generated monodisperse pH-degradable PVA microdroplets loaded with BMSCs and BMP-2. The microdroplets were then crosslinked to form microgels, providing microenvironments with tunable mechanical properties and degradation rates in which release profiles of the growth factor were controlled [176]. Prolonged survival, proliferation, migration, and osteogenic differentiation of BMSCs were reported in these microgels, making them promising cell vehicles for bone regeneration applications. In another study, single MSCs were continuously loaded within Ca-alginate microgels via integrating microfluidic encapsulation, gelation, and de-emulsification [236]. By implementing this approach at a cell density of 4×10^6 cells ml^{-1}, about 21.6% of the generated microgels contained single cells, and the rest were empty or had multiple cells. Accelerated osteogenesis and rapid mineralization of hydrogel matrix were established 7 d after induction *in vitro* and enhanced bone formation was observed *in vivo* (figure 20(b)). These single cell-laden microgels are good candidates as injectable fillers for bone regeneration.

In other application of droplet-based microfluidics in tissue engineering, Weaver *et al* proposed a microfluidic-based encapsulation platform, which produced synthetic poly(ethylene glycol)-based microgels with small sizes. The gels enhanced islet insulin reaction compared to alginate capsules and provided vascularized tissue regions. The authors showed that a single pancreatic donor syngeneic islet mass showed enhanced long-term function compared to conventional alginate capsules and incorporated

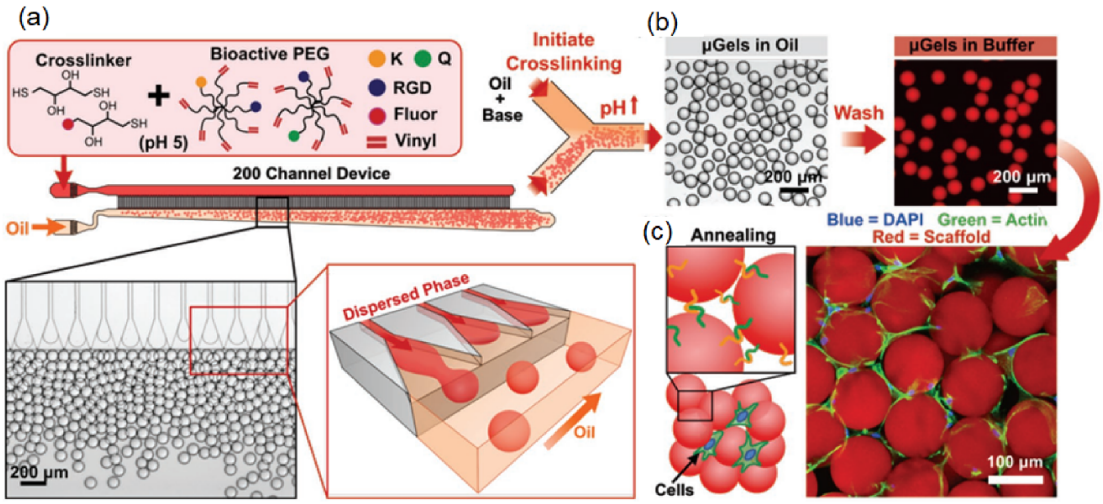

Figure 21. Summary of μgel generation and scaffold creation. (a) Mixture of crosslinkers and bioactive hydrogel precursors are introduced into the microfluidic device at a nonreactive pH. (b) Organic base is mixed with the oil phase in flow to raise pH and encourage crosslinking. Crosslinked μgels are isolated from the oil phase and washed. (c) μgels are seeded with cells in solution and covalently connected together using enzymatic reaction between Q and K peptides to create cell-laden microporous scaffolds. [241] John Wiley & Sons.

into the native vasculature system [237]. Cai *et al* prepared an engineered porous scaffold with drug loading ability via a capillary microfluidic device to heal intrauterine adhesions (IUAs). In this respect, monodisperse droplets were generated from an aqueous solution of GelMA and sodium alginate and then solidified using UV illumination and a bath of calcium chloride solution. To construct porous scaffolds with a desired shape, the products were transferred to a container, which induced the shape of the uterine cavity to the collected building blocks. Microfluidics enabled a precise control over the pore size of the scaffold by tuning flow rates during droplet formation. Furthermore, the porous structure of the scaffold can be used for sustained drug release. To confirm the anti-adhesion and restoration of drug-loaded scaffolds, the performance of the built scaffold was evaluated using rat models of IUAs, and it was revealed that scaffolds were capable to increase neovascularization, repair the endometrium, and cellularize the damaged tissue [238]. Vascular development of thin endometrium was improved by microfluidic-generated methacrylated hyaluronic acid (HAMA) microspheres loaded with VEGF to induce angiogenesis [239]. Microfluidic electrospray technique was implemented to achieve microspheres with uniform size of an average diameter of about 400 μm and porous structure, which were biocompatible for endometrial regeneration. *In vitro* and *in vivo* tests revealed that the combination of HA and VEGF promoted new blood vessel formation. Although the angiogenic microspheres showed potential for thin endometrium repair, periodic treatment is required due to their limited drug-release ability.

A remarkable investigation was performed by Zhu *et al* with a focus on neural tissue repair utilizing microfluidic hydrogel microcapsules [240]. Microgels were fabricated in a microfluidic electrospray system containing two-phase fluid inlets, droplet generation part, and microcapsule fabrication unit to encapsulate human induced pluripotent stem cells-derived neural cells within alginate-based hydrogels. Brain organoids along with vascular networks were successfully formed by suspending endothelial cells, fibroblasts, and neural cell-loaded microgels in the fibrin matrix and their co-culture. The resulting vascularized brain tissue was then injected to a rat model with traumatic brain injury and showed favorable neural regeneration.

Hydrogel scaffolds are extensively employed in regeneration of tissue structures. Still, there is a trade-off between the properties of material, including interconnected pore size and stiffness. To resolve this trade-off, Rutte *et al* introduced microporous annealed particle scaffolds by conserving a flowable precursor. However, production throughput, flexibility, and reproducibility of microparticle components were restricted, hampering their extensive implementation. A high-throughput production of monodisperse microgels was attained by employing a parallelized and scalable step emulsification platform. The hydrogel crosslinking was introduced downstream of droplet production via pH adjustment using proton acceptors dissolved in the oil phase. Their proposed method provides generation of microgels for over 12 h in a continuous manner, while guaranteeing uniform properties. Moreover, they investigated the effects of local stiffness of the matrix on cell growth orthogonal to the scaffold

porosity. Additionally, the creation of injectable cell-laden heterogeneous microporous scaffolds was revealed. Their proposed method is mostly suitable for the creation of modular and multimaterial scaffolds, which can be used for construction of more intricate scaffolds to improve regeneration of irregular wounds as well as in 3D bioprinting applications [241] (figure 21).

5. Conclusion and future directions

The research in droplet-based microfluidics systems has been growing remarkably during the recent years. In this review, the most typical methods for droplet generation were described. Then, different applications of droplet-based microfluidics in biomedical applications including particle synthesis, biomolecular analysis, cell biology, diagnostics, drug delivery, and drug screening were reviewed. Droplet microfluidic technology enables microdroplet generation with precise control over the size, size distribution, chemical content, and morphology of droplets.

Despite remarkable progress in droplet-based microfluidics, several limitations and challenges still exist for further progress in the field. One major obstacle to further commercialization of the microfluidic droplet generator chips is their low throughout. Although the parallelizing methods have improved the throughput by a factor of 10 or more, it is still insufficient to fulfill the requirement for many purposes. Furthermore, the parallelization of encapsulated structures is challenging because complex surface treatment and geometry of microchannels are required [18]. Although droplet-based microfluidics devices have shown promise in the development of the particulate DDS synthesis, more progress needs to be made before they can be transformed into industry-scale manufacturing. Two requirements should be fulfilled for further widespread adoption of droplet-based microfluidics in various applications including improving their versatility and scalability. Droplet-based microfluidics applications for drug carrier synthesis in industrial scale need a high-throughput generation system. Efforts have been already made to fabricate microfluidic devices that support the production of droplets/particles at high rates by implementation of parallel generators in a single chip [242, 243]. As miniaturization is a main characteristic of microfluidics devices, hundreds of these chips can be fabricated to work simultaneously to produce DDS. The drug production procedure also requires to be versatile so that DDS with various properties can be produced and sorted with a high efficiency. Current microfluidics-based particle synthesis for drug carriers is largely passive, where the properties of the particle are regulated by changing the flow rates of two immiscible phases. One of the restrictions is that any variation at input has a long reaction time [244]. To address this issue, an automated active droplet generation device was presented in which valves were used to externally regulate the infusion of two phases to tune the droplet volume [244]. This can improve the versatility of the microfluidics-based platforms for drug carrier synthesis as carrier properties can be appropriately regulated. After the synthesis of drug carriers, steps need to be considered to sort them based on their properties in terms of their size or shell thickness. For this purpose, functions such as particle separation or sorting can be incorporated into the microfluidic device appropriately due to the flexibility of microfluidic devices for multistep processing [245].

Droplet microfluidic technology faces some challenges that limit its widespread application in tissue engineering and regenerative medicine. As discussed earlier, droplets and microgels loaded with cells are more effective for tissue repair. Another issue in this field is relatively lower cellular viability in the process of droplet generation in microfluidic devices, shear stress of droplet separation damages the cells to a small degree [246]. Precise control of cell number in droplets, as well as cell escapement, is significantly challenging [236, 247]. This problem is highlighted in heterogeneous tissues where co-culture of multiple cell types is required. Another challenge arising from multiple cell cultures is providing specific microenvironment and cell media for each cell type. Designing core–shell structures for the generated droplets solves this problem to some extent [248]. In the case of microfluidic encapsulation of cells within hydrogels, gelation of the generated droplet is essential. To attain efficient automation, extra microfluidic compartments must be integrated into the droplet generator to introduce the curing agent and maintain its reaction with the gel material. On-chip gelation compartments lead to a higher complexity of fabrication and operation [249].

Despite the significant advances in the droplet-based microfluidic platforms, a few commercial products of these devices have established themselves as central tools in the biological and chemical sciences [250]. Some of the commercial products of this technology, which are related to biomedical applications include Drop-seq, 10× Genomics, and nucleic acid quantification using Droplet Digital™ PCR systems from BioRad [251]. Fujifilm Dimatrix printer (DMP2800) and cluster technology (DeskViewer™) are two commercial piezoelectric drop-on-demand products, which are established for Bacterial cells to investigate cell-to-cell interactions and liver tissue chips containing HUVECs and hepatocytes (HepG2), respectively [252]. Additionally, RegenHU Ltd BioFactoryR is a commercial solenoid micro-valve in 3D bioprinter technology is proposed for lung tissue containing Matrigel™, A549 cells and A.hy926 cells [253].

It is expected that future improvements and standardization of these devices will further enable

microfluidic adaptation. Additionally, further efforts in commercialization will drive extensive adaptation of microfluidic platforms from the research community into commercial biomedical applications [250, 254]. To enable out-of-lab application of droplet-based microfluidics, the employment of additive manufacturing methods will become more central in fabricating advanced microfluidic devices [255]. Moreover, the use of pumpless fluid manipulation methods [256] enables using droplet-based analysis devices in remote and resource-limited manner [257]. Step emulsification can be beneficial in the future application in diagnostic applications including digital droplet PCR or isothermal as well as large-scale screening/selection applications [252]. Moreover, Raman spectroscopy is a favorable method for analysis of single-cell. Hence, the integration of droplet microfluidics with Raman spectroscopy can provide a special possibility for downstream single-cell analysis, including culturing cells as well as DNA/RNA extraction. Additionally, analytical detection methods including mass spectrometry, Raman spectroscopy, and electrochemical detection, can be combined to broaden their use in droplet microfluidics [252].

Data availability statement

No new data were created or analyzed in this study.

Acknowledgment

Rohollah Nasiri acknowledges the Ministry of Science, Research and Technology of Iran for financial support of this work.

ORCID iDs

Mohsen Besanjideh https://orcid.org/0000-0003-0098-7856
Amir Shamloo https://orcid.org/0000-0002-0131-0567
Ali Khademhosseini https://orcid.org/0000-0002-2692-1524

References

[1] Teh S-Y, Lin R, Hung L-H and Lee A P 2008 Droplet microfluidics *Lab Chip* **8** 198–220
[2] Lu H, Caen O, Vrignon J, Zonta E, El Harrak Z, Nizard P, Baret J C and Taly V 2017 High throughput single cell counting in droplet-based microfluidics *Sci. Rep.* **7** 1366
[3] Wu C-Y, Ouyang M, Wang B, de Rutte J, Joo A, Jacobs M, Ha K, Bertozzi A L and di Carlo D 2020 Monodisperse drops templated by 3D-structured microparticles *Sci. Adv.* **6** eabb9023
[4] Zhang Y and Jiang H-R 2016 A review on continuous-flow microfluidic PCR in droplets: advances, challenges and future *Anal. Chim. Acta* **914** 7–16
[5] Madadelahi M, Ghazimirsaeed E and Shamloo A 2019 Design and fabrication of a two-phase diamond nanoparticle aided fast PCR device *Anal. Chim. Acta* **1068** 28–40
[6] Shembekar N, Chaipan C, Utharala R and Merten C A 2016 Droplet-based microfluidics in drug discovery, transcriptomics and high-throughput molecular genetics *Lab Chip* **16** 1314–31
[7] Salomon R, Kaczorowski D, Valdes-Mora F, Nordon R E, Neild A, Farbehi N, Bartonicek N and Gallego-Ortega D 2019 Droplet-based single cell RNAseq tools: a practical guide *Lab Chip* **19** 1706–27
[8] Madadelahi M and Shamloo A 2017 Droplet-based flows in serpentine microchannels: chemical reactions and secondary flows *Int. J. Multiph. Flow* **97** 186–96
[9] Ghazimirsaeed E, Madadelahi M, Dizani M and Shamloo A 2021 Secondary flows, mixing, and chemical reaction analysis of droplet-based flow inside serpentine microchannels with different cross sections *Langmuir* **37** 5118–30
[10] Solvas X C I and DeMello A 2011 Droplet microfluidics: recent developments and future applications *Chem. Commun.* **47** 1936–42
[11] Zhao C-X 2013 Multiphase flow microfluidics for the production of single or multiple emulsions for drug delivery *Adv. Drug Deliv. Rev.* **65** 1420–46
[12] Salehi S S, Shamloo A and Hannani S K 2020 Microfluidic technologies to engineer mesenchymal stem cell aggregates—applications and benefits *Biophys. Rev.* **12** 123–33
[13] Wehking J D, Gabany M, Chew L and Kumar R 2014 Effects of viscosity, interfacial tension, and flow geometry on droplet formation in a microfluidic T-junction *Microfluid. Nanofluidics* **16** 441–53
[14] Christopher G F and Anna S L 2007 Microfluidic methods for generating continuous droplet streams *J. Phys. D: Appl. Phys.* **40** R319
[15] Anna S L 2016 Droplets and bubbles in microfluidic devices *Annu. Rev. Fluid Mech.* **48** 285–309
[16] Zhao C-X and Middelberg A P 2011 Two-phase microfluidic flows *Chem. Eng. Sci.* **66** 1394–411
[17] Mou C L, Wang W, Li Z L, Ju X J, Xie R, Deng N N, Wei J, Liu Z and Chu L Y 2018 Trojan-horse-like stimuli-responsive microcapsules *Adv. Sci.* **5** 1700960
[18] Sattari A, Hanafizadeh P and Hoorfar M 2020 Multiphase flow in microfluidics: from droplets and bubbles to the encapsulated structures *Adv. Colloid Interface Sci.* **282** 102208
[19] Garstecki P, Fuerstman M J, Stone H A and Whitesides G M 2006 Formation of droplets and bubbles in a microfluidic T-junction—scaling and mechanism of break-up *Lab Chip* **6** 437–46
[20] Besanjideh M, Shamloo A and Kazemzadeh Hannani S 2021 Enhanced oil-in-water droplet generation in a T-junction microchannel using water-based nanofluids with shear-thinning behavior: a numerical study *Phys. Fluids* **33** 012007
[21] Christopher G F, Noharuddin N N, Taylor J A and Anna S L 2008 Experimental observations of the squeezing-to-dripping transition in T-shaped microfluidic junctions *Phys. Rev.* E **78** 036317
[22] Umbanhowar P, Prasad V and Weitz D A 2000 Monodisperse emulsion generation via drop break off in a coflowing stream *Langmuir* **16** 347–51
[23] de Menech M, Garstecki P, Jousse F and Stone H A 2008 Transition from squeezing to dripping in a microfluidic T-shaped junction *J. Fluid Mech.* **595** 141–61
[24] Abate A R, Kutsovsky M, Seiffert S, Windbergs M, Pinto L F, Rotem A, Utada A S and Weitz D A 2011 Synthesis of monodisperse microparticles from non-Newtonian polymer solutions with microfluidic devices *Adv. Mater.* **23** 1757–60
[25] Zhu P and Wang L 2017 Passive and active droplet generation with microfluidics: a review *Lab Chip* **17** 34–75

[26] Utada A S, Fernandez-Nieves A, Stone H A and Weitz D A 2007 Dripping to jetting transitions in coflowing liquid streams *Phys. Rev. Lett.* **99** 094502
[27] Castro-Hernandez E, Gundabala V, Fernández-Nieves A and Gordillo J M 2009 Scaling the drop size in coflow experiments *New J. Phys.* **11** 075021
[28] Wang W, Xie R, Ju X-J, Luo T, Liu L, Weitz D A and Chu L-Y 2011 Controllable microfluidic production of multicomponent multiple emulsions *Lab Chip* **11** 1587–92
[29] Nasiri R, Shamloo A, Akbari J, Tebon P, Dokmeci M R and Ahadian S 2020 Design and simulation of an integrated centrifugal microfluidic device for CTCs separation and cell lysis *Micromachines* **11** 699
[30] Salehi S S, Shamloo A and Hannani S K 2020 Parametric study of droplet formation and characteristics within microfluidic devices—a case study *Int. J. Appl. Mech.* **12** 2050077
[31] Wang W, Liu Z, Jin Y and Cheng Y 2011 LBM simulation of droplet formation in micro-channels *Chem. Eng. J.* **173** 828–36
[32] Salkin L, Schmit A, Courbin L and Panizza P 2013 Passive breakups of isolated drops and one-dimensional assemblies of drops in microfluidic geometries: experiments and models *Lab Chip* **13** 3022–32
[33] Li X-B, Li F-C, Yang J-C, Kinoshita H, Oishi M and Oshima M 2012 Study on the mechanism of droplet formation in T-junction microchannel *Chem. Eng. Sci.* **69** 340–51
[34] Hong Y and Wang F 2007 Flow rate effect on droplet control in a co-flowing microfluidic device *Microfluid. Nanofluidics* **3** 341–6
[35] Peng L, Yang M, Guo S-S, Liu W and Zhao X-Z 2011 The effect of interfacial tension on droplet formation in flow-focusing microfluidic device *Biomed. Microdevices* **13** 559–64
[36] Husny J and Cooper-White J J 2006 The effect of elasticity on drop creation in T-shaped microchannels *J. Nonnewton Fluid Mech.* **137** 121–36
[37] Bai L, Fu Y, Zhao S and Cheng Y 2016 Droplet formation in a microfluidic T-junction involving highly viscous fluid systems *Chem. Eng. Sci.* **145** 141–8
[38] Murshed S S and Estellé P 2017 A state of the art review on viscosity of nanofluids *Renew. Sustain. Energy Rev.* **76** 1134–52
[39] Yao X, Liu Z, Ma M, Chao Y, Gao Y and Kong T 2018 Control of particle adsorption for stability of pickering emulsions in microfluidics *Small* **14** 1802902
[40] Besanjideh M, Hajabdollahi M and Nassab S G 2016 CFD based analysis of laminar forced convection of nanofluid separated flow under the presence of magnetic field *J. Mech.* **32** 777–85
[41] Feng S, Shirani E and Inglis D W 2019 Droplets for sampling and transport of chemical signals in biosensing: a review *Biosensors* **9** 80
[42] Seemann R, Brinkmann M, Pfohl T and Herminghaus S 2011 Droplet based microfluidics *Rep. Prog. Phys.* **75** 016601
[43] Chong Z Z, Tan S H, Gañán-Calvo A M, Tor S B, Loh N H and Nguyen N-T 2016 Active droplet generation in microfluidics *Lab Chip* **16** 35–58
[44] Liu M 1995 Fluid dynamics of colloidal magnetic and electric liquid *Phys. Rev. Lett.* **74** 4535
[45] Xi H-D, Zheng H, Guo W, Gañán-Calvo A M, Ai Y, Tsao C-W, Zhou J, Li W, Huang Y and Nguyen N-T 2017 Active droplet sorting in microfluidics: a review *Lab Chip* **17** 751–71
[46] Stan C A, Tang S K and Whitesides G M 2009 Independent control of drop size and velocity in microfluidic flow-focusing generators using variable temperature and flow rate *Anal. Chem.* **81** 2399–402
[47] Huang Y, Wang Y and Wong T 2017 AC electric field controlled non-Newtonian filament thinning and droplet formation on the microscale *Lab Chip* **17** 2969–81
[48] Shojaeian M and Hardt S 2018 Fast electric control of the droplet size in a microfluidic T-junction droplet generator *Appl. Phys. Lett.* **112** 194102
[49] Malloggi F, Vanapalli S A, Gu H, van den Ende D and Mugele F 2007 Electrowetting-controlled droplet generation in a microfluidic flow-focusing device *J. Phys.: Condens. Matter* **19** 462101
[50] Tan S-H, Nguyen N-T, Yobas L and Kang T G 2010 Formation and manipulation of ferrofluid droplets at a microfluidic T-junction *J. Micromech. Microeng.* **20** 045004
[51] Bijarchi M A, Favakeh A, Sedighi E and Shafii M B 2020 Ferrofluid droplet manipulation using an adjustable alternating magnetic field *Sens. Actuators* A **301** 111753
[52] Odenbach S 2003 Ferrofluids—magnetically controlled suspensions *Colloids Surf.* A **217** 171–8
[53] Campelj S, Makovec D and Drofenik M 2008 Preparation and properties of water-based magnetic fluids *J. Phys.: Condens. Matter* **20** 204101
[54] Chen H, Wang Y, Qu J, Hong R and Li H 2011 Preparation and characterization of silicon oil based ferrofluid *Appl. Surf. Sci.* **257** 10802–7
[55] Wang S, Yang C and Bian X 2012 Magnetoviscous properties of Fe_3O_4 silicon oil based ferrofluid *J. Magn. Magn. Mater.* **324** 3361–5
[56] Yan Q, Xuan S, Ruan X, Wu J and Gong X 2015 Magnetically controllable generation of ferrofluid droplets *Microfluid. Nanofluidics* **19** 1377–84
[57] Zhang K, Liang Q, Ai X, Hu P, Wang Y and Luo G 2011 On-demand microfluidic droplet manipulation using hydrophobic ferrofluid as a continuous-phase *Lab Chip* **11** 1271–5
[58] Shamloo A and Besanjideh M 2019 Investigation of a novel microfluidic device for label-free ferrohydrodynamic cell separation on a rotating disk *IEEE Trans. Biomed. Eng.* **67** 372–8
[59] Zhao W, Cheng R, Lim S H, Miller J R, Zhang W, Tang W, Xie J and Mao L 2017 Biocompatible and label-free separation of cancer cells from cell culture lines from white blood cells in ferrofluids *Lab Chip* **17** 2243–55
[60] Chen L, Zheng X L, Hu N, Yang J, Luo H Y, Jiang F and Liao Y J 2015 Research progress on microfluidic chip of cell separation based on dielectrophoresis *Chin. J. Anal. Chem.* **43** 300–8
[61] Yoon S, Kim J A, Lee S H, Kim M and Park T H 2013 Droplet-based microfluidic system to form and separate multicellular spheroids using magnetic nanoparticles *Lab Chip* **13** 1522–8
[62] Chen C and Lee G 2006 Formation of microdroplets in liquids utilizing active pneumatic choppers on a microfluidic chip *J. Microelectromech. Syst.* **15** 1492–8
[63] Bransky A, Korin N, Khoury M and Levenberg S 2009 A microfluidic droplet generator based on a piezoelectric actuator *Lab Chip* **9** 516–20
[64] Zhu P, Tang X and Wang L 2016 Droplet generation in co-flow microfluidic channels with vibration *Microfluid. Nanofluidics* **20** 47
[65] Tan S-H, Murshed S S, Nguyen N-T, Wong T N and Yobas L 2008 Thermally controlled droplet formation in flow focusing geometry: formation regimes and effect of nanoparticle suspension *J. Phys. D: Appl. Phys.* **41** 165501
[66] Lorenz T, Bojko S, Bunjes H and Dietzel A 2018 An inert 3D emulsification device for individual precipitation and concentration of amorphous drug nanoparticles *Lab Chip* **18** 627–38
[67] Adams L, Kodger T E, Kim S-H, Shum H C, Franke T and Weitz D A 2012 Single step emulsification for the generation of multi-component double emulsions *Soft Matter* **8** 10719–24
[68] Piccin E, Ferraro D, Sartori P, Chiarello E, Pierno M and Mistura G 2014 Generation of water-in-oil and oil-in-water microdroplets in polyester-toner microfluidic devices *Sens. Actuators* B **196** 525–31

[69] Nie Z, Park J I, Li W, Bon S A and Kumacheva E 2008 An 'inside-out' microfluidic approach to monodisperse emulsions stabilized by solid particles *J. Am. Chem. Soc.* **130** 16508–9
[70] Fouilloux S, Malloggi F, Daillant J and Thill A 2016 Aging mechanism in model pickering emulsion *Soft Matter* **12** 900–4
[71] Pan M, Lyu F and Tang S K 2017 Methods to coalesce fluorinated pickering emulsions *Anal. Methods* **9** 4622–9
[72] Saeki D, Sugiura S, Kanamori T, Sato S and Ichikawa S 2010 Microfluidic preparation of water-in-oil-in-water emulsions with an ultra-thin oil phase layer *Lab Chip* **10** 357–62
[73] Nisisako T, Okushima S and Torii T 2005 Controlled formulation of monodisperse double emulsions in a multiple-phase microfluidic system *Soft Matter* **1** 23–27
[74] Nabavi S A, Vladisavljević G T, Gu S and Ekanem E E 2015 Double emulsion production in glass capillary microfluidic device: parametric investigation of droplet generation behaviour *Chem. Eng. Sci.* **130** 183–96
[75] Yang S, Guo F, Kiraly B, Mao X, Lu M, Leong K W and Huang T J 2012 Microfluidic synthesis of multifunctional Janus particles for biomedical applications *Lab Chip* **12** 2097–102
[76] Hao N, Nie Y and Zhang J X 2018 Microfluidic synthesis of functional inorganic micro-/nanoparticles and applications in biomedical engineering *Int. Mater. Rev.* **63** 461–87
[77] Dendukuri D and Doyle P S 2009 The synthesis and assembly of polymeric microparticles using microfluidics *Adv. Mater.* **21** 4071–86
[78] Langer R 1990 New methods of drug delivery *Science* **249** 1527–33
[79] Uhrich K E, Cannizzaro S M, Langer R S and Shakesheff K M 1999 Polymeric systems for controlled drug release *Chem. Rev.* **99** 3181–98
[80] Zeng S, Yong K-T, Roy I, Dinh X-Q, Yu X and Luan F 2011 A review on functionalized gold nanoparticles for biosensing applications *Plasmonics* **6** 491
[81] Li Z, Sun Q, Zhu Y, Tan B, Xu Z P and Dou S X 2014 Ultra-small fluorescent inorganic nanoparticles for bioimaging *J. Mater. Chem.* B **2** 2793–818
[82] Kolosnjaj-Tabi J, Wilhelm C, Clément O and Gazeau F 2013 Cell labeling with magnetic nanoparticles: opportunity for magnetic cell imaging and cell manipulation *J. Nanobiotechnol.* **11** S7
[83] Lan W, Li S, Xu J and Luo G 2011 Controllable preparation of nanoparticle-coated chitosan microspheres in a co-axial microfluidic device *Lab Chip* **11** 652–7
[84] Zhang J, Yan S, Sluyter R, Li W, Alici G and Nguyen N T 2014 Inertial particle separation by differential equilibrium positions in a symmetrical serpentine micro-channel *Sci. Rep.* **4** 4527
[85] Lim Z-Z J, Li J-E J, Ng C-T, Yung L-Y L and Bay B-H 2011 Gold nanoparticles in cancer therapy *Acta Pharmacol. Sin.* **32** 983–90
[86] Zhong Y, Chen Y, Yao L, Zhao D, Zheng L, Liu G, Ye Y and Chen W 2016 Gold nanoparticles based lateral flow immunoassay with largely amplified sensitivity for rapid melamine screening *Microchim. Acta* **183** 1989–94
[87] Lazarus L L, Yang A S-J, Chu S, Brutchey R L and Malmstadt N 2010 Flow-focused synthesis of monodisperse gold nanoparticles using ionic liquids on a microfluidic platform *Lab Chip* **10** 3377–9
[88] Bandulasena M V, Vladisavljević G T and Benyahia B 2019 Droplet-based microfluidic method for robust preparation of gold nanoparticles in axisymmetric flow focusing device *Chem. Eng. Sci.* **195** 657–64
[89] Cheng L, Cai B, Zuo Y, Xiao L, Rao L, He Z, Yang Y, Liu W, Guo S and Zhao X-Z 2017 Janus droplet parallel arrangements using a simple Y-channel flow-focusing microfluidic device *Chem. Phys. Lett.* **673** 93–98
[90] Li W, Dong H, Tang G, Ma T and Cao X 2015 Controllable microfluidic fabrication of Janus and microcapsule particles for drug delivery applications *RSC Adv.* **5** 23181–8
[91] Li W, Liu D, Zhang H, Correia A, Mäkilä E, Salonen J, Hirvonen J and Santos H A 2017 Microfluidic assembly of a nano-in-micro dual drug delivery platform composed of halloysite nanotubes and a pH-responsive polymer for colon cancer therapy *Acta Biomater.* **48** 238–46
[92] Zhang H, Liu D, Shahbazi M A, Mäkilä E, Herranz-Blanco B, Salonen J, Hirvonen J and Santos H A 2014 Fabrication of a multifunctional nano-in-micro drug delivery platform by microfluidic templated encapsulation of porous silicon in polymer matrix *Adv. Mater.* **26** 4497–503
[93] Chen R, Chen X, Jin X and Zhu X 2017 Morphology design and control of polymer particles by regulating the droplet flowing mode in microfluidic chips *Polym. Chem.* **8** 2953–8
[94] Hessberger T, Braun L, Henrich F, Müller C, Gießelmann F, Serra C and Zentel R 2016 Co-flow microfluidic synthesis of liquid crystalline actuating Janus particles *J. Mater. Chem.* C **4** 8778–86
[95] Ghosh S and Schurtenberger P 2019 Microfluidic production of snowman-shaped Janus hydrogel particles *Colloids Surf.* A **573** 205–10
[96] Kozlíková B, Krone M, Falk M, Lindow N, Baaden M, Baum D, Viola I, Parulek J and Hege H C 2017 Visualization of biomolecular structures: state of the art revisited *Comput. Graph. Forum* **36** 178–204
[97] Dressler O J, Casadevall I Solvas X and deMello A J 2017 Chemical and biological dynamics using droplet-based microfluidics *Annu. Rev. Anal. Chem.* **10** 1–24
[98] Macaulay I C and Voet T 2014 Single cell genomics: advances and future perspectives *PLoS Genet.* **10** e1004126
[99] Beer N R, Hindson B J, Wheeler E K, Hall S B, Rose K A, Kennedy I M and Colston B W 2007 On-chip, real-time, single-copy polymerase chain reaction in picoliter droplets *Anal. Chem.* **79** 8471–5
[100] Zhang Y, Park S, Yang S and Wang T-H 2010 An all-in-one microfluidic device for parallel DNA extraction and gene analysis *Biomed. Microdevices* **12** 1043–9
[101] Abate A R, Hung T, Sperling R A, Mary P, Rotem A, Agresti J J, Weiner M A and Weitz D A 2013 DNA sequence analysis with droplet-based microfluidics *Lab Chip* **13** 4864–9
[102] Zubaite G, Simutis K, Galinis R, Milkus V, Kiseliovas V and Mazutis L 2017 Droplet microfluidics approach for single-DNA molecule amplification and condensation into DNA-magnesium-pyrophosphate particles *Micromachines* **8** 62
[103] Okura N, Nakashoji Y, Koshirogane T, Kondo M, Tanaka Y, Inoue K and Hashimoto M 2017 A compact and facile microfluidic droplet creation device using a piezoelectric diaphragm micropump for droplet digital PCR platforms *Electrophoresis* **38** 2666–72
[104] Stark A, Shin D J and Wang T-H 2018 A sample-to-answer droplet magnetofluidic assay platform for quantitative methylation-specific PCR *Biomed. Microdevices* **20** 31
[105] Lee S H, Lee H W, Kwon H G, Lee J H, Kim Y-H, Jeong O C and Ahn J-Y 2018 A droplet-based microfluidic approach and microsphere-PCR amplification for single-stranded DNA amplicons *J. Vis. Exp.* **141** e57703
[106] Bian X, Jing F, Li G, Fan X, Jia C, Zhou H, Jin Q and Zhao J 2015 A microfluidic droplet digital PCR for simultaneous detection of pathogenic *Escherichia coli* O157 and Listeria monocytogenes *Biosens. Bioelectron.* **74** 770–7
[107] Pellegrino M, Sciambi A, Treusch S, Durruthy-Durruthy R, Gokhale K, Jacob J, Chen T X, Geis J A, Oldham W and Matthews J 2018 High-throughput single-cell DNA sequencing of acute myeloid leukemia tumors with droplet microfluidics *Genome Res.* **28** 1345–52
[108] Bustin S 2002 INVITED REVIEW quantification of mRNA using real-time reverse transcription PCR (RT-PCR): trends and problems *J. Mol. Endocrinol.* **29** 23–39

[109] Beer N R, Wheeler E K, Lee-Houghton L, Watkins N, Nasarabadi S, Hebert N, Leung P, Arnold D W, Bailey C G and Colston B W 2008 On-chip single-copy real-time reverse-transcription PCR in isolated picoliter droplets *Anal. Chem.* **80** 1854–8
[110] Prakash R, Pabbaraju K, Wong S, Wong A, Tellier R and Kaler K 2015 Multiplex, quantitative, reverse transcription PCR detection of influenza viruses using droplet microfluidic technology *Micromachines* **6** 63–79
[111] Schwartz S L and Lowen A C 2016 Droplet digital PCR: a novel method for detection of influenza virus defective interfering particles *J. Virol. Methods* **237** 159–65
[112] Yucha R W, Hobbs K S, Hanhauser E, Hogan L E, Nieves W, Ozen M O, Inci F, York V, Gibson E A and Thanh C 2017 High-throughput characterization of HIV-1 reservoir reactivation using a single-cell-in-droplet PCR assay *EBioMedicine* **20** 217–29
[113] Chaipan C, Pryszlak A, Dean H, Poignard P, Benes V, Griffiths A D and Merten C A 2017 Single-virus droplet microfluidics for high-throughput screening of neutralizing epitopes on HIV particles *Cell Chem. Biol.* **24** 751–7
[114] Shin D J, Trick A Y, Hsieh Y-H, Thomas D L and Wang T-H 2018 Sample-to-answer droplet magnetofluidic platform for point-of-care hepatitis C viral load quantitation *Sci. Rep.* **8** 9793
[115] Zhang H, Jenkins G, Zou Y, Zhu Z and Yang C J 2012 Massively parallel single-molecule and single-cell emulsion reverse transcription polymerase chain reaction using agarose droplet microfluidics *Anal. Chem.* **84** 3599–606
[116] Eastburn D J, Sciambi A and Abate A R 2013 Ultrahigh-throughput mammalian single-cell reverse-transcriptase polymerase chain reaction in microfluidic drops *Anal. Chem.* **85** 8016–21
[117] Kim S C, Clark I C, Shahi P, and Abate A R 2018 Single cell RT-PCR in microfluidic droplets with integrated chemical lysis *Anal. Chem.* **90** 1273–9
[118] Notomi T, Okayama H, Masubuchi H, Yonekawa T, Watanabe K, Amino N and Hase T 2000 Loop-mediated isothermal amplification of DNA *Nucleic Acids Res.* **28** e63
[119] Azizi M, Zaferani M, Cheong S H and Abbaspourrad A 2019 Pathogenic bacteria detection using RNA-based loop-mediated isothermal-amplification-assisted nucleic acid amplification via droplet microfluidics *ACS Sens.* **4** 841–8
[120] Costa C, Giménez-Capitán A, Karachaliou N and Rosell R 2013 Comprehensive molecular screening: from the RT-PCR to the RNA-seq *Transl. Lung Cancer Res.* **2** 87
[121] Klein A M, Mazutis L, Akartuna I, Tallapragada N, Veres A, Li V, Peshkin L, Weitz D A and Kirschner M W 2015 Droplet barcoding for single-cell transcriptomics applied to embryonic stem cells *Cell* **161** 1187–201
[122] Macosko E Z, Basu A, Satija R, Nemesh J, Shekhar K, Goldman M, Tirosh I, Bialas A R, Kamitaki N and Martersteck E M 2015 Highly parallel genome-wide expression profiling of individual cells using nanoliter droplets *Cell* **161** 1202–14
[123] Adamson B, Norman T M, Jost M, Cho M Y, Nuñez J K, Chen Y, Villalta J E, Gilbert L A, Horlbeck M A and Hein M Y 2016 A multiplexed single-cell CRISPR screening platform enables systematic dissection of the unfolded protein response *Cell* **167** 1867–82
[124] Fu Y, Chen H, Liu L and Huang Y 2016 Single cell total RNA sequencing through isothermal amplification in picoliter-droplet emulsion *Anal. Chem.* **88** 10795–9
[125] Kang H M, Subramaniam M, Targ S, Nguyen M, Maliskova L, McCarthy E, Wan E, Wong S, Byrnes L and Lanata C M 2018 Multiplexed droplet single-cell RNA-sequencing using natural genetic variation *Nat. Biotechnol.* **36** 89
[126] Liu Y, Chen X, Zhang Y and Liu J 2019 Advancing single-cell proteomics and metabolomics with microfluidic technologies *Analyst* **144** 846–58
[127] Berman H M, Westbrook J, Feng Z, Gilliland G, Bhat T N, Weissig H, Shindyalov I N and Bourne P E 2000 The protein data bank *Nucleic Acids Res.* **28** 235–42
[128] McPherson A 2004 Introduction to protein crystallization *Methods* **34** 254–65
[129] Maeki M, Yamazaki S, Pawate A S, Ishida A, Tani H, Yamashita K, Sugishima M, Watanabe K, Tokeshi M and Kenis P J 2016 A microfluidic-based protein crystallization method in 10 micrometer-sized crystallization space *CrystEngComm* **18** 7722–7
[130] Maeki M, Yamaguchi H, Yamashita K, Nakamura H, Miyazaki M and Maeda H 2012 A method for generating single crystals that rely on internal fluid dynamics of microdroplets *Chem. Commun.* **48** 5037–9
[131] Maeki M, Teshima Y, Yoshizuka S, Yamaguchi H, Yamashita K and Miyazaki M 2014 Controlling protein crystal nucleation by droplet-based microfluidics *Chem. Eur. J.* **20** 1049–56
[132] Zheng B, Roach L S and Ismagilov R F 2003 Screening of protein crystallization conditions on a microfluidic chip using nanoliter-size droplets *J. Am. Chem. Soc.* **125** 11170–1
[133] Pham N, Radajewski D, Round A, Brennich M, Pernot P, Biscans B A, Bonnete´ F O and Teychene´ S B 2017 Coupling high throughput microfluidics and small-angle x-ray scattering to study protein crystallization from solution *Anal. Chem.* **89** 2282–7
[134] Ferreira J, Castro F, Rocha F and Kuhn S 2018 Protein crystallization in a droplet-based microfluidic device: hydrodynamic analysis and study of the phase behaviour *Chem. Eng. Sci.* **191** 232–44
[135] Zhang S, Gerard C J, Ikni A, Ferry G, Vuillard L M, Boutin J A, Ferte N, Grossier R, Candoni N and Veesler S 2017 Microfluidic platform for optimization of crystallization conditions *J. Cryst. Growth* **472** 18–28
[136] Gerard C J, Ferry G, Vuillard L M, Boutin J A, Ferte N, Grossier R, Candoni N and Veesler S 2018 A chemical library to screen protein and protein–ligand crystallization using a versatile microfluidic platform *Cryst. Growth Des.* **18** 5130–7
[137] Selzer D, Spiegel B, and Kind M 2018 A generic polycarbonate based microfluidic tool to study crystal nucleation in microdroplets *J. Cryst. Process Technol.* **8** 1–17
[138] Joensson H N, Samuels M L, Brouzes E R, Medkova M, Uhlén M, Link D R and Andersson-Svahn H 2009 Detection and analysis of low-abundance cell-surface biomarkers using enzymatic amplification in microfluidic droplets *Angew. Chem., Int. Ed.* **48** 2518–21
[139] Li L, Wang Q, Feng J, Tong L and Tang B 2014 Highly sensitive and homogeneous detection of membrane protein on a single living cell by aptamer and nicking enzyme assisted signal amplification based on microfluidic droplets *Anal. Chem.* **86** 5101–7
[140] Srisa-Art M, Kang D K, Hong J, Park H, Leatherbarrow R J, Edel J B, Chang S I and Demello A J 2009 Analysis of protein–protein interactions by using droplet-based microfluidics *Chem. Bio. Chem.* **10** 1605–11
[141] Choi J-W, Kang D-K, Park H, deMello A J and Chang S-I 2012 High-throughput analysis of protein–protein interactions in picoliter-volume droplets using fluorescence polarization *Anal. Chem.* **84** 3849–54
[142] Benz C, Retzbach H, Nagl S and Belder D 2013 Protein–protein interaction analysis in single microfluidic droplets using FRET and fluorescence lifetime detection *Lab Chip* **13** 2808–14
[143] Lu Y, Yang L, Wei W and Shi Q 2017 Microchip-based single-cell functional proteomics for biomedical applications *Lab Chip* **17** 1250–63
[144] Li Z-Y, Huang M, Wang X-K, Zhu Y, Li J-S, Wong C C and Fang Q 2018 Nanoliter-scale oil-air-droplet chip-based single cell proteomic analysis *Anal. Chem.* **90** 5430–8
[145] Chaturvedi S, Singh A K, Keshari A K, Maity S, Sarkar S and Saha S 2016 Human metabolic enzymes deficiency: a genetic mutation based approach *Scientifica* **2016** 9828672

[146] Mair P, Gielen F and Hollfelder F 2017 Exploring sequence space in search of functional enzymes using microfluidic droplets *Curr. Opin. Chem. Biol.* **37** 137–44
[147] Hammer S C, Knight A M and Arnold F H 2017 Design and evolution of enzymes for non-natural chemistry *Curr. Opin. Green Sustain. Chem.* **7** 23–30
[148] Kintses B, Hein C, Mohamed M F, Fischlechner M, Courtois F, Lainé C and Hollfelder F 2012 Picoliter cell lysate assays in microfluidic droplet compartments for directed enzyme evolution *Chem. Biol.* **19** 1001–9
[149] Beneyton T, Coldren F, Baret J-C, Griffiths A D and Taly V 2014 CotA laccase: high-throughput manipulation and analysis of recombinant enzyme libraries expressed in *E. coli* using droplet-based microfluidics *Analyst* **139** 3314–23
[150] Hosokawa M, Hoshino Y, Nishikawa Y, Hirose T, Yoon D H, Mori T, Sekiguchi T, Shoji S and Takeyama H 2015 Droplet-based microfluidics for high-throughput screening of a metagenomic library for isolation of microbial enzymes *Biosens. Bioelectron.* **67** 379–85
[151] Obexer R, Pott M, Zeymer C, Griffiths A D and Hilvert D 2016 Efficient laboratory evolution of computationally designed enzymes with low starting activities using fluorescence-activated droplet sorting *Protein Eng. Des. Sel.* **29** 355–66
[152] Ma F, Chung M T, Yao Y, Nidetz R, Lee L M, Liu A P, Feng Y, Kurabayashi K and Yang G-Y 2018 Efficient molecular evolution to generate enantioselective enzymes using a dual-channel microfluidic droplet screening platform *Nat. Commun.* **9** 1030
[153] Gielen F, Hours R, Emond S, Fischlechner M, Schell U and Hollfelder F 2016 Ultrahigh-throughput–directed enzyme evolution by absorbance-activated droplet sorting (AADS) *Proc. Natl Acad. Sci.* **113** E7383–E7389
[154] Sjostrom S L, Bai Y, Huang M, Liu Z, Nielsen J, Joensson H N and Svahn H A 2014 High-throughput screening for industrial enzyme production hosts by droplet microfluidics *Lab Chip* **14** 806–13
[155] Beneyton T, Thomas S, Griffiths A D, Nicaud J-M, Drevelle A and Rossignol T 2017 Droplet-based microfluidic high-throughput screening of heterologous enzymes secreted by the yeast Yarrowia lipolytica *Microb. Cell Factories* **16** 18
[156] Rakszewska A, Tel J, Chokkalingam V and Huck W T 2014 One drop at a time: toward droplet microfluidics as a versatile tool for single-cell analysis *NPG Asia Mater.* **6** e133
[157] Chou W L, Lee P Y, Yang C L, Huang W Y and Lin Y S 2015 Recent advances in applications of droplet microfluidics *Micromachines* **6** 1249–71
[158] Dong L, Chen D-W, Liu S-J and Du W 2016 Automated chemotactic sorting and single-cell cultivation of microbes using droplet microfluidics *Sci. Rep.* **6** 24192
[159] Zhang Q, Wang T, Zhou Q, Zhang P, Gong Y, Gou H, Xu J and Ma B 2017 Development of a facile droplet-based single-cell isolation platform for cultivation and genomic analysis in microorganisms *Sci. Rep.* **7** 41192
[160] Chen Q, Utech S, Chen D, Prodanovic R, Lin J-M and Weitz D A 2016 Controlled assembly of heterotypic cells in a core–shell scaffold: organ in a droplet *Lab Chip* **16** 1346–9
[161] Salehi-Reyhani A, Ces O and Elani Y 2017 Artificial cell mimics as simplified models for the study of cell biology *Exp. Biol. Med.* **242** 1309–17
[162] Sharma S, Srisa-Art M, Scott S, Asthana A and Cass A 2013 Droplet-based microfluidics *Microfluidic Diagnostics* (Berlin: Springer) pp 207–30
[163] Periyannan Rajeswari P K, Joensson H N and Andersson-Svahn H 2017 Droplet size influences division of mammalian cell factories in droplet microfluidic cultivation *Electrophoresis* **38** 305–10
[164] Guo M T, Rotem A, Heyman J A and Weitz D A 2012 Droplet microfluidics for high-throughput biological assays *Lab Chip* **12** 2146–55
[165] Mahler L, Tovar M, Weber T, Brandes S, Rudolph M M, Ehgartner J, Mayr T, Figge M T, Roth M and Zang E 2015 Enhanced and homogeneous oxygen availability during incubation of microfluidic droplets *RSC Adv.* **5** 101871–8
[166] Huang H, Yu Y, Hu Y, He X, Usta O B and Yarmush M L 2017 Generation and manipulation of hydrogel microcapsules by droplet-based microfluidics for mammalian cell culture *Lab Chip* **17** 1913–32
[167] Siltanen C, Diakatou M, Lowen J, Haque A, Rahimian A, Stybayeva G and Revzin A 2017 One step fabrication of hydrogel microcapsules with hollow core for assembly and cultivation of hepatocyte spheroids *Acta Biomater.* **50** 428–36
[168] Headen D M, García J R and García A J 2018 Parallel droplet microfluidics for high throughput cell encapsulation and synthetic microgel generation *Microsyst. Nanoeng.* **4** 17076
[169] Chokkalingam V, Tel J, Wimmers F, Liu X, Semenov S, Thiele J, Figdor C G and Huck W T 2013 Probing cellular heterogeneity in cytokine-secreting immune cells using droplet-based microfluidics *Lab Chip* **13** 4740–4
[170] Tumarkin E, Tzadu L, Csaszar E, Seo M, Zhang H, Lee A, Peerani R, Purpura K, Zandstra P W and Kumacheva E 2011 High-throughput combinatorial cell co-culture using microfluidics *Integr. Biol.* **3** 653–62
[171] Lu Y-C, Song W, An D, Kim B J, Schwartz R, Wu M and Ma M 2015 Designing compartmentalized hydrogel microparticles for cell encapsulation and scalable 3D cell culture *J. Mater. Chem.* B **3** 353–60
[172] Chan H F, Zhang Y and Leong K W 2016 Efficient one-step production of microencapsulated hepatocyte spheroids with enhanced functions *Small* **12** 2720–30
[173] Zhang L, Chen K, Zhang H, Pang B, Choi C H, Mao A S, Liao H, Utech S, Mooney D J and Wang H 2018 Microfluidic templated multicompartment microgels for 3D encapsulation and pairing of single cells *Small* **14** 1702955
[174] Siltanen C, Yaghoobi M, Haque A, You J, Lowen J, Soleimani M and Revzin A 2016 Microfluidic fabrication of bioactive microgels for rapid formation and enhanced differentiation of stem cell spheroids *Acta Biomater.* **34** 125–32
[175] Zhao X, Liu S, Yildirimer L, Zhao H, Ding R, Wang H, Cui W and Weitz D 2016 Injectable stem cell-laden photocrosslinkable microspheres fabricated using microfluidics for rapid generation of osteogenic tissue constructs *Adv. Funct. Mater.* **26** 2809–19
[176] Hou Y, Xie W, Achazi K, Cuellar-Camacho J L, Melzig M F, Chen W and Haag R 2018 Injectable degradable PVA microgels prepared by microfluidic technology for controlled osteogenic differentiation of mesenchymal stem cells *Acta Biomater.* **77** 28–37
[177] Martino C and deMello A J 2016 Droplet-based microfluidics for artificial cell generation: a brief review *Interface Focus* **6** 20160011
[178] Elani Y 2016 Construction of membrane-bound artificial cells using microfluidics: a new frontier in bottom-up synthetic biology *Biochem. Soc. Trans.* **44** 723–30
[179] Elani Y, Solvas X C, Edel J B, Law R V and Ces O 2016 Microfluidic generation of encapsulated droplet interface bilayer networks (multisomes) and their use as cell-like reactors *Chem. Commun.* **52** 5961–4
[180] Baxani D K, Morgan A J, Jamieson W D, Allender C J, Barrow D A and Castell O K 2016 Bilayer networks within a hydrogel shell: a robust chassis for artificial cells and a platform for membrane studies *Angew. Chem., Int. Ed.* **55** 14240–5
[181] Czekalska M A, Kaminski T S, Makuch K and Garstecki P 2019 Passive and parallel microfluidic formation of droplet interface bilayers (DIBs) for measurement of leakage of small molecules through artificial phospholipid membranes *Sens. Actuators* B **286** 258–65
[182] Findlay H E, Harris N J and Booth P J 2016 *In vitro* synthesis of a major facilitator transporter for specific active transport across droplet interface bilayers *Sci. Rep.* **6** 39349

[183] Czekalska M, Kaminski T, Horka M, Jakiela S and Garstecki P 2017 An automated microfluidic system for the generation of droplet interface bilayer networks *Micromachines* **8** 93
[184] Nishigami Y, Ito H, Sonobe S and Ichikawa M 2016 Non-periodic oscillatory deformation of an actomyosin microdroplet encapsulated within a lipid interface *Sci. Rep.* **6** 18964
[185] Miyazaki M, Chiba M, Eguchi H, Ohki T and Ishiwata S I 2015 Cell-sized spherical confinement induces the spontaneous formation of contractile actomyosin rings *in vitro Nat. Cell Biol.* **17** 480
[186] Kaminski T S, Scheler O and Garstecki P 2016 Droplet microfluidics for microbiology: techniques, applications and challenges *Lab Chip* **16** 2168–87
[187] Juul S, Nielsen C J, Labouriau R, Roy A, Tesauro C, Jensen P W, Harmsen C, Kristoffersen E L, Chiu Y-L and Frøhlich R 2012 Droplet microfluidics platform for highly sensitive and quantitative detection of malaria-causing plasmodium parasites based on enzyme activity measurement *ACS Nano* **6** 10676–83
[188] Kang D-K, Ali M M, Zhang K, Huang S S, Peterson E, Digman M A, Gratton E and Zhao W 2014 Rapid detection of single bacteria in unprocessed blood using integrated comprehensive droplet digital detection *Nat. Commun.* **5** 5427
[189] Churski K, Kaminski T S, Jakiela S, Kamysz W, Baranska-Rybak W, Weibel D B and Garstecki P 2012 Rapid screening of antibiotic toxicity in an automated microdroplet system *Lab Chip* **12** 1629–37
[190] Sabhachandani P, Sarkar S, Zucchi P C, Whitfield B A, Kirby J E, Hirsch E B and Konry T 2017 Integrated microfluidic platform for rapid antimicrobial susceptibility testing and bacterial growth analysis using bead-based biosensor via fluorescence imaging *Microchim. Acta* **184** 4619–28
[191] Kang W, Sarkar S, Lin Z S, McKenney S and Konry T 2019 Ultra-fast parallelized microfluidic platform for antimicrobial susceptibility testing of gram positive and negative bacteria *Anal. Chem.* **91** 6242–9
[192] Postek W, Gargulinski P, Scheler O, Kaminski T S and Garstecki P 2018 Microfluidic screening of antibiotic susceptibility at a single-cell level shows the inoculum effect of cefotaxime on *E. coli Lab Chip* **18** 3668–77
[193] Simpson C, Lee S S, Lee C-S and Yamauchi Y 2018 Microfluidics: an untapped resource in viral diagnostics and viral cell biology *Curr. Clin. Microbiol. Rep.* **5** 245–51
[194] Tao Y, Rotem A, Zhang H, Chang C B, Basu A, Kolawole A O, Koehler S A, Ren Y, Lin J S and Pipas J M 2015 Rapid, targeted and culture-free viral infectivity assay in drop-based microfluidics *Lab Chip* **15** 3934–40
[195] Fischer A E, Wu S K, Proescher J B, Rotem A, Chang C B, Zhang H, Tao Y, Mehoke T S, Thielen P M and Kolawole A O 2015 A high-throughput drop microfluidic system for virus culture and analysis *J. Virol. Methods* **213** 111–7
[196] Mashaghi S and van Oijen A M 2016 Droplet microfluidics for kinetic studies of viral fusion *Biomicrofluidics* **10** 024102
[197] Kang D-K, Ali M M, Zhang K, Pone E J and Zhao W 2014 Droplet microfluidics for single-molecule and single-cell analysis in cancer research, diagnosis and therapy *TrAC Trends Anal. Chem.* **58** 145–53
[198] Yu Z, Zhou L, Zhang T, Shen R, Li C, Fang X, Griffiths G and Liu J 2017 Sensitive detection of MMP9 enzymatic activities in single cell-encapsulated microdroplets as an assay of cancer cell invasiveness *ACS Sens.* **2** 626–34
[199] Ng E X, Sun G, Wei S-C, Miller M A, DasGupta R, Lam P Y P and Chen C-H 2018 Ultrafast single-cell level enzymatic tumor profiling *Anal. Chem.* **91** 1277–85
[200] Sengupta D, Mongersun A, Kim T J, Mongersun K, von Eyben R, Abbyad P and Pratx G 2019 Multiplexed single-cell measurements of FDG uptake and lactate release using droplet microfluidics *Technol. Cancer Res. Treat.* **18** 1533033819841066
[201] Del Ben F, Turetta M, Celetti G, Piruska A, Bulfoni M, Cesselli D, Huck W T and Scoles G 2016 A method for detecting circulating tumor cells based on the measurement of single-cell metabolism in droplet-based microfluidics *Angew. Chem., Int. Ed.* **55** 8581–4
[202] Cong L, Liang L, Cao F, Sun D, Yue J, Xu W, Liang C and Xu S 2019 Distinguishing cancer cell lines at a single living cell level via detection of sialic acid by dual-channel plasmonic imaging and by using a SERS-microfluidic droplet platform *Microchim. Acta* **186** 367
[203] Jang M, Koh I, Lee S J, Cheong J-H and Kim P 2017 Droplet-based microtumor model to assess cell-ECM interactions and drug resistance of gastric cancer cells *Sci. Rep.* **7** 1–10
[204] Sun Q, Tan S H, Chen Q, Ran R, Hui Y, Chen D and Zhao C-X 2018 Microfluidic formation of coculture tumor spheroids with stromal cells as a novel 3D tumor model for drug testing *ACS Biomater. Sci. Eng.* **4** 4425–33
[205] Du X, Li W, Du G, Cho H, Yu M, Fang Q, Lee L P and Fang J 2018 Droplet array-based 3D coculture system for high-throughput tumor angiogenesis assay *Anal. Chem.* **90** 3253–61
[206] Agarwal P, Wang H, Sun M, Xu J, Zhao S, Liu Z, Gooch K J, Zhao Y, Lu X and He X 2017 Microfluidics enabled bottom-up engineering of 3D vascularized tumor for drug discovery *ACS Nano* **11** 6691–702
[207] Chen W W, Balaj L, Liau L M, Samuels M L, Kotsopoulos S K, Maguire C A, LoGuidice L, Soto H, Garrett M and Zhu L D 2013 Beaming and droplet digital PCR analysis of mutant IDH1 mRNA in glioma patient serum and cerebrospinal fluid extracellular vesicles *Mol. Ther. Nucleic Acids* **2** e109
[208] Pekin D and Taly V 2017 Multiplex detection of KRAS mutations using passive droplet fusion *Microchip Diagnostics* (Berlin: Springer) pp 133–42
[209] Pekin D and Taly V 2017 Droplet-based microfluidics digital PCR for the detection of KRAS mutations *Microchip Diagnostics* (Berlin: Springer) pp 143–64
[210] Vanova B, Kalman M, Jasek K, Kasubova I, Burjanivova T, Farkasova A, Kruzliak P, Busselberg D, Plank L and Lasabova Z 2019 Droplet digital PCR revealed high concordance between primary tumors and lymph node metastases in multiplex screening of KRAS mutations in colorectal cancer *Clin. Exp. Med.* **19** 1–6
[211] Watanabe M *et al* 2015 Ultra-sensitive detection of the pretreatment EGFR T790M mutation in non-small cell lung cancer patients with an EGFR-activating mutation using droplet digital PCR *Clin. Cancer Res.* **21** 3552–60
[212] Tsao S C-H, Weiss J, Hudson C, Christophi C, Cebon J, Behren A and Dobrovic A 2015 Monitoring response to therapy in melanoma by quantifying circulating tumour DNA with droplet digital PCR for BRAF and NRAS mutations *Sci. Rep.* **5** 11198
[213] Ou C-Y, Vu T, Grunwald J T, Toledano M, Zimak J, Toosky M, Shen B, Zell J A, Gratton E and Abram T J 2019 An ultrasensitive test for profiling circulating tumor DNA using integrated comprehensive droplet digital detection *Lab Chip* **19** 993–1005
[214] Li Y, Yan D, Fu F, Liu Y, Zhang B, Wang J, Shang L, Gu Z and Zhao Y 2017 Composite core-shell microparticles from microfluidics for synergistic drug delivery *Sci. China Mater.* **60** 543–53
[215] He F, Zhang M J, Wang W, Cai Q W, Su Y Y, Liu Z, Faraj Y, Ju X J, Xie R and Chu L Y 2019 Designable polymeric microparticles from droplet microfluidics for controlled drug release *Adv. Mater. Technol.* **4** 1800687
[216] Xue P, Wu Y, Menon N V and Kang Y 2015 Microfluidic synthesis of monodisperse PEGDA microbeads for sustained release of 5-fluorouracil *Microfluid. Nanofluidics* **18** 333–42

[217] Kong F, Zhang X and Hai M 2014 Microfluidics fabrication of monodisperse biocompatible phospholipid vesicles for encapsulation and delivery of hydrophilic drug or active compound *Langmuir* **30** 3905–12
[218] Yang J, Zhu Y, Wang F, Deng L, Xu X and Cui W 2020 Microfluidic liposomes-anchored microgels as extended delivery platform for treatment of osteoarthritis *Chem. Eng. J.* **400** 126004
[219] Yu L, Sun Q, Hui Y, Seth A, Petrovsky N and Zhao C-X 2019 Microfluidic formation of core-shell alginate microparticles for protein encapsulation and controlled release *J. Colloid Interface Sci.* **539** 497–503
[220] Ling K, Wu H, Neish A S and Champion J A 2019 Alginate/chitosan microparticles for gastric passage and intestinal release of therapeutic protein nanoparticles *J. Control. Release* **295** 174–86
[221] Labie H, Perro A, Lapeyre V, Goudeau B, Catargi B, Auzély R and Ravaine V 2019 Sealing hyaluronic acid microgels with oppositely-charged polypeptides: a simple strategy for packaging hydrophilic drugs with on-demand release *J. Colloid Interface Sci.* **535** 16–27
[222] Sabhachandani P, Motwani V, Cohen N, Sarkar S, Torchilin V and Konry T 2016 Generation and functional assessment of 3D multicellular spheroids in droplet based microfluidics platform *Lab Chip* **16** 497–505
[223] Schaich M, Cama J, Al Nahas K, Sobota D, Sleath H, Jahnke K, Deshpande S, Dekker C and Keyser U F 2019 An integrated microfluidic platform for quantifying drug permeation across biomimetic vesicle membranes *Mol. Pharm.* **16** 2494–501
[224] Yu L, Chen M C and Cheung K C 2010 Droplet-based microfluidic system for multicellular tumor spheroid formation and anticancer drug testing *Lab Chip* **10** 2424–32
[225] Sabhachandani P, Sarkar S, Mckenney S, Ravi D, Evens A M and Konry T 2019 Microfluidic assembly of hydrogel-based immunogenic tumor spheroids for evaluation of anticancer therapies and biomarker release *J. Control. Release* **295** 21–30
[226] Shi N, Moniruzzaman M and Easley C J 2020 Tissue Engineering and Analysis in Droplet Microfluidics *Droplet Microfluidics* Ren Carolyn and Lee Abraham (R. Soc. Chem.) 223–60
[227] Jang M, Yang S and Kim P 2016 Microdroplet-based cell culture models and their application *Biochip J.* **10** 310–7
[228] Chung B G, Lee K-H, Khademhosseini A and Lee S-H 2012 Microfluidic fabrication of microengineered hydrogels and their application in tissue engineering *Lab Chip* **12** 45–59
[229] Sheikhi A, de Rutte J, Haghniaz R, Akouissi O, Sohrabi A, di Carlo D and Khademhosseini A 2019 Microfluidic-enabled bottom-up hydrogels from annealable naturally-derived protein microbeads *Biomaterials* **192** 560–8
[230] Yu J, Huang T-R, Lim Z H, Luo R, Pasula R R, Liao L-D, Lim S and Chen C-H 2016 Production of hollow bacterial cellulose microspheres using microfluidics to form an injectable porous Scaffold for wound healing *Adv. Healthcare Mater.* **5** 2983–92
[231] Chen G, Yu Y, Wu X, Wang G, Gu G, Wang F, Ren J, Zhang H and Zhao Y 2019 Microfluidic electrospray niacin metal-organic frameworks encapsulated microcapsules for wound healing *Research* **2019** 6175398
[232] Shi M, Zhang H, Song T, Liu X, Gao Y, Zhou J and Li Y 2019 Sustainable dual release of antibiotic and growth factor from pH-responsive uniform alginate composite microparticles to enhance wound healing *ACS Appl. Mater. Interfaces* **11** 22730–44
[233] Zhang H, Xu R, Yin Z, Yu J, Liang N and Geng Q 2021 Antibacterial hydrogel microparticles with drug loading for wound healing *Mater. Res. Express* **8** 095403
[234] Galván-Chacón V P, Costa L, Barata D and Habibovic P 2021 Droplet microfluidics as a tool for production of bioactive calcium phosphate microparticles with controllable physicochemical properties *Acta Biomater.* **128** 486–501
[235] Sun J, Zhang Y, Li B, Gu Y and Chen L 2017 Controlled release of BMP-2 from a collagen-mimetic peptide-modified silk fibroin–nanohydroxyapatite scaffold for bone regeneration *J. Mater. Chem.* B **5** 8770–9
[236] An C *et al* 2020 Continuous microfluidic encapsulation of single mesenchymal stem cells using alginate microgels as injectable fillers for bone regeneration *Acta Biomater.* **111** 181–96
[237] Weaver J D, Headen D M, Coronel M M, Hunckler M D, Shirwan H and García A J 2019 Synthetic poly(ethylene glycol)-based microfluidic islet encapsulation reduces graft volume for delivery to highly vascularized and retrievable transplant site *Am. J. Transplant.* **19** 1315–27
[238] Cai Y, Wu F, Yu Y, Liu Y, Shao C, Gu H, Li M and Zhao Y 2019 Porous scaffolds from droplet microfluidics for prevention of intrauterine adhesion *Acta Biomater.* **84** 222–30
[239] Lei L, Lv Q, Jin Y, An H, Shi Z, Hu G, Yang Y, Wang X and Yang L 2021 Angiogenic microspheres for the treatment of a thin endometrium *ACS Biomater. Sci. Eng.* **7** 4914–20
[240] Zhu Y, Sun L, Fu X, Liu J, Liang Z, Tan H, Li W and Zhao Y 2021 Engineering microcapsules to construct vascularized human brain organoids *Chem. Eng. J.* **424** 130427
[241] de Rutte J M, Koh J and di Carlo D 2019 Scalable high-throughput production of modular microgels for *in situ* assembly of microporous tissue scaffolds *Adv. Funct. Mater.* **29** 1900071
[242] Nisisako T and Torii T 2008 Microfluidic large-scale integration on a chip for mass production of monodisperse droplets and particles *Lab Chip* **8** 287–93
[243] Kobayashi I, Neves M A, Wada Y, Uemura K and Nakajima M 2012 Large microchannel emulsification device for mass producing uniformly sized droplets on a liter per hour scale *Green Process. Synth.* **1** 353–62
[244] Guzowski J, Korczyk P M, Jakiela S and Garstecki P 2011 Automated high-throughput generation of droplets *Lab Chip* **11** 3593–5
[245] Feng H, Zheng T, Li M, Wu J, Ji H, Zhang J, Zhao W and Guo J 2019 Droplet-based microfluidics systems in biomedical applications *Electrophoresis* **40** 1580–90
[246] Kim S, Oh J and Cha C 2016 Enhancing the biocompatibility of microfluidics-assisted fabrication of cell-laden microgels with channel geometry *Colloids Surf.* B **147** 1–8
[247] Benavente-Babace A, Haase K, Stewart D J and Godin M 2019 Strategies for controlling egress of therapeutic cells from hydrogel microcapsules *J. Tissue Eng. Regen. Med.* **13** 612–24
[248] Husman D *et al* 2020 Multiphasic microgel-in-gel materials to recapitulate cellular mesoenvironments *in vitro* *Biomater. Sci.* **8** 101–8
[249] Luo R-C and Chen C-H 2012 Structured microgels through microfluidic assembly and their biomedical applications *Soft* **1** 1–23
[250] Dressler O J, MacEiczyk R M, Chang S-I and deMello A J 2013 Droplet-based microfluidics: enabling impact on drug discovery *J. Biomol. Screen.* **19** 483–96
[251] Lignos I *et al* 2018 Exploration of near-infrared-emissive colloidal multinary lead halide perovskite nanocrystals using an automated microfluidic platform *ACS Nano* **12** 5504–17
[252] Sohrabi S, Kassir N and Keshavarz Moraveji M 2020 Droplet microfluidics: fundamentals and its advanced applications *RSC Adv.* **10** 27560–74
[253] Horváth L, Umehara Y, Jud C, Blank F, Petri-Fink A and Rothen-Rutishauser B 2015 Engineering an *in vitro* air-blood barrier by 3D bioprinting *Sci. Rep.* **5** 7974
[254] Nasiri R *et al* 2020 Microfluidic-based approaches in targeted cell/particle separation based on physical properties: fundamentals and applications *Small* **16** 2000171

[255] Waheed S, Cabot J M, MacDonald N P, Lewis T, Guijt R M, Paull B and Breadmore M C 2016 3D printed microfluidic devices: enablers and barriers *Lab Chip* **16** 1993–2013
[256] Zhao B, Cui X, Ren W, Xu F, Liu M, and Ye Z-G 2017 A controllable integrated pump-enabled microfluidic chip and its application in droplets generating *Sci. Rep.* **7** 11319
[257] Suea-Ngam A, Howes P D, Srisa-Art M and deMello A J 2019 Droplet microfluidics: from proof-of-concept to real-world utility? *Chem. Commun.* **55** 9895–903